DISS. ETH NO. 17142

MODELING DIELECTRIC ELASTOMER ACTUATORS

A dissertation submitted to the

SWISS FEDERAL INSTITUTE OF TECHNOLOGY in ZURICH

for the degree of

Doctor of Sciences

presented by

MICHAEL TOBIAS WISSLER

Dipl. Werkstoff.-Ing. ETH

born 25th October 1976

citizen of Sumiswald (BE)

accepted on the recommendation of
Prof. Dr. E. Mazza, examiner
Prof. Dr. P. Ermanni, co-examiner
Prof. Dr. M. Farshad, co-examiner
Dr. G. Kovacs, co-examiner

2007

Acknowledgments

I wish to express my sincere gratitude to

- My supervisor Prof. Dr. Edoardo Mazza, for his kind support and encouragement during this work, the many fruitful discussions and his interest in my research work.

- My co-examiners, Prof. Dr. Paolo Ermanni, Prof. Dr. Mehdi Farshad and Dr. Gabor Kovacs for carefully reviewing this thesis.

- All my colleagues and supervisors at the laboratory for Materials and Engineering at Empa for the good atmosphere, especially: Silvain Michel, Patrick Lochmatter, Rui Zhang, Christian Dürager, Claudio Iseli and Lukas Kessler for the interesting and helpful discussions concerning dielectric elastomers; Alfred Schmidlin, Urs Hintermüller, Bernd Jähne and Kurt Gantner for technical support; Dr. Luc Wullschleger, Christian Affolter and Bernhard Weisse for assisting me with finite element simulations.

- Jonas Wyrsch, Riya Bhattacharya, Patrick Grau, Marcel Birrer and Julien Egger for writing their semester thesis on topics directly related to my research.

- Dr. Alessandro Nava for performing the aspiration experiments.

- The Swiss National Science Foundation (SNF) for the financial support of this thesis (Project number: 200021-107661/1).

- My family and my friends for their encouragement and support. This work is dedicated to my parents.

Michael Wissler
Zürich, April 2007

Table of contents

Abstract

Dielectric elastomer actuators belong to the group of so called “electroactive polymers” and are used in active structures where large strains are required. Dielectric elastomers have many potential applications as actuators. Models and simulation techniques are required for the design and optimization of actuator applications in order to determine states of stress and strain as functions of the applied voltage. Several aspects have to be considered in the modeling and simulation of dielectric elastomer actuators, including the constitutive model of the elastomer, the electromechanical coupling, numerical implementation and experimental validation of the models. So far no adequate models exist which are able to predict the actuator behavior over a large deformation and time range.

In the present work, actuators made of an acrylic elastomer (the widely used material VHB 4910 by 3M) are investigated. The passive mechanical response of the elastomer is decoupled from the electromechanical problem. Electrostatic forces arise only at the interface between the electrodes and the elastomer. The elastomer behaves as a passive layer and there is no direct interaction between electric field and its mechanical properties. The electromechanical coupling, an equation proposed by Pelrine et al. (Sensors and Actuators A, 64, 1998), is evaluated by analytical and numerical methods. The dielectric constant of VHB 4910 is determined by LCR measurements for various prestrain levels as well as by spring roll experiments. The passive mechanical response of the elastomer is described using a ‘quasilinear visco-hyperelastic model’ suitable for large strains and viscoelasticity. The constitutive model and the electromechanical coupling are implemented in finite element models for simulating the behavior of circular actuators. A systematic experimental characterization of circular actuators under various prestrain and voltage conditions has been carried out. Over 40 actuators have been tested at 11 different prestrain/voltage levels. These experimental data are essential for model definition and validation purposes. The constitutive model is further evaluated using different deformation configurations. Uniaxial tensile and relaxation tests, aspiration tests and compression tests have been carried out and compared to corresponding simulations.

The mechanical model (with an optimized parameter set) is valid over a wide deformation and time range, as shown for circular actuator tests at different prestrain and voltage levels as well as for uniaxial, aspiration and compression tests. The concept of quasilinear viscoelasticity was validated by uniaxial relaxation tests which showed that the normalized stress-relaxation function is independent of the magnitude of the deformation. For the simulation of the circular actuators, a novel finite element

technique was developed which allows direct simulation of the actuator activation by the applied voltage. An analytical model was derived for circular actuators. An equation was obtained that links the voltage, the prestrain and the active strain. The analytical model is valid for hyperelastic materials (time-dependent effects are neglected) and can be used for the design of silicone actuators, with less pronounced viscoelastic behavior. It has been demonstrated that fitting the strain energy forms of Yeoh, Ogden and Mooney-Rivlin to uniaxial data leads to different simulation results in the VHB 4910 actuator behavior. This illustrates the importance of characterizing the biaxial response of the elastomer. This step was omitted in previous work on dielectric elastomers, where material models were based only on uniaxial test data. The numerical analysis for the evaluation of the electromechanical coupling provides the charge, electric field and electrostatic force distribution for a circular actuator. It is found that the electromechanical pressure acts in thickness direction and with the same magnitude in lateral direction. By considering a superimposed hydrostatic stress state, the resulting out-of-plane pressure corresponds to the equation proposed by Pelrine et al. This analysis provides a new physical interpretation for the electromechanical coupling. Measurements of the dielectric constant demonstrated that its value decreases by increasing prestrain. The dielectric constant of VHB 4910 is about 3.2 in the relevant prestrain range and not 4.7 as was proposed by Kofod et al. (Journal of Intelligent Material Systems and Structures, 14, 2003) and used by many researchers. This result was also confirmed by spring roll experiments.

The results of the present work represent fundamental contributions to the modeling and characterization of dielectric elastomer actuators. On the basis of these findings suitable numerical models can be defined for the design and optimization of general actuator applications. The next challenge is to describe the failure behavior of these material systems. These investigations are necessary in order to achieve the commercialization of actuator applications.

Zusammenfassung

Dielektrische Elastomere gehören zur Gruppe der so genannten „elektroaktiven Polymere“ und werden in aktiven Strukturen für die Erzeugung von grossen Dehnungen verwendet. Dielektrische Elastomere verfügen über verschiedene Anwendungen als Aktuatoren. Für die Auslegung und die Optimierung solcher Aktuatoren sind Modelle und Simulationstechniken erforderlich, welche mechanische Spannungs- und Dehnungszustände in Abhängigkeit der angelegten elektrischen Spannung beschreiben. Verschiedene Aspekte sind bei der Modellierung und Simulation von Aktuatoren aus dielektrischen Elastomeren zu berücksichtigen: Das konstitutive Modell des Elastomers, die elektromechanische Kopplung, numerische Implementierung der Modelle und ihre experimentelle Verifizierung. Bis anhin existieren keine geeigneten Modelle, um das Aktuator-Verhalten über grosse Deformations- und Zeitbereiche zu beschreiben.

In der vorliegenden Arbeit wird das Material VHB 4910 von 3M untersucht, welches sehr häufig für dielektrische Elastomer-Aktuatoren verwendet wird. Das passive mechanische Verhalten des Elastomers wird vom elektromechanischen Problem getrennt betrachtet. Elektrostatische Kräfte treten nur beim Übergangsbereich zwischen Elektroden und Elastomer auf. Das Elastomer verhält sich wie eine passive Schicht und keine direkte Wechselwirkung zwischen elektrischem Feld und den mechanischen Eigenschaften treten auf, deshalb ist diese getrennte Betrachtung zulässig. Die elektromechanische Kopplung wurde mit der Gleichung von Pelrine et al. (Sensors and Actuators A, 64, 1998) berücksichtigt. Die Gültigkeit dieser Gleichung wurde hier mit analytischen und numerischen Methoden untersucht. Die dielektrische Konstante von VHB 4910 wurde mit LCR-Messungen bei unterschiedlichen Vordehnungen und mit Zylinderaktuator-Experimenten ermittelt. Das passive mechanische Verhalten des Elastomers wird mit einem konstitutiven Modell, dem ‚quasi-linearen visko-hyperelastischen Modell’, beschrieben. Dieses Modell berücksichtigt grosse Dehnungen und Viskoelastizität. Für die Simulation von Kreisaktuatoren wurde das konstitutive Modell und die elektromechanische Kopplung in ein Finite Elemente Modell implementiert. Eine systematische, experimentelle Charakterisierung von Kreisaktuatoren bei verschiedenen Vordehnungen und elektrischen Spannungen wurde durchgeführt. Über 40 Aktuatoren wurden bei 11 unterschiedlichen Vordehnungs-/Spannungsbedingungen gestestet. Einachsige Zug- und Relaxationsversuche, Aspirationsversuche und Kompressionsversuche wurden durchgeführt und mit den entsprechenden Simulationen verglichen.

Das mechanische Modell (einschliesslich den entsprechenden Parametern) ist über einen weiten Deformations- und Zeitbereich gültig. Dies wurde sowohl für Kreisaktuatoren bei unterschiedlichen Vordehnungen und elektrischen Spannungen als auch für einachsige Versuche, Aspirationsversuche und Kompressionsversuche gezeigt. Das Konzept der quasilinearen Viskoelastizität wurde mit einachsigen Relaxationsversuchen verifiziert, in denen gezeigt wurde, dass die mechanische, relative Spannungsrelaxationsfunktion unabhängig vom Ausmass der Deformation ist. Für die Simulation der Kreisaktuatoren wurde eine neuartige Finite Elemente Technik entwickelt, welche es erlaubt, eine direkte Simulation mit der elektrischen Spannung als Input-Parameter durchzuführen.

Ein analytisches Modell wurde für Kreisaktuatoren hergeleitet, welches die elektrische Spannung, die Vordehnung und die aktivierte Dehnung verknüpft. Das analytische Modell ist für hyperelastische Materialien gültig (zeitabhängige Effekte wurden vernachlässigt) und könnte sehr nützlich für das Design von Silikon-Aktuatoren sein, welche kein ausgeprägtes viskoelastisches Verhalten aufweisen. Es wurde gezeigt, dass die Kalibrierung des Modells anhand von einachsigen Daten für die Dehnungsenergiepotentiale von Yeoh, Ogden und Mooney-Rivlin zu unterschiedlichen Resultaten im Aktuatorverhalten führt. Dieses Ergebnis betont die Wichtigkeit, das biaxiale Verhalten des Elastomers zu charakterisieren. Dies wurde in vorhergehenden Arbeiten über dielektrische Elastomere vernachlässigt. Die numerische Analyse des elektromechanischen Verhaltens liefert die Ladungs-, elektrische Feld- und elektrostatische Kräfteverteilung für den Kreisaktuator. Es wurde gezeigt, dass der elektromechanische Druck in Dickenrichtung mit demselben Ausmass auch in seitlicher Richtung wirkt. Bei der Betrachtung eines überlagerten hydrostatischen Spannungszustandes entspricht der resultierende Druck in Dickenrichtung der Gleichung von Pelrine et al. Diese Analyse liefert eine neue physikalische Interpretation der elektromechanischen Kopplung. Kapazitätsmessungen zeigten eine Abnahme der dielektrischen Konstante bei zunehmender Vordehnung. Die dielektrische Konstante von VHB 4910 hat einen Wert von ungefähr 3.2 im relevanten Vordehnungsbereich und nicht 4.7 (wie von Kofod et al. publiziert (Journal of Intelligent Material Systems and Structures, 14, 2003) und von vielen Forschern verwendet). Dieses Ergebnis wurde durch Zylinderaktuator–Experimente bestätigt.

Die Resultate der vorliegenden Arbeit liefern grundlegende Beiträge betreffend Modellierung und Charakterisierung von Aktuatoren aus dielektrischen Elastomeren. Für die Auslegung und die Optimierung von Aktuator-Anwendungen können die vorliegenden Ergebnisse mittels passender numerischer Modelle verwendet werden. Die nächste Herausforderung stellt die Untersuchung von Schadensmechanismen dar, welche wichtig für die Kommerzialisierung von Aktuator-Anwendungen ist.

1 Introduction

1.1 General remarks

Electroactive polymers (EAP) are functional materials that can be used as actuators in active structures, in particular when large deformations are required. EAP actuators transform electrical energy directly into mechanical work and produce large strains, in the order of 10% to 30%.

There are two classes of so called “electroactive polymers”: electric EAPs [Kim 2000, Pelrine 1998, Pelrine 2000a, Su 1999, Zhang 1998 and Zhang 2002] and ionic EAPs [Baughman 1999, Calvert 1998, Gandhi 1995 and Shahinpoor 2001]. The mode of action of electric EAPs is based on Coulomb forces generated by electric fields. In ionic EAPs, the mobility or diffusion of ions is exploited to produce large elongations. The rapid development in EAP technology that has occurred in the last ten years is the result of collaboration between scientists from various disciplines such as mechanics, physics, materials science, chemistry and electrical engineering.

One class, the dielectric elastomers (DE), belongs to the electric EAPs and has outstanding properties. The combination of large elongation, high energy density, good efficiency and high speed of response [Bar Cohen 2001 and Pelrine 2000a] is unique to dielectric EAPs and is essential to certain applications such as mobile (micro-) robots.

Actuators made of dielectric elastomers consist basically of a capacitor with a thin passive elastomer film sandwiched between two compliant electrodes [Pelrine 1998], see Figure 1.1. According to [Pelrine 1998], the electrostatic pressure p_{el} acting on the insulating elastomer film can be calculated for a given applied voltage, U, and film thickness, d:

$$p_{el} = \varepsilon_0 \cdot \varepsilon_r \cdot \left(\frac{U}{d}\right)^2 \tag{1.1}$$

where ε_0 is the free-space permittivity ($8.85 \cdot 10^{-12}$ As/Vm) and ε_r is the relative dielectric constant of the elastomer. Due to the mechanical compression, the elastomer film contracts in the thickness direction and expands in the film's planar directions. Ideally, the electrodes have to behave as very compliant layers in order to present a minimum of resistance to the deformation. This in-plane expansion is exploited to

generate motion or forces. Dielectric elastomers are pre-stretched, typically up to five times their in-plane dimensions, in order to improve their performance.

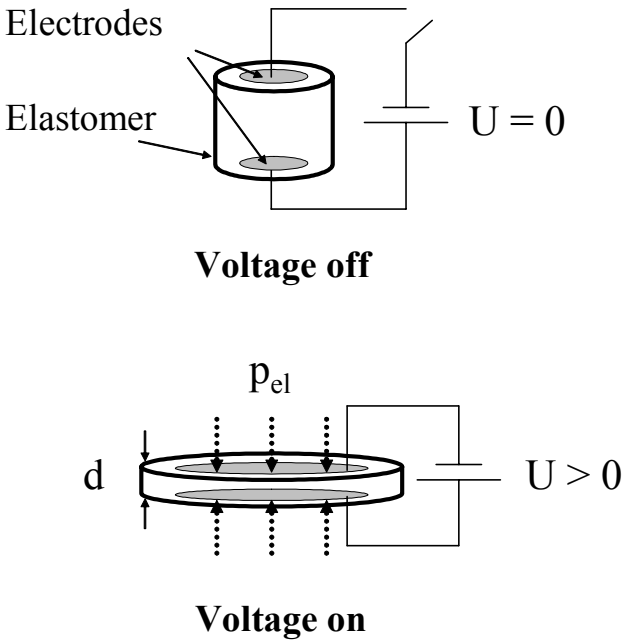

Figure 1.1. Working principle of a dielectric elastomer actuator: activation with a high voltage leads to vertical contraction and in-plane expansion

Dielectric elastomers have many potential applications as actuators. Examples of such actuators include artificial muscles [Kovacs 2006, Pei 2003 and Pelrine 2002], mini- and micro-robots [Pelrine 2001a], color displays [Aschwanden 2006], electroacoustic transducers [Heydt 1998], in aircraft [Michel 2006], diaphragm actuators for pumps [Ashley 2003 and Pelrine 2001a] and generators [Pelrine 2001b].

It has to be pointed out that the denotation “electroactive polymer” is somewhat misleading in the case of dielectric elastomers. In fact the polymer itself behaves as a passive layer. In this sense, it would be more accurate to denote a dielectric elastomer actuator as an “electroactive system”.

1.2 Design of dielectric elastomer actuators

For the design and optimization of actuator applications, models and simulation techniques are required in order to determine stress and strain states as functions of the applied voltage. There are various aspects which have to be considered in the modeling and simulation of dielectric elastomer actuators:

(i) Constitutive model of the elastomer. The constitutive model is the link between the stress and strain states of the elastomeric film. The preferred elastomer for DE actuators is VHB 4910 (3M), see section 2.3. This material undergoes large strains, shows a dissipative behavior and is incompressible [Pelrine 1998, Pelrine 2000a and Kofod 2001a]. In order to model such a material, a constitutive model is required which describes the large strains and time-dependence of the mechanical response with an appropriate mathematical formulation, as well as the corresponding material parameters. More information about the constitutive model is given in section 1.3.

(ii) Electromechanical coupling. The relationship between the applied voltage and the stress and strain states in the actuator has to be described with suitable equations.

(iii) Numerical models. Numerical models are required for the design and optimization of 'real' actuators. The constitutive model of the elastomer and the electromechanical coupling equations have to be implemented into a numerical model for simulation of the actuator behavior.

(iv) Experimental validation. The formulation and the verification of the constitutive model, the electromechanical coupling and the numerical model require experimental data. Experiments have to be representative of relevant actuator configurations.

A general simplification for modeling dielectric elastomers proposed by Bhattacharya in [Bar-Cohen 2001] is that the passive mechanical response of the elastomer can be decoupled from the electromechanical problem. Electrostatic forces arise only at the interface between the electrodes and the elastomer. The elastomer behaves as a passive layer and no direct interaction occur between electrical field and its mechanical properties. This fact was confirmed experimentally by [Kofod 2003], who demonstrated that electrostrictive effects are negligibly small for VHB 4910. Thus, the constitutive model of the elastomer includes only purely mechanical equations while the electromechanical coupling is considered through kinetic boundary conditions representing the electrostatic forces.

The generally accepted approach to electromechanical coupling in dielectric elastomer actuators is described by eq. (1.1). This equation was proposed by [Pelrine 1998] and verified experimentally for silicone actuators by [Kofod 2005]. No comprehensive analysis of this expression has been carried out so far.

The determination of suitable constitutive equations capable of describing the large strain response (with prestrain) and time-dependence over a large deformation range

represents the main challenge in modeling dielectric elastomer actuators, as described in the next section.

1.3 Constitutive equations

Equations that specify the stress components of the elastomer in terms of strain components [Holzapfel 2000] are necessary for the constitutive model. The framework of nonlinear continuum mechanics is used for this purpose. A few comments on constitutive equations in nonlinear continuum mechanics are given here.

For the description of materials which undergo large strains, the theory of hyperelasticity is used [Holzapfel 2000] to describe the non-dissipative mechanical response. The existence of a Helmholtz free-energy function is postulated for so-called hyperelastic material. When this function is solely dependent on the deformation gradient, the Helmholtz free-energy function is referred to as a strain energy potential, see section 2.1.

A large number of constitutive equations have been proposed for hyperelastic materials, e.g. see [Holzapfel 2000 and Truesdell 1992]. Most of the equations follow the so-called phenomenological approach, describing the macroscopic nature of the observed mechanical behaviour of materials. By contrast, the statistical approach (see for example [Boyce 2000] for a review) represents an attempt to take the microstructure of the materials into consideration.

Generally the phenomenological approach, but inevitably also the statistical approach, is concerned with fitting mathematical equations to experimental data. The fitting parameters correspond to the parameters of the strain energy potential. The constitutive model must be able to describe the three-dimensional stress / strain behavior. This means that the model has to correctly predict the material response for various types of experimental configurations. Thus, different types of experimental data are required for the formulation and verification of the constitutive model.

In addition to the large strain elastic response, time effects have to be included in the model formulation. This is relevant especially for materials with a pronounced dissipative behavior such as VHB 4910.

Time-dependent response can be described within the framework of the theory of large deformations by so called quasilinear viscoelastic models [Fung 1993]. These models describe the time dependence through hereditary integrals and therefore imply that no microstructural changes occur in the material due to the strain history.

In order to describe microstructural changes, nonlinear viscoelastic or viscoplastic models can be used. For example, Rubin [Rubin 2002] proposed a model with internal variables that allow for the description of history-dependence for large deformations in materials with dissipative behavior.

1.4 Literature review on modeling of DE-actuators

In the present section, a review is provided on previous work dealing with modeling and simulation of dielectric elastomer actuators. The purely hyperelastic models without viscoelastic effects were considered with the following works:

Kofod [Kofod 2001a] performed uniaxial tensile tests and verified the range of validity of various hyperelastic material models for the one-dimensional stress state for the elastomer VHB 4910. The best results were obtained with a four-parameter Ogden [Ogden 1972] model, which allows the fitting of the stress-strain curves for elongations up to four times the initial length.

An analytical model for cylindrical silicone actuators was derived by [Carpi 2004] using linear elastic theories. The Young's modulus was obtained by fitting a uniaxial tensile test. The comparison between experiments and modeling of one single actuator showed good agreement.

Kofod [Kofod 2005] proposed an analytical model for a stripe actuator made on a laminate of two silicone films. The Ogden strain energy function was used for the constitutive model of the elastomer. The material parameters were obtained by fitting uniaxial data. Two different kinds of experiments were performed: (i) constant strain experiments where the force was measured and (ii) constant load experiments where the strain was measured. A comparison of experimental data and modeling resulted in an experimental verification of eq. (1.1) for silicone for the constant strain experiment. The discrepancy between the model and experimental data varied between 15 and 37% for the strain values for the constant load experiments.

In [Goulbourne 2005], an analytical model is derived for the investigation of the behavior of an inflatable dielectric elastomer membrane which has a potential application as a cardiac pump. The material parameters of the mechanical model (an Ogden strain energy form is used here) are obtained by fitting a uniaxial tensile test. The model is used to study the behavior of the inflatable membrane by changing a number of design variables. A comparison between the model and experimental data of the elastomer membrane is missing.

Lochmatter [Lochmatter 2006a] investigated the performance of a planar DE actuator with a hyperelastic film model. The material parameters were obtained by fitting uniaxial tensile test data. A quasi-static activation cycle of the planar actuator was simulated. The theoretical efficiency (10%) of the planar actuator was calculated.

Models that also take into account the time-dependence have been presented, as summarized below:

The dynamic behavior of a VHB 4910 stripe actuator loaded with a constant weight was investigated by [Sommer-Larsen 2002]. The mechanical model considered viscoelasticity and large deformations by using the Rivlin-Sawyer equation [Rivlin 1971]. The model parameters were fitted to a uniaxial tensile and a uniaxial relaxation test. The dynamic strain response of the stripe actuator was calculated, but not verified experimentally.

In [Mockensturm 2006], an analytical model is derived for the dynamic behavior of a spherical inflatable membrane fabricated from VHB 4910. A Mooney-Rivlin [Mooney 1940] strain energy form was used for the constitutive model. Time effects are included. The model is used for the design of pumps. There is no comparison between the model and experimental data.

Yang [Yang 2005] proposed an analytical model to model an annular membrane made of dielectric elastomers. Finite strains (Mooney-Rivlin strain energy form) and viscoelasticity [Christensen 1981] were applied for the mechanical model. The material parameters were fitted to uniaxial creep tests and the strain behavior of the annular membrane was predicted for a stretch ratio up to three.

In [Plante 2006a and Plante 2006b] a detailed study on modeling was carried out by considering so-called circular actuators and diamond actuators. A modified Bergström-Boyce model [Bergström 1998], a constitutive model which describes viscoelasticity and large strains, was applied for the diamond actuators. The hyperelastic part of the model was adapted: The eight-chain model was replaced by an Ogden strain energy form.

An analytical model which combines the constitutive model and electromechanical coupling was proposed. The model was used to predict the work cycles of diamond actuators. Diamond actuators at a single prestrain level were created and work cycles with five different velocities were driven for experimental verification. The material parameters of the adapted Bergström-Boyce model (ten in total) were found by fitting the model to experimental data for a single velocity. The actuator behavior was then predicted for the other four velocities and compared to the experimental data. The agreement between the model and experiments was reasonable. By considering a

power balance, the analytical model also was used to calculate the current consumption. There are two points which restrict the model proposed by Plante:

(i) The material parameters are only fitted for a single prestrain configuration. Validity for different prestrains is not verified.

(ii) The material parameters were fitted to a diamond actuator which has a deformation state that is to a certain extent equi-biaxial. It was not evaluated whether the model with the material parameter fitted by the diamond actuator is able to describe different deformation states, e.g. the uniaxial behavior. Uniaxial tests were carried out experimentally but not used for model verification.

Failure criteria and an analytical model were used to investigate failure mechanism for the circular actuators. The constitutive behavior of the analytical model was given by the Ogden strain energy form. Viscoelasticity was not considered in the constitutive equations but indirectly, by fitting tensile tests with the Ogden strain energy form at 'low' and 'high' stretch rates of the tensile test. The two sets of material parameters (at low and high stretch rates) were used to predict the failure of circular actuators which were activated slowly and rapidly. For rapidly activated actuators, the model overestimated the experimental critical strain up to 57%. For slowly activated actuators, the prediction of the model was reasonable, but only experimental data for three different prestrains were used for verification. In order to draw serious conclusions about the failure mechanism, more detailed information is required. A quantitative relationship between the circular actuator and the diamond actuator is missing.

In all cases the electromechanical coupling was considered either with the full electrostatic pressure as proposed by Pelrine (eq. (1.1)) or else by half of it [Goulbourne 2005, Mockensturm 2006 and Yang 2005]. Even though Pelrine's equation is generally established for the mechanical coupling, some researchers [Goulbourne 2005, Mockensturm 2006 and Yang 2005] use half of the electrostatic pressure proposed by Pelrine, corresponding to the behavior of a plate capacitor. A detailed theoretical and experimental investigation of the electromechanical coupling is thus required.

The majority of the models in literature describes large strains and neglects viscoelasticity. The material parameters of all cited references except [Plante 2006a] are evaluated by means of uniaxial tensile tests. This is not sufficient for the characterization of the three-dimensional material behavior [Boyce 2000]. Therefore, most of the models are successful in describing the uniaxial behavior but are either restricted to one activation configuration or fail to make reasonable predictions for the

actuator behavior. This is due to the missing characterization of the multiaxial behavior for material parameter evaluation.

Plante's model [Plante 2006a] is calibrated for a biaxial state and is able to predict actuation cycles at different velocities for diamond actuators. The model is, however, restricted to one single prestrain (5x2.2) and is not verified for different deformation states.

From a scientific point of view, the 'three-dimensionality' of a model in continuum mechanics is important. Otherwise the model is reduced to a sterile curve fitting exercise. A phenomenological approach in continuum mechanics is always restricted to specific deformation and time ranges, and material parameters are determined by fitting experimental data. Therefore, an essential step consists in the verification whether the model and experimental data agree for all relevant deformation states.

The application of all cited models is in practice of limited usefulness; most models do not describe the actuator behavior reasonably or have not been verified experimentally. All models are restricted to a small deformation range in their predictive capabilities. For general actuator design and optimization, a 'global' constitutive model is required which is able to describe (i) the actuator behavior over a large strain and time range, and (ii) various deformation configurations (uniaxial as well as multiaxial).

Dielectric elastomer actuators are usually pre-stretched by a stretch ratio of between 3 and 5. Systematic investigations considering this deformation range are required, but corresponding experimental studies are absent from literature.

1.5 Objectives of the present work

The main objectives of the present thesis concern (i) constitutive model formulation, (ii) electromechanical coupling, (iii) numerical implementation of the models, (iv) experimental characterization and (v) an overall verification with different types of actuators.

(i) The first aim is to define **a three-dimensional constitutive model** that includes large strains and viscoelasticity and which is able to predict the states of stress and strain of arbitrary actuator configurations as a function of the applied voltage, over a large deformation and time range. The material parameters of the model have to be determined by optimization techniques. The model should be able to rationalize the observations from different experiments: actuator tests, uniaxial tensile and relaxation tests, aspiration tests [Nava 2007] and compression tests. Circular actuators are considered as a basic model system. Different strain energy

potential formulations have to be investigated for large-strain elasticity. In literature, the Mooney-Rivlin or the Ogden form (see section 1.4) are used for modeling dielectric elastomer actuators. Both strain energy forms are able to well describe the uniaxial response. Along with the Ogden and the Mooney-Rivlin form, the Yeoh [Yeoh 1990] and the Arruda-Boyce [Arruda 1993] form are also evaluated here. The Yeoh form is a third degree polynomial of the first invariant of the right Green deformation tensor (see section 2.1). The Arruda-Boyce strain energy form has two material parameters which can be related to physical properties of the elastomer.

(ii) A **fundamental investigation of the electromechanical coupling** has to be carried out. The aim is to verify Pelrine's equation theoretically as well as experimentally. The difference in electrostatic force distributions in a dielectric elastomer and a plate capacitor is investigated. For the theoretical understanding of electromechanical coupling, numerical analysis is performed to determine the charges and electrostatic forces. The experimental verification of the electromechanical coupling considers measurement of the dielectric constant for different pre-stretches as well as experiments with spring rolls.

(iii) **Numerical models** must include the implementation of both the constitutive model and the electromechanical coupling. Commercial finite element programs are used for the numerical calculations. Various constitutive models are implemented. The challenge lies in the algorithm development for electromechanical coupling. Various methods have been investigated. In one approach, the measured displacement of the active zone is imposed as kinetic boundary condition (by prescribing the membrane thickness variation) and the 'required' activation voltage represents the result of the calculation. In a second approach, the activation voltage is the input while the time history of the radial strain is the output of the calculation. This is achieved by an iterative algorithm included into a user program. The advantage of this direct approach is that the voltage is a direct input parameter. The disadvantage is that it is time-consuming and might present convergence problems (especially when large strains occur).

(iv) A **systematic experimental characterization** of the material VHB 4910 has to be performed. Experiments under different prestrain and voltage conditions are carried out for the circular actuators. Thus a large deformation range is included. Several experiments are carried out for each condition. This is important since statistical aspects have to be considered (the electrode is applied by hand). Uniaxial tensile and relaxation tests, aspiration tests and compression tests are performed to describe the passive mechanical behavior in different deformation

states. The experiments serve for the formulation and verification of the constitutive model.

(v) **Spring rolls** are used for **a further verification** of the whole model system. By blocking the strain of a spring roll in an experiment, the electromechanical coupling is studied by measuring the force. This leads to an evaluation of both the mathematical form of eq. (1.1) and the dielectric constant of the elastomer.

2 Theoretical Background and Material Details

This chapter provides an introduction to the theoretical framework of nonlinear continuum mechanics, to the optimization methods applied in this work and to the utilized materials.

2.1 Nonlinear continuum mechanics

2.1.1 Finite strains

The following part is adapted from [Holzapfel 2000]. In continuum mechanics, two different configurations are considered for the description of the deformation of a body B, viz. the reference and the current configuration. The position of a particle, Y, in the body, B, is given by the position vector, $\underline{x}$, in the current configuration and by the position vector, $\underline{X}$, in the reference configuration. In this section, vectors are singly underlined and tensors doubly underlined.

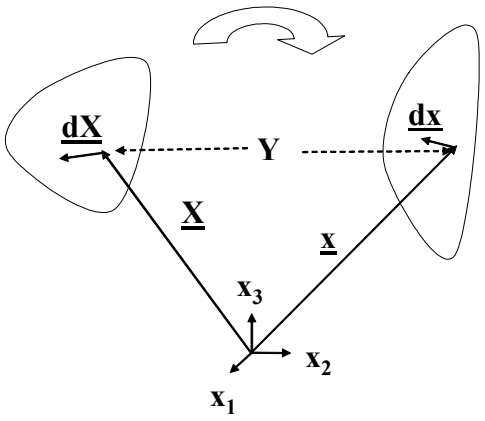

Figure 2.1. Deformation of a solid body

The reference configuration is a single-constant configuration and is independent of time. The current configuration describes the position of each particle Y at time t. The mapping relation between the current and the reference configuration is given by a function, f, which specifies how the particle Y moves through space as time progresses.

$$\underline{x} = f(\underline{X}, t) \tag{2.1}$$

The deformation of the body is described by the deformation gradient, $\underline{F}$, which gives the incremental deformation of a material line element, $d\underline{X}$ (in the reference configuration), to the material line element $d\underline{x}$ (in the current configuration).

$$\underline{\underline{F}} = \frac{\partial \underline{x}}{\partial \underline{X}} \tag{2.2}$$

The relationship between a material line element, $d\underline{X}$, of the reference configuration and the line element, $d\underline{x}$, of the current configuration is given by

$$d\underline{x} = \underline{\underline{F}} d\underline{X} \tag{2.3}$$

The magnitude, $|d\underline{s}|$, of the material line element, $d\underline{x}$, in the current configuration may be calculated using eq. (2.3) such that

$$(|d\underline{s}|)^2 = d\underline{x} \cdot d\underline{x} = d\underline{X} \cdot \underline{\underline{F}}^T \underline{\underline{F}} d\underline{X} = d\underline{X} \cdot \underline{\underline{C}} d\underline{X} \tag{2.4}$$

where $\underline{\underline{C}}=\underline{\underline{F}}^T\underline{\underline{F}}$ is called the right Green deformation tensor. It is also convenient to define the left Green deformation tensor, $\underline{\underline{B}}=\underline{\underline{F}}\underline{\underline{F}}^T$. With the help of this tensor, the magnitude, $|d\underline{S}|$, of the material line element, $d\underline{X}$, in the reference configuration is given:

$$(|d\underline{S}|)^2 = d\underline{X} \cdot d\underline{X} = d\underline{x} \cdot \underline{\underline{B}}^{-1} d\underline{x} \tag{2.5}$$

The stretch ratio, λ, of a material line element is defined in terms of the ratio of the lengths $|d\underline{s}|$ and $|d\underline{S}|$,

$$\lambda = \frac{|d\underline{s}|}{|d\underline{S}|} \tag{2.6}$$

There are various tensors which define the strain state. One of them is the Lagrangian strain tensor $\underline{\underline{E}}$.

$$\underline{\underline{E}} = \frac{1}{2}(\underline{\underline{C}} - \underline{\underline{I}}) \tag{2.7}$$

where $\underline{\underline{I}}$ is the unit tensor. Strain states can also be characterized by scalar terms, the so-called invariants. There are three invariants for the right Green deformation tensor and the left Green deformation tensor:

$$I_1 = \underline{\underline{C}} \cdot \underline{\underline{I}} = \underline{\underline{B}} \cdot \underline{\underline{I}} \tag{2.8}$$

$$I_2 = \frac{1}{2}\left[(\underline{\underline{C}} \cdot \underline{\underline{I}})^2 - \underline{\underline{C}} \cdot \underline{\underline{I}}\right] = \frac{1}{2}\left[(\underline{\underline{B}} \cdot \underline{\underline{I}})^2 - \underline{\underline{B}} \cdot \underline{\underline{I}}\right] \tag{2.9}$$

$$I_3 = \det(\underline{\underline{C}}) = \det(\underline{\underline{B}}) = J^2 \tag{2.10}$$

where J corresponds to the ratio between a volume element in the current configuration, dv, and the same in the reference configuration, dV:

$$J = \det(\underline{\underline{F}}) = \frac{dv}{dV} \tag{2.11}$$

The determinant of $\underline{\underline{F}}$ is a pure measure of dilatation. For an incompressible material, J is equal to 1.

A further strain measure which is used later is the rate of deformation tensor, $\underline{\underline{D}}$. It is related to the velocity gradient, $\underline{\underline{L}}$, the derivative of the velocity field, $\underline{v}(\underline{x},t)$, in the current configuration:

$$\underline{\underline{L}} = \frac{\partial \underline{v}}{\partial \underline{x}} = \underline{\underline{D}} + \underline{\underline{W}} \tag{2.12}$$

where $\underline{\underline{D}}$ is the symmetrical part of the velocity gradient, $\underline{\underline{L}}$:

$$\underline{\underline{D}} = sym(\underline{\underline{L}}) = \frac{1}{2}(\underline{\underline{L}} + \underline{\underline{L}}^T) = \underline{\underline{D}}^T \tag{2.13}$$

$\underline{\underline{W}}$ is the spin tensor, the skew symmetric part of $\underline{\underline{L}}$:

$$\underline{\underline{W}} = \frac{1}{2}(\underline{\underline{L}} - \underline{\underline{L}}^T) = -\underline{\underline{W}}^T \tag{2.14}$$

2.1.2 Stresses

An elastic material for which a strain energy function exists is called a Green elastic or hyperelastic material. The strain energy function, W, represents the elastic energy stored in the material. The stress state depends only on the deformation state of the material itself (no time-dependent effects occur) and is given by

$$\underline{\underline{P}} = \underline{\underline{F}} \frac{\partial W}{\partial \underline{\underline{E}}} = 2\underline{\underline{F}} \frac{\partial W}{\partial \underline{\underline{C}}} \tag{2.15}$$

where $\underline{\underline{P}}$ is the first Piola-Kirchhoff (or nominal) stress tensor. The first Piola-Kirchhoff stress tensor characterizes the stress state in the reference configuration. By multiplying the first Piola-Kirchhoff stress tensor by a unit vector, $\underline{N}$, in the reference configuration, the first Piola-Kirchhoff (or nominal) traction vector, $\underline{p}$, in the reference configuration is obtained. For the stress states in the present configuration, the Cauchy stress tensor, $\underline{\underline{T}}$, is used:

$$\underline{\underline{T}} = 2\underline{\underline{F}}\frac{\partial W}{\partial \underline{\underline{C}}}\underline{\underline{F}}^T \tag{2.16}$$

Multiplying the Cauchy stress tensor with a unit vector, $\underline{n}$, in the current configuration gives the Cauchy (or true) traction vector, $\underline{t}$, in the current configuration. Numerous definitions exist for stress tensors. The Kirchhoff stress tensor, $\underline{\underline{\tau}}$, is introduced for later reference:

$$\underline{\underline{\tau}} = J\underline{\underline{T}} \tag{2.17}$$

where J is the volume ratio. The Kirchhoff stress tensor is work conjugate [Holzapfel 2000] to the rate of deformation tensor, $\underline{\underline{D}}$. Work conjugate means that the double contraction of a stress tensor and the associated rate of deformation tensor describes the real physical power during a dynamic process [Holzapfel 2000], i.e. the rate of internal mechanical work per unit reference volume, denoted by w_{int}

$$w_{\text{int}} = \underline{\underline{\tau}} \cdot \underline{\underline{D}} \tag{2.18}$$

2.1.3 Strain energy functions and nearly incompressible materials

As mentioned previously, the stress tensor in hyperelastic materials is described using a strain energy function. Strain energy potentials are given either as a function of the invariants or of stretch ratios. An example is the so-called Yeoh form [Yeoh 1990]:

$$W = \sum_{i=1}^{3} C_{i0}(I_1 - 3)^i \tag{2.19}$$

For finite element simulations, mixed formulations which use both displacement and pressure degrees of freedom have been shown to be very efficient and accurate in the solution of problems for nearly or totally incompressible materials. The material laws have to be modified in order to treat the pressure as a separate variable. To separate the hydrostatic pressure from the stress tensor, the following strain energy function is used [Sussmann 1987]:

$$\overline{W} = W(I_{r1}, I_{r2}) + W_h(I_{r3}) \tag{2.20}$$

where I_{r1}, I_{r2} and I_{r3} are the reduced invariants and W_h represents a hydrostatic work term. For the Yeoh form (eq. 2.19), the strain energy is adapted as follows:

$$\overline{W} = \sum_{i=1}^{3} C_{i0}(I_{r1} - 3)^i + \frac{K_0}{2}(J-1)^2 \tag{2.21}$$

where C_{i0} and K_0 (bulk modulus) are material parameters. The reduced invariants are [e.g. Sussmann 1987]:

$$I_{r1} = I_3^{-1/3} I_1 \tag{2.22}$$

$$I_{r2} = I_3^{-2/3} I_2 \tag{2.23}$$

$$I_{r3} = \sqrt{I_3} \tag{2.24}$$

2.1.4 Quasilinear viscoelasticity

In order to introduce time-dependent effects, the concept of quasilinear viscoelasticity [Fung 1993] is used. For infinitesimal strains, linear viscoelasticity is given by the basic hereditary formulation:

$$\underline{\underline{P}}(t) = \int_0^t 2G(t-t')\dot{\underline{\underline{e}}}dt' + \underline{\underline{I}}\int_0^t K(t-t')\dot{\varphi}dt' \tag{2.25}$$

where $\underline{\underline{e}}$ is the mechanical deviatoric strain tensor, φ is the mechanical volumetric strain and $\underline{\underline{P}}$ is the nominal stress tensor. The time-dependent functions, G(t) and K(t), are the shear and bulk relaxation moduli. In the present work the time dependence of the volumetric behavior is neglected, i.e. $K(t)=K_0$, while G(t) is expressed in terms of an exponential series known as the Prony series:

$$G(t) = G_0\left(1 - \sum_{i=1}^{M} g_i e^{-t/\tau_i}\right) \tag{2.26}$$

where G_0 is the instantaneous shear modulus, τ_i are the relaxation times that characterize the decay time and g_i are the corresponding weighting factors that define the amount of decay of the stress response. Using integration by parts, eq. (2.25) can be rewritten as

$$\underline{\underline{P}}(t) = 2G_0\underline{\underline{e}}(t) + \int_0^t 2\dot{G}\underline{\underline{e}}(t-t')dt' + K_0\varphi(t)\underline{\underline{I}} \tag{2.27}$$

A suitable generalization for the finite strains of the hereditary integral formulation is obtained as follows [ABAQUS 2004]:

$$\underline{\underline{\tau}}(t) = \underline{\underline{\tau}}_0(t) + sym\left[\int_0^t \underline{\underline{F_t}}^{-1}(t-t')\left(\frac{\dot{G}(t')}{G_0}\underline{\underline{\tau}}_0^{\,D}(t-t')\right)\underline{\underline{F_t}}\,(t-t')dt'\right] \tag{2.28}$$

where $\underline{\underline{\tau}}_0^D$ is the deviatoric part of the instantaneous Kirchhoff stress, $\underline{\underline{\tau}}_0$, and $\underline{\underline{F}}_t(t\text{-}t')$ is the deformation gradient of the state t-t' relative to the state at time t. A transformation is performed on the stress relating the state at time t-t' to the state at time t.

2.2 Optimization procedure

To determine the material parameters of the constitutive model, the 'inverse problem' has to be solved. In other words the material parameters are adapted iteratively by an optimization procedure until experimental data and the corresponding finite element calculations agree to a specified extent.

For example, for a circular strain test, the material parameters (x_1, x_2, …, x_n) have to be chosen in such a way that the experimental and calculated nominal radial strain history (the finite element output) agree. The calculated strain history, $s_c(t)$, is given by discrete strain values, $s_{c,k}$ (k=1..n), at corresponding time values, t_k. In order to obtain the n material parameters (x_1, x_2, …, x_n), a minimum has to be found for the error function, f_e. The function f_e is the sum of the squares of the differences between the calculated strains, $s_{c,k}$, and the experimental strains, $s_{e,k}$:

$$f_e(x_1, x_2, ..., x_n) = \sum_k (s_{c,k}(x_1, x_2, ..., x_n) - s_{e,k})^2 \tag{2.29}$$

where $s_{e,k}$ are discrete points of the experimental strain history, $s_e(t)$. The minimum of a function with n independent variables is searched for in a mathematical way. An iterative solution technique is used to find the minimum of the function, f_e.

There are two classes of optimization algorithms, viz. direct and indirect methods. The direct methods require only the function values. The indirect methods also require derivatives of the error function. In the present work, the function f_e is evaluated with the output of the finite element simulation and hence only the function value is known and not its derivatives. Therefore, a direct method is required. A review of direct methods is given by [Lewis 2000]. An effective and computationally compact direct method [Lewis 2000] is the simplex algorithm of Nelder and Mead [Nelder 1965] which is used in the present work. A simplex is a polytope of N+1 vertices in N dimensions, e.g. for N=2 the simplex is a triangle, for N=3 the simplex is a tetrahedron.

The Nelder-Mead method can be understood in principle for the simple example of two material parameters, x_1 and x_2, with N=2. The method is a pattern search that compares function values at the three vertices of the triangle. The diameter of the simplex is calculated after each step. The aim of the algorithm is to minimize the

diameter of the simplex. The so-called 'worst' vertex which 'causes a large diameter' is rejected and replaced with a new vertex. A new triangle is formed and the search is continued. The process generates a sequence of triangles for which the function values at the vertices get smaller and smaller. The size of the triangles is reduced until the diameter of the simplex is less than the specified tolerance. Further details on the Nelder-Mead method are given in [Lagarias 1998 and Nelder 1965].

Like all general purpose multidimensional optimization algorithms, Nelder-Mead occasionally gets stuck in a rut. The standard approach to handle this is to restart the algorithm with a new simplex starting at the current best value.

2.3 Material details

2.3.1 Elastomers

Actuator technologies are often compared by different actuator output parameters [Bar-Cohen 2001]: maximum strain, maximum pressure, efficiency and speed of response.

For dielectric elastomer actuators, SRI International [Kornbluh 1999, Kornbluh 2000 and Pelrine 2000a] evaluated different elastomers by circular strain tests and theoretical considerations regarding the actuator parameters. The conclusion [Pelrine 2000a] was that acrylic and silicone actuators are the most promising materials for the dielectric elastomer technology.

In particular, the acrylic elastomer VHB 4910, commercially available from the company 3M (in the form of a membrane with 1 mm thickness, 23 mm width and user-defined length), has shown the largest activation strain (over 200%) [Kornbluh 2000 and Pelrine 2000a], a high elastic energy density (3.4 J/cm^3) [Kornbluh 2000] and a high electrical breakdown strength (218 MV/m) [Kofod 2003]. The material is widely used in the research community and has also been used in the present work. The chemical composition is not declared by the manufacturer.

VHB 4910 is usually prestrained in two directions, see Figure 2.2. The pre-stretch ratio (or prestrain) in the x-direction is defined as $\lambda_x = x_1/X$ and the pre-stretch ratio (or prestrain) in the y-direction is defined as $\lambda_y = y_1/Y$. For an equi-biaxial deformation state, $\lambda_x = \lambda_y$, the pre-stretch ratio is described by λ_p with $\lambda_p = \lambda_x = \lambda_y$.

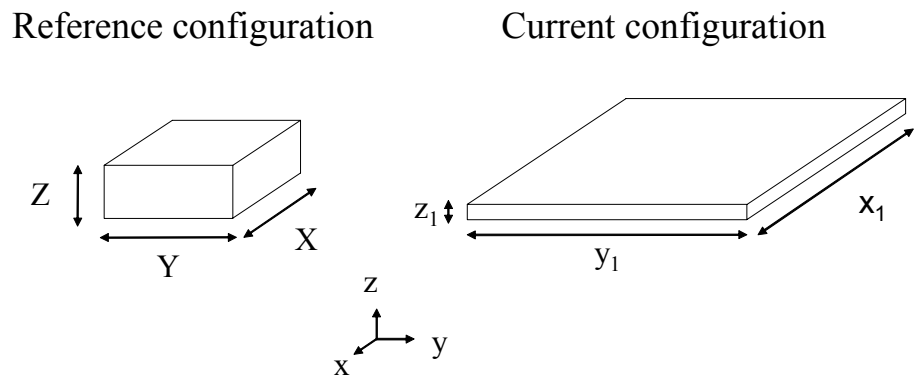

Figure 2.2. Illustration of the prestrain

The reasons for pre-stretching the elastomeric film are:

(i) The electrical breakdown strength increases from 18 to 218 MV/m by equi-biaxially pre-stretching the film from no prestrain to λ_p=6 [Kofod 2003]

(ii) The thickness of the film decreases. A lower voltage has to be applied to obtain the same electrostatic pressure (see eq. (1.1))

(iii) The prestrain avoids so-called pull-in failures [Plante 2006a]

2.3.2 Electrodes

Various electrode materials have been investigated in [Carpi 2003 and Kofod 2001a]. So far, several different types of electrodes are being used in the research community. No theoretical study has been performed, nor has one electrode material shown any major advantages. In general, the electrode should be conductive and compliant.

Gold electrodes [Zhang 2004] were used in the first part of the present work. Thin layers (thickness: 250 nm) of beaten gold (from Brandenberger AG, Thalwil, Switzerland) were applied (article 1). Beaten gold has the advantage that so-called 'self healing' effects occur. At the position of the electrode where an electrical breakdown occurs, the thin gold layer evaporates and the actuator does not fail.

In the second part of this work (article 3), the gold electrodes were replaced with silicone/graphite electrodes. The reason for this was that gold electrodes constrain the elongation of the actuator mechanically, in contrast to the silicone/graphite electrodes, see section 4.2. The silicone/graphite electrode is a mixture of 11 g graphite powder (TIMREX SP30) and 10 ml silicone oil (DC 200/100 cs).

3 Modeling Dielectric Elastomer Actuators

3.1 Article 1

This section contains a reprint of the article:

M. Wissler and E. Mazza, Modeling and simulation of dielectric elastomer actuators, Smart Materials and Structures, 2005, vol. 14, pp. 1396-1402

Background motivation: The motivation for this article was to create a model for the simulation of a circular actuator including large strains and viscoelasticity. The model was compared to experimental data.

Summary of methods: Uniaxial tensile and relaxation tests were carried out. A finite element model for a uniaxial tensile test was created and the material parameters were extracted by an optimization procedure which led to a good agreement between experimental data and simulation. The 'quasilinear visco-hyperelastic model' was used as a constitutive model for the elastomer as a general model formulation. For the hyperelastic part, the strain energy form of Yeoh and for the viscoelastic part the Prony series were applied. The concept of 'quasilinear viscoelasticity' was evaluated by uniaxial relaxation tests.

A circular actuator with prestrain 4 was created and experimentally activated by a constant voltage (3.5 kV). A corresponding finite element model was created. For the simulation of the activation, the inverse problem was solved. The thickness of the actuator was prescribed corresponding to the experimental strain history. The output of the simulation was the out-of-plane stress which corresponded to the electrostatic pressure in eq. (1.1). With this equation, the voltage history was calculated and compared to the experimental voltage history.

Summary of results: The uniaxial relaxation tests show that the concept of 'quasilinear viscoelasticity' is able to describe the mechanical response of the material VHB 4910. A set of parameters was determined by fitting uniaxial tensile test data. Experimental results from the circular actuator test agree to a great extent with the corresponding simulations.

Main conclusions, link to the next article: The ‘three-dimensionality’ of the model is warranted for both the uniaxial and the multi-axial (actuator) behavior. Experimental data and simulations agree to a great extent. Different strain energy forms will be investigated in article 2 in order to evaluate their predictive capabilities for the same data sets. Further analytical models are required for the optimization of the actuators, due also to the duration of the numerical calculations, see article 2.

Modeling and simulation of dielectric elastomer actuators

Michael Wissler[1] and Edoardo Mazza[2]

[1] Swiss Federal Laboratories for Materials Testing and Research (EMPA), 8600 Dübendorf, Switzerland
[2] Swiss Federal Institute of Technology (ETH), Dept. of Mechanical Engineering, 8092 Zürich, Switzerland

Abstract

Dielectric elastomers are used as base material for so called electroactive polymer (EAP) actuators. A procedure and a specific constitutive model (for the acrylic elastomer VHB 4910) are presented in this work for finite element modeling and simulation of dielectric elastomer actuators of general shape and set-up. The Yeoh strain energy potential and the Prony series are used for describing the large strain time dependent mechanical response of the dielectric elastomer. Material parameters were determined from uniaxial experiments (relaxation tests and tensile tests). Thereby the inverse problem was solved using iterative finite element calculations. A pre-strained circular actuator was built and activated with a predefined voltage. A three dimensional finite element model of the circular actuator was created and the electromechanical activation process simulated. Simulation and actual measurements agree to a great extent, thus leading to a validation of both, the constitutive model and the actuator simulation procedure proposed in this work.

1 Introduction

Electroactive polymers (EAP) are functional materials that can be used as actuators in adaptive structures, in particular when large deformations are required. EAP transform electric energy directly into mechanical work and produce large strains, in the order of 10% to 30%. Modeling of actuators made of dielectric elastomers is investigated in this paper. Dielectric elastomer actuators are a category of EAP which were shown to provide excellent overall performance [1], combining large elongation, high energy density, good efficiency and high speed of response. Examples of applications [2, 3] of dielectric elastomers as actuators include mobile mini- and microrobots, micropumps and microvalves, micro air vehicles, disk drives, prosthetic devices and flat panel loudspeakers.

Actuators made of dielectric elastomers consist basically of a compliant capacitor, with a thin passive elastomer film sandwiched between two compliant electrodes [2, 4]. The electrostatic pressure acting on the insulating elastomer film can be calculated for a given applied voltage and film thickness [2]. Due to the mechanical compression, the elastomer film contracts in the thickness direction and expands in the film plane directions. This in-plane expansion is exploited to generate motion or forces. In order to improve their performance dielectric elastomers are pre-stretched, typically up to five times of their in-plane dimensions.

Models are required for the design and optimization of EAP actuators. So far only few works were presented in literature on modeling and simulation of dielectric elastomers [1, 5-9]. In most cases functioning of EAP actuators is predicted by using analytical expressions which directly relate voltage with displacement or force exerted. These analytical models assume a linear or non-linear elastic mechanical response of the elastomer and do neither account for its three dimensional viscoelastic behavior nor for the anisotropy induced by pre-stretching of EAP. Analytical models describe the behavior of simple actuator set-up (such as planar actuators with simple kinematic boundary conditions) and thus their application in practice for general actuator design and optimization is of limited use.

The finite element (FE) method is used here for simulating the behavior of dielectric elastomer actuators. In a FE analysis there is no limitation in actuator geometry and set-up. The main difficulties in the FE simulation of EAP actuators lay in (i) modeling the activation through an applied voltage and (ii) the definition of the elastomer constitutive model. Dielectric elastomers behave as insulating layers; do not change their shape as a consequence of the electric field but only as a consequence of the electrostatic mechanical pressure exerted by the electrodes in the thickness direction. Since the electric field between the electrodes is inversely proportional to the film thickness, the activation pressure depends on the deformation of the actuator, thus leading to electromechanical coupling.

The problem can be treated however as fully uncoupled according to the procedure applied in the present work: (i) the contraction in thickness direction and thus the current thickness is imposed as a kinematic boundary condition, (ii) the required compressive forces are calculated, (iii) from the mechanical pressure in thickness direction and the current film thickness, the corresponding voltage is determined. Motion of the actuator is considered as an input whereas the required voltage to realize it is the output of the calculation. The results of the FE calculation depend on the electrical properties and on the (passive) mechanical properties of the elastomer film.

The determination of the relative dielectric constant can be accomplished through standard methods [10]. The main challenge for the realization of a FE model of an EAP actuator consists therefore in the definition of its constitutive model. The acrylic elastomer used in the present work behaves as a nonlinear viscoelastic material.

The experiments performed for determining the constitutive equations of the elastomer are described in section 2 of this paper: these are large strain uniaxial relaxation tests, large strain uniaxial tensile tests and experiments with a biaxially pre-strained circular actuator. The nonlinear viscoelastic model used for the description of the mechanical behavior of the dielectric elastomer is presented in section 3. In section 4 the FE models for the analysis of the experiments are outlined along with the procedure for determining the material parameters from curve fitting and optimization algorithms. Section 5 presents the results of the uniaxial tests with the corresponding material model. The FE simulation of the circular actuator described in section 6 provides a validation of both, the constitutive model and the FE procedure applied for the analysis of EAP actuators.

2 Experiments

The dielectric elastomer used in the present work is the commercially available acrylic elastomer VHB 4910 (3M), which has been shown to produce large strains and high elastic energy density [11].

2.1 Relaxation tests

Uniaxial relaxation tests were performed at room temperature (23° C) by stretching the samples to a predefined elongation and measuring the force decrease over a time period of approximately 0.5 hour. For each sample the elongation was quickly (0.2-0.4 s.) applied using a hand-operated set-up. The nominal or engineering strain s_1 (the change of length divided by the original length) was defined for a gauge length corresponding to the whole length of the sample between the clamping points. Fourteen experiments have been performed: the nominal strain was 20, 50, 100, 200, 300, 400 and 500%, and two tests were carried out for each elongation. The resulting force history has been measured with a force transducer (HBM type S2) which was connected to a PC LabView system for data acquisition. The undeformed sample geometry was set to a ratio between length and width of 10:1, in order to ensure uniaxial stress conditions. The undeformed thickness of the samples was 1 mm.

2.2 Tensile tests

Uniaxial tensile tests have been performed for two samples with a Zwick (Z010) machine at room temperature (23 °C). The time history of the nominal strain (for both samples) is shown in figure 1: the sample was first loaded up to 300% nominal strain linearly over a time period of 900 s, the strain was hold fix for 900 s, and the sample was than unloaded with a negative strain rate of -0.33 %/s. The sample geometry corresponded to the one of the relaxation tests. The strain in these tests was not determined from the relative displacement of the clamping points but monitored with an elongation sensor (Zwick multisens) in the middle of the sample, over an undeformed gauge length of 50 mm.

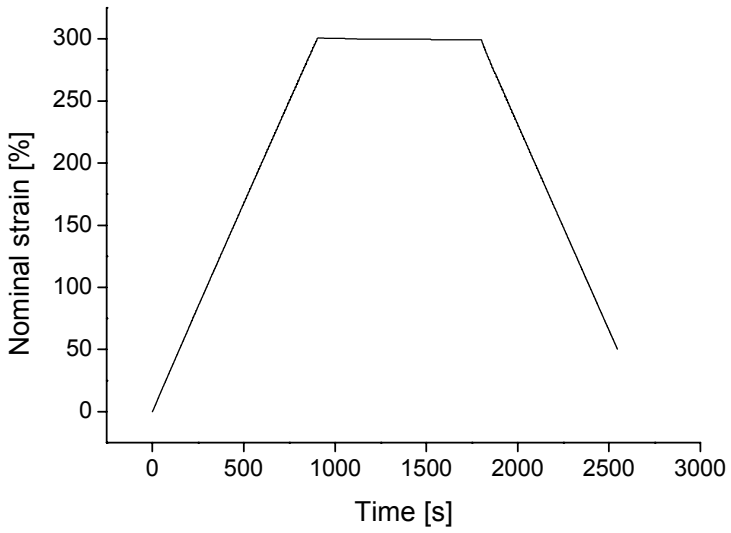

Figure 1. Control profile of the strain controlled tensile test.

2.3 Circular strain test

A multi-axial electromechanical experiment has been performed on a biaxially prestrained circular actuator (in a so called circular strain test [4, 12]) at room temperature (23° C). The elastomer film was pre-strained radially up to a nominal radial strain of 308% (according to the procedure described in [13]) and fixed on a circular frame (radius R = 75 mm), see figure 2. The thickness of the film was measured by a thickness sensor (Mitutoyo ID-F125/150) before (1 mm) and after (0.06 mm) prestraining.

After prestraining, a circular area (radius r_0 = 22 mm) at the center of the film was coated with beaten gold (Brandenberger AG, Thalwil, Switzerland) used as electrode on the upper and lower side. The electrodes were connected to a high voltage supplier

through a thin metal wire. A constant voltage of 3.5 kV was applied for 3 min. The nominal radial strain $s_r = r_1/r_0 - 1$ of the coated area was measured with a video-extensometer (Ovex ME-46) connected to a PC LabView system.

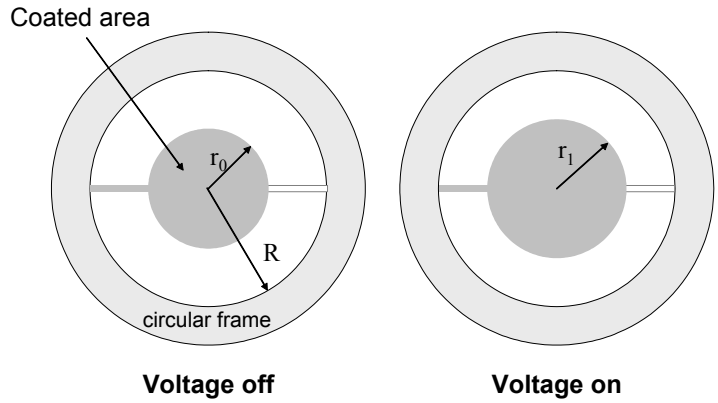

Figure 2. Arrangement of the circular actuator for electromechanical measurements (r_0 = 22 mm and R = 75 mm). The maximum nominal radial strain s_r under activation was 14%.

3 Constitutive model

In order to describe the mechanical behavior of the dielectric elastomer a three dimensional constitutive model is required and the material parameters have to be determined from the experiments. In this work large strain elastic response is modeled using the strain energy potential of Yeoh [14] and the so called Prony series are used to describe the time dependence of the mechanical response (quasi-linear viscoelasticity, [15]). The material is considered to be incompressible, an assumption justified by previous measurements in uniaxial tension in which lateral contraction was monitored.

3.1 Strain energy potential

In continuum mechanics large strain elastic (i.e. hyperelastic) materials are characterized through a strain energy potential W, which represents the strain energy of the material as a function of the deformation. The Yeoh-form [14] of the strain energy potential (a particular type of the so called reduced polynomial form) is described by three material parameters C_{10}, C_{20} and C_{30}, according to the following equation:

$$W = C_{10}(I_1 - 3) + C_{20}(I_1 - 3)^2 + C_{30}(I_1 - 3)^3 \qquad (1)$$

I_1 in eq. (1) is the first invariant of the left Cauchy-Green deformation tensor and depends on the principal stretch ratios λ_i (i = 1, 2 and 3) as

$$I_1 = \lambda_1^2 + \lambda_2^2 + \lambda_3^2 \tag{2}$$

The stretch ratio λ_i (i = 1, 2 and 3) is defined as the current length divided by the original length in the principal directions of the deformation. For a totally incompressible material, the nominal or engineering stress σ_i (the current force per unit area of the undeformed configuration) is given by the derivative of the strain energy potential with respect to the stretch ratio λ_i:

$$\sigma_i = \frac{\partial W}{\partial \lambda_i} - \frac{1}{\lambda_i} p \tag{3}$$

In eq. (3) p is the hydrostatic pressure which depends on the kinetic boundary conditions. For the uniaxial tensile test (loading in direction 1), the nominal stresses in the directions 2 and 3 are zero ($\sigma_2 = \sigma_3 = 0$). With this boundary condition, the nominal stress for the Yeoh form can be calculated as

$$\sigma_1 = 2 \cdot (\lambda_1 - \frac{1}{\lambda_1^2}) \cdot [C_{10} + 2 \cdot C_{20} \cdot (\lambda_1^2 + \frac{2}{\lambda_1} - 3) + 3 \cdot C_{30} \cdot (\lambda_1^2 + \frac{2}{\lambda_1} - 3)^2] \tag{4}$$

In the last expression, the relation

$$\lambda_2 = \lambda_3 = 1/\sqrt{\lambda_1} \tag{5}$$

has been used which corresponds to an isochoric deformation ($\lambda_1\lambda_2\lambda_3=1$). Eq. (4) is used to determine the hyperelastic material parameters C_{10}, C_{20} and C_{30} from uniaxial test data.

3.2 Viscoelasticity

Time dependence of the mechanical response in a so called quasi-linear viscoelastic model [15] is described by using time dependent coefficients in the strain energy potential. The time function for these parameters is described here with the so called Prony series [15]. The hyperelastic material parameters C_{ij}^R (in this case $C_{10} = C_{10}^R$, $C_{20} = C_{20}^R$ and $C_{30} = C_{30}^R$) are defined as

$$C_{ij}^R(t) = C_{ij}^0 \cdot [1 - \sum_{k=1}^{N} g_k \cdot (1 - \exp(-\frac{t}{t_k}))] = C_{ij}^0 \cdot f(t) \tag{6}$$

where C_{ij}^0 describe the instantaneous elastic response and g_k and t_k characterize the relaxation behavior. The relaxation function f(t) characterizes the relaxation behavior,

with f(t=0)=1. The material parameters g_k and t_k are determined from uniaxial relaxation tests. The relaxation curves for the measured nominal stress can be fitted through the parameters σ_∞, σ_i and τ_i in the following equation

$$\sigma(t) = \sigma_\infty + \sum_{i=1}^{N} \sigma_i \cdot \exp(-\frac{t}{\tau_i}) \tag{7}$$

where σ_∞ is the long term nominal stress, σ_i and τ_i are parameters which depend on the relaxation behavior. The instantaneous nominal stress σ_0 is

$$\sigma_0 = \sigma(t=0) = \sigma_\infty + \sum_{i=1}^{N} \sigma_i \tag{8}$$

The assumption of quasi-linear viscoelasticity is that the stress relaxation function is independent of the magnitude of the deformation. This can be verified experimentally through the function $s_\infty(t)$:

$$s_\infty(t) = \frac{\sigma(t)}{\sigma_\infty} = \frac{\sigma_\infty + \sum_{i=1}^{N} \sigma_i \cdot \exp(-\frac{t}{\tau_i})}{\sigma_\infty} \tag{9}$$

A material is quasi-linear viscoelastic when the function $s_\infty(t)$ is independent of the imposed elongation in the relaxation test. The parameters of the Prony series are evaluated by combining eq. (6) and eq. (9):

$$s_\infty(t) = \frac{\sigma(t)}{\sigma_\infty} = \frac{\sigma_\infty + \sum_{i=1}^{N} \sigma_i \cdot \exp(-\frac{t}{\tau_i})}{\sigma_\infty} = \frac{1 - \sum_{k=1}^{N} g_k \cdot (1 - \exp(-\frac{t}{t_k}))}{1 - \sum_{k=1}^{N} g_k} \tag{10}$$

From eq. (10) the following relation is obtained, where g_k and t_k can be obtained by coefficient comparison from the parameters σ_∞, σ_i and τ_i:

$$\sum_{i=1}^{N} \frac{\sigma_i}{\sigma_\infty} \cdot \exp(-\frac{t}{\tau_i}) = \frac{\sum_{k=1}^{N} g_k \cdot \exp(-\frac{t}{t_k})}{1 - \sum_{k=1}^{N} g_k} \tag{11}$$

The stress relaxation function is normalized here with respect to the long term stress σ_∞ (and not the instantaneous stress σ_0) due to the experimental conditions. In fact the initial strain is applied over a short ramp of variable duration so that determination of the initial stress value is uncertain. The influence of this uncertainty vanishes due to the fading memory of the material.

4 Numerical calculations

4.1 Finite Element models

The general purpose FE program ABAQUS [16] has been used for the present calculations. Two FE-models have been created. The model used for simulation of the tensile test consists of triangular plane stress elements. The 3D model for the analysis of the circular actuator experiment is shown in figure 3 and consists of 140 solid hybrid elements (8-node linear brick).

For the tensile test simulation the time history of uniaxial displacement corresponded to the elongation control profile of figure 1. True (Cauchy) and nominal stresses were determined as a function of time for each parameter set of the quasi-linear viscoelastic model and compared with the experimental results.

The circular actuator simulation included three steps: (i) prestrain in radial direction by 308%, by imposing the displacement of the nodes at the model boundary, (ii) relaxation for 1 hour, and (iii) actuation by imposing a time history of thickness variation in the activated region corresponding to the measured radial displacement from the experiments. The required voltage was determined from the calculated stresses in thickness direction in the activated region. Thereby was assumed that the compressive forces arise from the electrostatic pressure [2]. Electrostrictive effects are neglected, which is a common simplification for dielectric elastomers [10]. The electrostatic pressure p_{el} corresponds to the negative Cauchy stress t_3 in the direction of the electric field and is defined by

$$p_{el} = \varepsilon_0 \cdot \varepsilon_r \cdot \left(\frac{U}{d} \right)^2 = -t_3 \tag{12}$$

ε_0 is the free-space permittivity ($8.85 \cdot 10^{-12}$ As/Vm), ε_r is the relative dielectric constant (4.7 for VHB 4910 [10]), U is the electrical voltage applied to the electrodes and d is the thickness of the polymer film. Eq. (12) has been implemented in the ABAQUS user subroutine UVAR and used to calculate the electric voltage from the current values of film thickness and stress t_3 as a function of time.

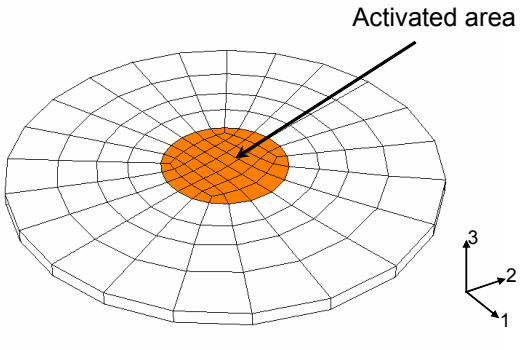

Figure 3. FE-model for the circular actuator. The activated area is indicated.

4.2 Procedure for material parameter extraction

The software Matlab with the standard tool 'cftool' has been used for determining the hyperelastic (eq. (4)) and the viscoelastic (eq. (7)) coefficients from the relaxation tests. Matlab has been used also for the optimization procedure applied for the material parameter identification in the tensile tests. The parameters were obtained as follows: (i) Matlab calls a FE tensile test simulation with a specific material parameter set; (ii) ABAQUS calculates the force versus time curve; (iii) the difference f_{error} between the time integrals of the simulated and the experimental curve is than calculated; (iv) a new material parameter set is determined by Matlab, according to a specific optimization algorithm (Nelder-Mead simplex method). The iteration has been stopped when a minimum of f_{error} had been found.

No material parameter optimization has been performed for the circular actuator simulation, which has been used as a validation of the present modeling approach.

5 Uniaxial test results

5.1 Relaxation tests

The experimental results of the relaxation tests for nominal strains of 50, 200 and 500 % are shown in figure 4. A simple curve fitting procedure has been used for determining the parameters σ_∞, σ_i and τ_i, eq. (7), from the experimental data. Good results were obtained with N=4 in eqs. (6) – (11) (four terms in the Prony series).

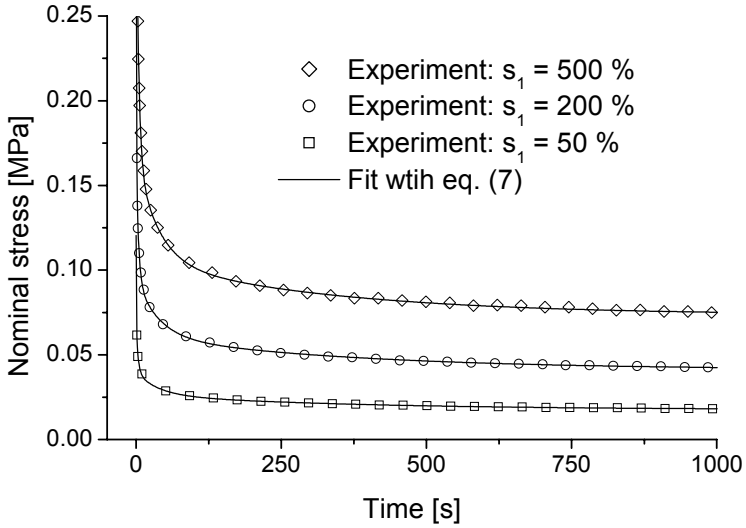

Figure 4. Nominal stress in function of time for nominal strains (s_1) of 50, 200 and 500%.

In figure 5 the relaxation function $s_\infty(t)$ is plotted against time for all relaxation experiments.

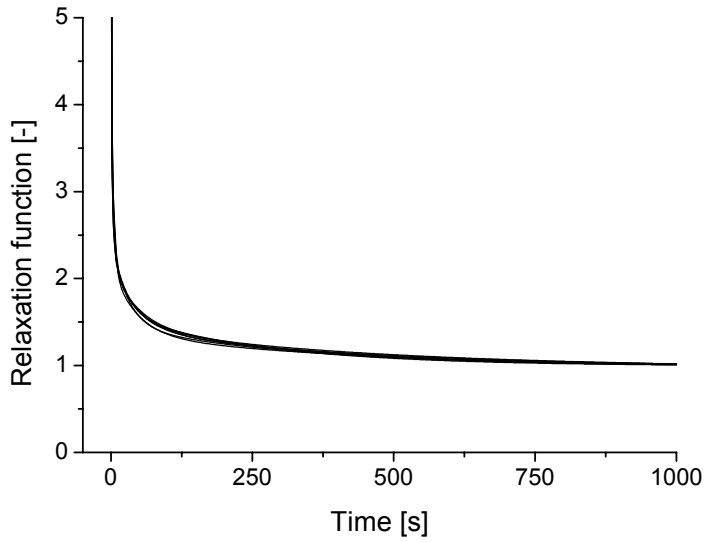

Figure 5. The relaxation function s_∞ from all relaxation tests.

The excellent agreement of the functions $s_\infty(t)$ for different elongations confirms that quasi-linear viscoelastic behavior can be assumed for this material. With the average of the relaxation functions $s_\infty(t)$, the material parameters g_k and t_k were determined according to the procedure of section 3.2. The results are reported in Table 1, column A.

From the measured stress relaxation functions the best fit parameters σ_∞, σ_i, τ_i and with eq. (8), the instantaneous nominal stresses σ_0 are determined. The hyperelastic behavior can be characterized from the instantaneous nominal stress in function of the corresponding stretch ratio, figure 6.

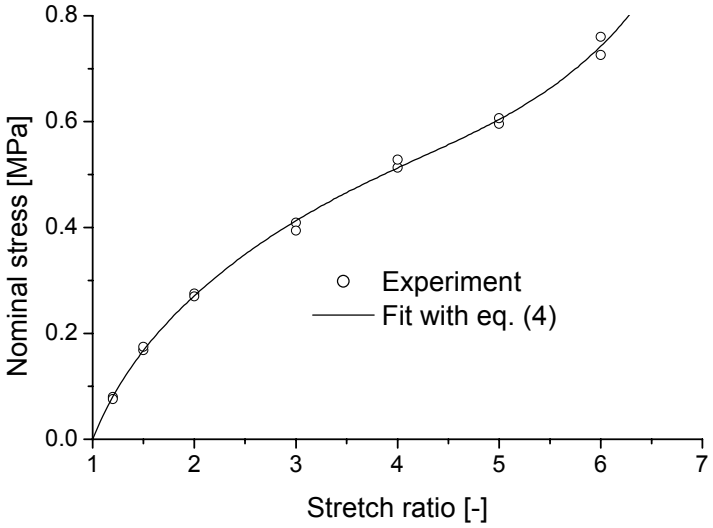

Figure 6. Evaluation of the hyperelastic material parameters for the Yeoh-form.

The parameters C_{10}^R, C_{20}^R and C_{30}^R were obtained by fitting the data of figure 6 with the Yeoh hyperelastic model, eq. (4). The corresponding values are reported in Table 1, column A.

5.2 Tensile tests

In figure 7 the experimental force time history is compared with the results of FE tensile test simulations. The dashed curve represents a simulation based on the material parameters from the relaxation tests, Table 1, column A. Specific optimization (for experiment 1) of the parameters C_{10}^R, C_{20}^R, C_{30}^R and g_k, t_k using the procedure described in section 4 led to the results of the continuous curve in figure 7. The corresponding material parameters are given in Table 1, column B.

The agreement of simulation and experiment obtained with the optimized material parameters is good, although the stress decrease in the relaxation phase of the simulation is too rapid. The results obtained with the material parameters from the relaxation tests are less satisfactory. As described in section 3, there are some uncertainties connected with the present relaxation tests: (i), the application of the initial strain was hand-controlled; (ii), strain was measured from the relative

displacement of the clamping points (end effects). The errors arising from these uncertainties might be responsible for the deviation between simulation and experiment shown in figure 7. The optimized parameters listed in Table 1, column B have been used for the circular actuator simulation, section 6.

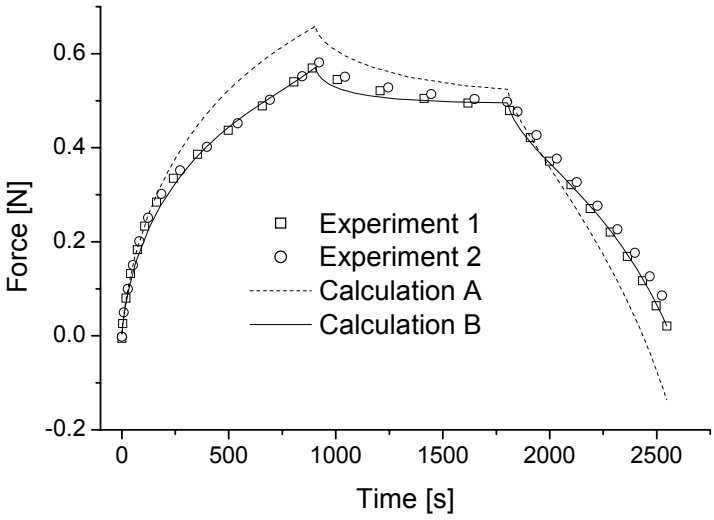

Figure 7. Force time history: Experimental data and simulations of the tensile tests. Calculation A: using data from relaxation tests. Calculation B: optimized parameters.

Table 1. Material parameters from relaxation tests (column A) and tensile tests (column B)

Parameter		A	B
C_{10}	[MPa]	0.0803	0.0693
C_{20}	[MPa]	-7.65×10^{-4}	-8.88×10^{-4}
C_{30}	[MPa]	9.84×10^{-6}	16.7×10^{-6}
g_1	[-]	0.570	0.547
t_1	[s]	0.311	0.135
g_2	[-]	0.189	0.198
t_2	[s]	3.35	0.382
g_3	[-]	0.0860	0.110
t_3	[s]	35.7	37.1
g_4	[-]	0.0543	0.0384
t_4	[s]	370	217

6 Results for the circular actuator

The experimental data of nominal radial strain reported in figure 8 were obtained with an activation voltage of 3.5 kV. The curve in figure 8 has been used in order to define the time history of the elastomer thickness imposed as kinematic boundary condition in the FE calculation.

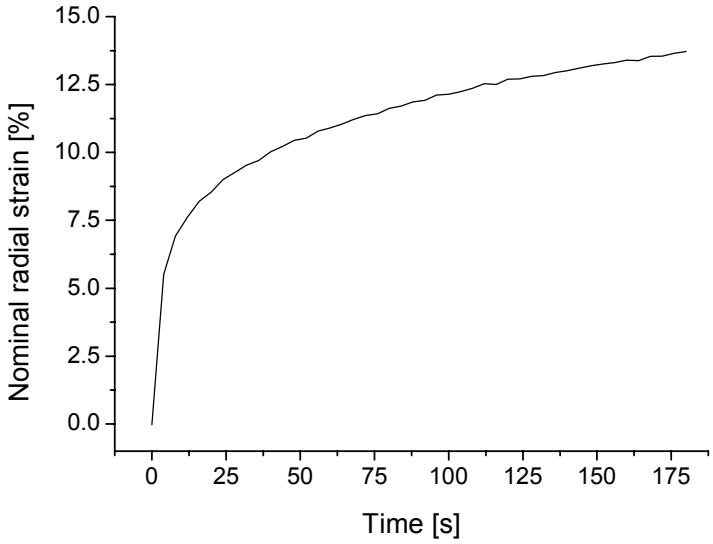

Figure 8. Measured nominal radial strain in the circular actuator activated by a constant voltage of 3.5 kV.

Figure 9 shows the FE-results for the activation voltage at different calculation time points. The time history of the calculated voltage is reported in figure 10. The agreement with the prescribed experimental voltage of 3.5 kV is excellent. The initial deviation of maximum 20% decreases with time and disappears after 80 s. Improvements of the short term relaxation model in the tensile test analysis would probably contribute reducing the voltage overestimation in the initial phase of the simulation.

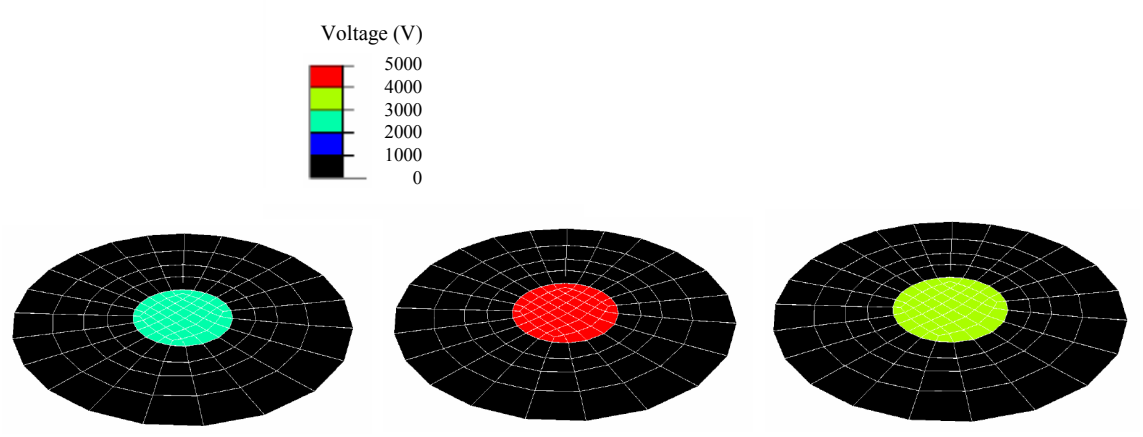

(a) (b) (c)

Figure 9. FE calculation of the applied voltage at time 1 s (a), 10 s (b) and 100 s (c).

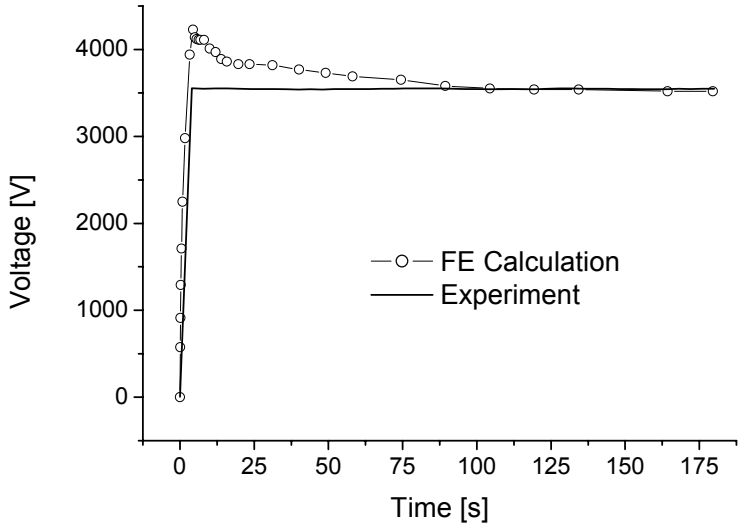

Figure 10. Circular actuator: experimental and calculated activation voltage.

7 Discussion and conclusions

A three dimensional constitutive model of the dielectric elastomer VHB 4910 has been derived from uniaxial tests and applied for the simulation of a biaxially pre-strained circular actuator. The good agreement between FE calculation and measurements with the circular actuator represents a validation of the constitutive model formulation proposed in this work.

The model parameters were determined from uniaxial data whereas a biaxial pre-straining and a three-axial stress state characterize the experiments with the circular

actuator. A number of strain energy formulations can be used for fitting the data from the uniaxial experiments. A comparison of the constitutive behavior predicted using the so called Mooney-Rivlin [17], Ogden [18] and Yeoh formulations for VHB 4910 is discussed in [19]: this work highlights the importance of performing multi-axial experiments in order to determine constitutive models of EAP materials. Other strain energy functions for hyperelastic materials will be evaluated in future with multi-axial large strain experiments. As well, the short term viscoelastic response has to be further characterized in order to eliminate the deviations between simulation and experiments observed in uniaxial (tensile test, figure 7) and in multi-axial (figure 10) experiments.

The results presented in section 6 confirm the validity of eq. (12) for the calculation of the electrostatic forces in EAP actuators. This relation along with the constitutive model represent the input for the procedure described in this paper which allow EAP actuators to be simulated by FE. This procedure can be used for design and optimization of EAP actuators of general shape.

The main disadvantage of the method presented here is the fact that the electrical voltage is the output of the calculation (with the elastomer film deformation as the input). Techniques for incorporating the electrical voltage as the input of the FE analysis are under evaluation and will be used for future simulations.

Future work on simulation and modeling of EAP actuators will also consider: (i) the influence of the compliant electrode layers (whose stiffness was neglected in the present study); and (ii) the material behavior in cyclic loading conditions and the microstructural damage mechanisms, which might lead to fatigue failure of the actuators.

8 References

[1] Y. Bar-Cohen, Electroactive Polymer (EAP) Actuators as Artificial Muscles - Reality, Potential and Challenges (2001) Washington, SPIE Press

[2] R.E. Pelrine, R.D. Kornbluh, J.P. Joseph, Electrostriction of polymer dielectrics with compliant electrodes as a means of actuation, Sens. Actuators A, 64 (1998) 77-85

[3] R. Pelrine, P. Sommer-Larsen, et al., Applications of dielectric elastomer actuators, Proc. SPIE, 4329 (2001) 335-349

[4] R. Pelrine, R. Kornbluh, et al., High-speed electrically actuated elastomers with strain greater than 100%, Science, 287 (2000) 836-839

[5] H. Kim, S. Oh, et al., Actuator model of electrostrictive polymers (EPs) for microactuators, Proc. SPIE, 4329 (2001) 482-490

[6] F. Carpi, D. Rossi, Dielectric elastomer cylindrical actuators: electromechanical modelling and experimental evaluation, Mat. Sci. Eng. C, 24 (2004) 555-562

[7] P. Sommer-Larsen, G. Kofod, et al., Performance of dielectric elastomer actuators and materials, Proc. SPIE, 4695 (2002) 158-166

[8] N. Goulbourne, M. Frecker, et al., Modeling of a dielectric elastomer diaphragm for a prosthetic blood pump, Proc. SPIE, 5051 (2003) 319-31

[9] G. Kofod, Dielectric elastomer actuators, PhD Thesis, (2001) Denmark, Riso-R-1286(EN)

[10] G. Kofod, P. Sommer-Larsen, et al., Actuation response of polyacrylate dielectric elastomers, J. Intel. Mat. Syst. Str., 14 (2003) 787-793

[11] R. Kornbluh, R. Pelrine, et al., Ultrahigh strain response of field-actuated elastomeric polymers, Proc. SPIE, 3987 (2000) 51-64

[12] R. Pelrine, R. Kornbluh, G. Kofod, High-strain actuator materials based on dielectric elastomers, Adv. Mater., 12 (2000), no. 16, 1223-1225

[13] R. Zhang, A. Kunz, et al., Dielectric elastomer actuators for a portable force feedback device, Proceedings of the 4th International Conference, EuroHaptics (2004) Munich, Germany, 300-307

[14] O.H. Yeoh, Characterization of elastic properties of carbon-black-filled rubber vulcanizates Rubber Chem. Technol., 63 (1990) 792-805

[15] Y. C. Fung, Biomechanics. Mechanical properties of living tissues, 2nd edn. (1993) New York, Springer-Verlag

[16] ABAQUS/Standard Manual, Version 6.4.1, Hibbitt, Karlsson, Sorensen, Inc., 2003

[17] M. Mooney, A theory of large elastic deformation, J. Appl. Phys., 11 (1940) 582-592

[18] R. W. Odgen, Large deformation isotropic elasticity – on the correlation of theory and experiment for incompressible rubberlike solids, Proc. R. Soc. Lond. A, 326 (1972) 565-584

[19] M. Wissler, E. Mazza, Modeling of a pre-strained circular actuator made of dielectric elastomers, Sens. Actuators A, 120 (2005) 184-192

3.2 Article 2

This section contains a reprint of the article:

M. Wissler and E. Mazza, Modeling of a pre-strained circular actuator made of dielectric elastomers, Sensors and Actuators A, 2005, vol. 120, pp. 184-192

Background motivation: An analytical model for the circular actuator is derived for optimization processes and for calculating the onset of electromechanical instabilities. In previous work, the Mooney-Rivlin or the Ogden strain energy forms are often used to model dielectric elastomer actuators. In this article, these two strain energy forms are investigated and compared to the Yeoh form which showed good predictive capabilities in article 1.

Summary of methods: A hyperelastic analytical model (without time-dependent effects) was derived for the circular actuator. Three strain energy functions (Yeoh, Ogden and Mooney-Rivlin form) were applied. The material parameters of the analytical model were obtained by fitting uniaxial data. A finite element model was created for the verification of the analytical model which includes simplifying assumptions. Time-dependent simulations were also performed (according to article 1) and the three strain energy functions were compared.

Summary of results: All three strain energy forms are able to fit the uniaxial data. For the actuator behavior, simulation and analytical results show large discrepancies between the applied voltage and strain, even though the uniaxial behavior is identical. Simulations with the Yeoh strain function agree to a great extent with the experiments (see also article 1). By contrast, the predictions for the Ogden form lay around 30% below the experimental values. The values of the Mooney-Rivlin form lay approximately 200% above the experimental values. The analytical models agree to a great extent to the hyperelastic finite element models. Electromechanical instability was predicted by the analytical models.

Main conclusions, link to the next article: The results show that the selection of an appropriate strain energy form is essential. The analytical model provides a relationship between voltage, prestrain and active strain. The circular actuator is a useful model system for investigating the main features of dielectric elastomer actuators. The analytical model describes electromechanical instabilities and can be

used for the optimization of the actuators. It was shown that the active strain is strongly dependent on the prestrain. The next steps are to broaden the experimental range, to find appropriate material parameters and to establish direct simulation techniques.

Modeling of a pre-strained circular actuator made of dielectric elastomers

Michael Wissler[1] and Edoardo Mazza[2]

[1] Swiss Federal Laboratories for Materials Testing and Research (EMPA), 8600 Dübendorf, Switzerland
[2] Swiss Federal Institute of Technology (ETH), Dept. of Mechanical Engineering, 8092 Zürich, Switzerland

Abstract

Dielectric elastomers are used for the realization of actuators with large deformations and belong to the group of so called electroactive polymers (EAP). Models are required for the design and optimization of EAP actuators. Thereby the constitutive behavior of the elastomer is of crucial importance and typically uniaxial experiments are performed in order to determine the mechanical properties of these materials. In this paper a pre-strained circular actuator made of a dielectric elastomer is investigated: constitutive models based on uniaxial data are verified by comparing calculation results with experimental observations. An analytical model is derived for the instantaneous response to an activation voltage in the pre-strained circular actuator and a finite element model is used to simulate the time dependent behavior. Hyperelastic models are used and three strain energy formulations (Yeoh, Ogden and Mooney-Rivlin) are compared in their predictive capabilities. The results of the calculations with the three strain energy forms differ significantly, although all forms were successfully fitted to the same uniaxial data set. Predictions of the actuator behavior with the Yeoh form agree to a great extent with the measurements. The results of the present work show that the circular actuator set-up represents a valid model system for the characterization and optimization of the electromechanical behavior of dielectric elastomers.

Keywords: EAP; modeling; dielectric elastomer; simulation; actuator

1 Introduction

Dielectric elastomers are used in actuator material systems able to generate large deformations by transforming electrical energy directly into mechanical work. They belong to the group of so called electroactive polymers (EAP). Several applications [1, 2] are envisaged for these actuator materials, such as mobile mini- and microrobots, micropumps and microvalves, micro air vehicles, disk drives, prosthetic devices and flat panel loudspeakers.

Actuators made of dielectric elastomers consist of a compliant capacitor, with a thin passive elastomer film sandwiched between two compliant electrodes [1, 3]. The electrostatic pressure acting on the insulating elastomer film can be calculated for a given applied voltage and film thickness [1]. Due to the mechanical compression, the elastomer film contracts in the thickness direction and expands in the film plane directions. This in-plane expansion is exploited to generate motion or forces in dielectric elastomer actuators. In order to increase the efficiency of the conversion of electrical energy into mechanical work dielectric elastomers are pre-stretched, typically up to five times their in-plane dimensions. Voltages are in the order of up to 5000 V (corresponding to an electric field of 200 MV/m in case of 25 μm film thickness) and deformations are in the order of 30% for pre-strained elastomer actuators.

Modeling techniques are required for the design and optimization of EAP actuators. An approach for modeling electromechanical coupling in dielectric EAP is proposed in [4]: the problem is solved by decoupling the electrostatic problem from the passive mechanical response of the material. The characterization of the constitutive behavior of the elastomeric film represents in this context the essential task for modeling purposes. The models have to describe time dependent mechanical response for large deformations.

Kofod [5] performed uniaxial tensile tests and verified the range of validity of various hyperelastic material models for the one dimensional stress state. Best results were obtained with a four-parameter Ogden model [6], which allows fitting the stress-strain curves for elongations up to 4 times the initial length. The influence of pre-straining in dielectric elastomer actuators has been studied with a Mooney-Rivlin model in [7]. Viscoelasticity and large deformations in dielectric elastomers have been investigated with uniaxial tests by Sommer-Larsen et al. [8] and the experimental data were rationalized by using the Rivlin-Sawyer model [9]. An analytical model for cylindrical silicone actuators has been derived in [10] by using linear elastic theories.

In-plane pre-straining and out-of-plane electrostatical activation induce a three-axial stress and deformation state in dielectric elastomer actuators. Under such circumstances hyperelastic-viscoelastic models derived from uniaxial tests are often inadequate for predicting the mechanical response: large strain biaxial and three-axial experiments have to be performed in order to determine the strain energy function that characterizes the non-dissipative component of the mechanical behavior.

In the present work a biaxially pre-strained circular actuator is proposed as model system for the characterization of the electromechanical behavior of a dielectric elastomer. In this system, like in all dielectric elastomer actuators, the deformation of the actuator for a given activation voltage depends on the three dimensional mechanical behavior of the film. The instantaneous (time independent) response is calculated analytically using hyperelastic models and a relationship between applied voltage and in-plane deformation is derived. Simplifications of the analytical model are verified through a finite element simulation of the circular actuator. Time dependent material behavior is than included in the finite element analysis by using hyperelastic-viscoelastic models determined from relaxation and tensile tests. The numerical results are compared with experimental observations. Three strain energy formulations are considered and compared in their predictive capabilities.

2 Hyperelastic material behavior

In the first part of this work analytical models are derived for a dielectric elastomer in a pre-strained circular actuator. In the analytical calculations the constitutive behavior is simplified by neglecting the time dependence of the mechanical response. Additional assumptions are that (i) the material is incompressible, and (ii) the material is isotropic in the reference undeformed configuration. Viscoelastic behavior is considered in the numerical calculations presented in section 5.

2.1 Strain energy functions

The mechanical behavior of hyperelastic materials is characterized by the strain energy function W. Many functional forms of the strain energy W exist [11]. In this work, three forms are considered, the Yeoh [12], Ogden [6] and Mooney-Rivlin [13] form. In the Yeoh form [12] the strain energy depends on I_1, the first invariant of the so called left Cauchy-Green deformation tensor:

$$W = C_{10}(I_1 - 3) + C_{20}(I_1 - 3)^2 + C_{30}(I_1 - 3)^3 \tag{1}$$

C_{10}, C_{20} and C_{30} are material parameters. I_1 can be calculated from the eigenvalues of the deformation gradient tensor, i.e. the so called principal stretch ratios λ_i (i=1,2 and 3) as

$$I_1 = \lambda_1^2 + \lambda_2^2 + \lambda_3^2 \tag{2}$$

The strain energy form of Mooney-Rivlin [13] is given by

$$W = C_{10}(I_1 - 3) + C_{01}(I_2 - 3) \tag{3}$$

C_{10} and C_{01} are material parameters. Here W depends on I_1 and on I_2, the second invariant of the left Cauchy-Green deformation tensor, which is given by

$$I_2 = \lambda_1^{-2} + \lambda_2^{-2} + \lambda_3^{-2} \tag{4}$$

The Ogden form [6] is expressed in function of the principal stretch ratios:

$$W = \sum_{i=1}^{N} \frac{\mu_i}{\alpha_i} \cdot (\lambda_1^{\alpha_i} + \lambda_2^{\alpha_i} + \lambda_3^{\alpha_i} - 3) \tag{5}$$

μ_i and α_i are material parameters and N is the number of terms. For an incompressible material, the principal Cauchy stresses t_i (force per unit area of the deformed configuration) can be determined from the derivative of the strain energy potential with respect to the stretch ratio λ_i (e.g. [6]):

$$t_i = \lambda_i \cdot \frac{\partial W}{\partial \lambda_i} - p \tag{6}$$

The hydrostatic pressure p in eq. (6) depends on the kinetic boundary conditions.

2.2 Uniaxial tension

For the uniform extension (here in direction 1) with simple (uniaxial) tension, lateral contraction occurs so that the stresses in the directions 2 and 3 are zero ($t_2 = t_3 = 0$). The isochoric deformation ($\lambda_1\lambda_2\lambda_3=1$) gives the following relation between the principal stretch ratios:

$$\lambda_2 = \lambda_3 = 1/\sqrt{\lambda_1} \tag{7}$$

By using the kinetic boundary conditions and eq. (7) the Cauchy principal stress t_1 can be calculated for the three strain energy forms as follows:

Yeoh form:

$$t_1 = 2\cdot(\lambda_1^{\,2} - \frac{1}{\lambda_1})\cdot\left[C_{10} + 2\cdot C_{20}\cdot(\lambda_1^{\,2} + \frac{2}{\lambda_1} - 3) + 3\cdot C_{30}\cdot(\lambda_1^{\,2} + \frac{2}{\lambda_1} - 3)^2\right] \quad (8\text{ a})$$

Ogden form:

$$t_1 = \sum_{i=1}^{N} \mu_i \cdot (\lambda_1^{\,\alpha_i} - \lambda_1^{\frac{-\alpha_i}{2}}) \quad (8\text{ b})$$

Mooney-Rivlin form:

$$t_1 = 2\cdot(\lambda_1^{\,2} - \frac{1}{\lambda_1})\cdot C_{10} + 2\cdot(\lambda_1 - \frac{1}{\lambda_1^{\,2}})\cdot C_{01} \quad (8\text{ c})$$

2.3 Biaxial tension

For the in-plane biaxial extension with equal stretches in the directions 1 and 2 ($\lambda_1=\lambda_2$), out-of-plane contraction occurs so that the stress in the direction 3 is zero ($t_3 = 0$). The isochoric deformation ($\lambda_1\lambda_2\lambda_3=1$) gives the following relation between the principal stretch ratios:

$$\lambda_3 = 1/\lambda_1^{\,2} = 1/\lambda_2^{\,2} \quad (9)$$

By using the kinetic boundary condition and eq. (6) the Cauchy principal stresses $t_1=t_2$ can be calculated for the three strain energy forms as follows:

$$t_1 = t_2 = \lambda_1 \frac{\partial W}{\partial \lambda_1} - \lambda_3 \frac{\partial W}{\partial \lambda_3} \quad (10)$$

$\lambda_k \cdot \frac{\partial W}{\partial \lambda_k}$ (k=1, 3) can be calculated as:

Yeoh form:

$$\lambda_k \cdot \frac{\partial W}{\partial \lambda_k} = 2\cdot\lambda_k^{\,2}\cdot\left[C_{10} + 2\cdot C_{20}\cdot(I_1 - 3) + 3\cdot C_{30}\cdot(I_1 - 3)^2\right] \quad (11\text{ a})$$

Ogden form:

$$\lambda_k \cdot \frac{\partial W}{\partial \lambda_k} = \sum_{i=1}^{N} \mu_i \cdot \lambda_k^{\,\alpha_i} \quad (11\text{ b})$$

Mooney-Rivlin form:

$$\lambda_k \cdot \frac{\partial W}{\partial \lambda_k} = 2\cdot\lambda_1^{\,2}\cdot C_{10} - 2\cdot\frac{1}{\lambda_1^{\,2}}\cdot C_{01} \quad (11\text{ c})$$

Cauchy principal stresses in directions 1 and 2 can be readily calculated from eq. (10) and (11).

3 Pre-strained circular actuator

3.1 Actuator set-up

A multi-axial electromechanical experiment has been performed on a biaxially pre-strained circular actuator (in a so called circular strain test [3, 14]) at room temperature (23° C). The elastomer film was pre-strained radially up to a nominal radial strain of 308% (according to the procedure described in [15]) and fixed on a circular frame (radius R = 75 mm), see Figure 1. The thickness of the film was measured by a thickness sensor (Mitutoyo ID-F125/150) before (1 mm) and after (0.06 mm) pre-straining.

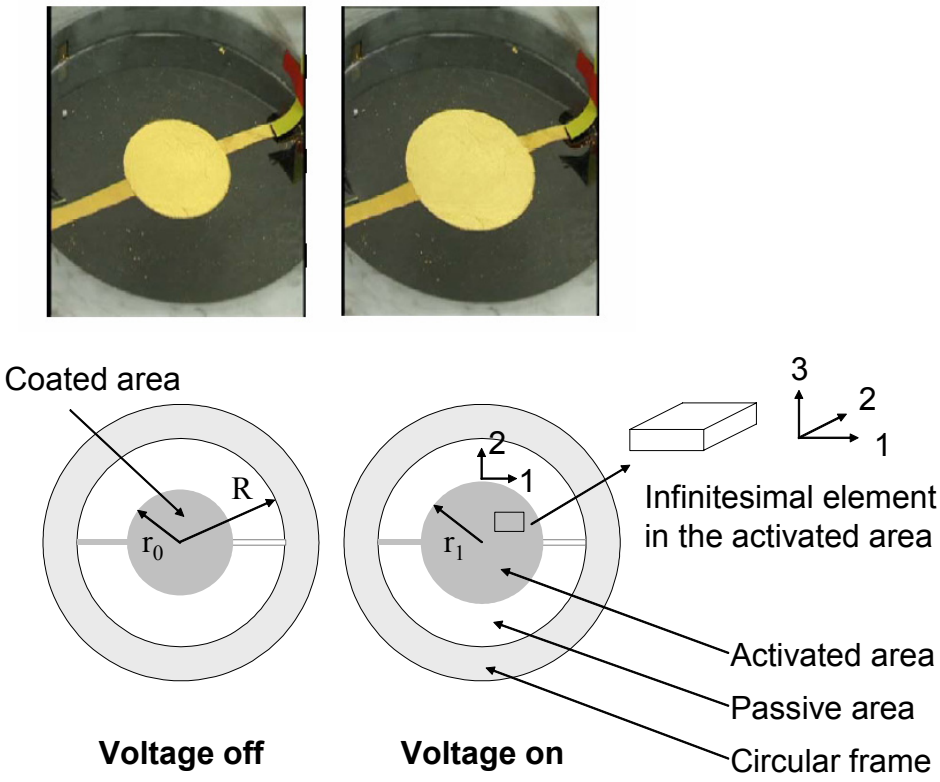

Figure. 1. Arrangement of the circular actuator for electromechanical measurements with pictures of the device (left: voltage off; right: voltage on).

After pre-straining, a circular area (radius r_0 = 22 mm) at the center of the film was coated with beaten gold (Brandenberger AG, Thalwil, Switzerland) used as electrode

on the upper and lower side. The electrodes were connected to a high voltage supplier through a thin metal wire. A constant voltage of 3.5 kV was applied for 3 min. The nominal radial strain $s_r = r_1/r_0 - 1$ of the coated area was measured with a video-extensometer (Ovex ME-46) connected to a PC LabView system.

3.2 Analytical model

The analytical model is derived for the elastomer film in the activated area (Figure 1), which is subjected to deformations in two steps: (I) pre-straining: homogeneous equibiaxial deformation in the film plane 1-2 with contraction in direction 3; (II) activation: compression in the out-of-plane direction through electrostatical forces with out-of-plane contraction and in-plane elongation. Three configurations are considered for the analytical model, see Figure 2: the undeformed or reference configuration 0 corresponds to the initial unstressed state of the elastomeric film; the pre-strained configuration I; the activated configuration II.

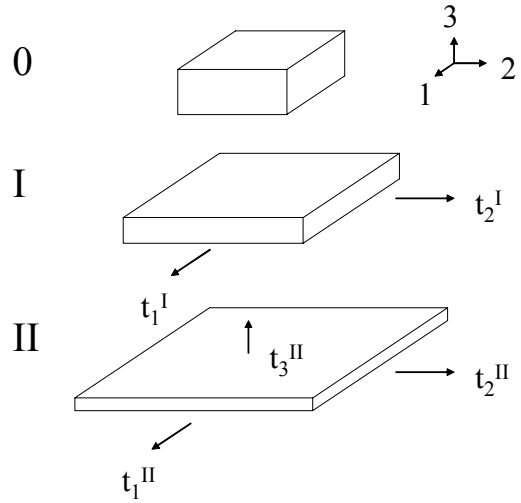

Figure. 2. Three configurations considered in the analytical model: 0 (undeformed configuration), I (pre-strained configuration) and II (activated configuration)

The basic assumptions for the present model are: (i) the material is incompressible, (ii) the material is isotropic in the reference configuration, (iii) the material is elastic (no time dependent response) and (iv) the electromechanical coupling is due solely to the electrostatic forces (no electrostriction). In the following, the index ^{I} refers to the pre-strained configuration and the index ^{II} to the activated configuration, Figure 2.

3.2.1 Pre-strained configuration

The deformation gradient of the in-plane isochoric equibiaxial deformation corresponds to the deformation described in section 2.3. Equations (10) and (11) give

the Cauchy stresses in the principal directions 1, 2 and 3 for each strain energy function.

3.2.2 Activated configuration

The activation of the dielectric elastomer leads to a further reduction of the film thickness. The principal stretch ratio λ_3^{II} in direction 3 is expressed as function of the pre-strain stretch ratio λ_1^{I} and the parameter k which characterizes the change of the thickness due to electrostatic forces:

$$\lambda_3^{II} = \lambda_3^{I} - k = \frac{1}{(\lambda_1^{I})^2} - k \tag{12}$$

Since only compressive forces are applied, the range of k is given by:

$$0 < k < \frac{1}{(\lambda_1^{I})^2} \tag{13}$$

Incompressibility yields

$$\lambda_3^{II} \cdot (\lambda_1^{II})^2 = 1 \tag{14}$$

so that the principal in-plane stretch ratios λ_1^{II} and λ_2^{II} can be written in function of the pre-strain stretch ratio λ_1^{I} and k

$$\lambda_1^{II} = \lambda_2^{II} = \frac{1}{\sqrt{\lambda_3^{II}}} = \frac{1}{\sqrt{\frac{1}{(\lambda_1^{I})^2} - k}} \tag{15}$$

In the following, the pre-strain stretch ratio is replaced by $\lambda_p = \lambda_1^{I} = \lambda_2^{I}$ and the index '$_p$' refers to the pre-strain phase. In the experiment the in-plane nominal strain s_1 is measured and is defined as:

$$s_1 = (\frac{\lambda_1^{II}}{\lambda_1^{I}} - 1) \cdot 100\% = (\frac{1}{\sqrt{1 - k \cdot \lambda_p^{\,2}}} - 1) \cdot 100\% \tag{16}$$

The definition of the kinetic boundary conditions for the activated configuration requires a simplification. In fact, due to the in-plane elongation of the activated region of the actuator, the in-plane stresses decrease (since the film is clamped at its outer radius, in the non-activated region). Consideration of the stress relaxation would require the non-activated region to be included in the mechanical analysis. However, if the radial elongation due to activation is small with respect to the pre-strain radial elongation, the reduction of the in-plane stress components can be neglected. The

errors arising from this approximation will be evaluated from a comparison with finite element calculations in section 4.

With eq. (6) the Cauchy principal stresses t_1^{II} and t_2^{II} in directions 1 and 2 are:

$$t_1^{II} = \lambda_1^{II} \frac{\partial W}{\partial \lambda_1^{II}} - p^{II} = t_1^I = t_p \tag{17 a}$$

$$t_2^{II} = \lambda_2^{II} \frac{\partial W}{\partial \lambda_2^{II}} - p^{II} = t_2^I = t_p \tag{17 b}$$

where t_p corresponds to the pre-stress which is equal in direction 1 and 2. From eq. (17a) the hydrostatic pressure p^{II} can be evaluated:

$$p^{II} = \lambda_1^{II} \frac{\partial W}{\partial \lambda_1^{II}} - t_p = \lambda_1^{II} \frac{\partial W}{\partial \lambda_1^{II}} - \lambda_1^I \frac{\partial W}{\partial \lambda_1^I} + \lambda_3^I \frac{\partial W}{\partial \lambda_3^I} \tag{18}$$

The Cauchy principal stress in direction 3, t_3^{II} becomes

$$t_3^{II} = \lambda_3^{II} \frac{\partial W}{\partial \lambda_3^{II}} - p^{II} = \lambda_3^{II} \frac{\partial W}{\partial \lambda_3^{II}} - \lambda_1^{II} \frac{\partial W}{\partial \lambda_1^{II}} + t_p = \lambda_3^{II} \frac{\partial W}{\partial \lambda_3^{II}} - \lambda_1^{II} \frac{\partial W}{\partial \lambda_1^{II}} + \lambda_1^I \frac{\partial W}{\partial \lambda_1^I} - \lambda_3^I \frac{\partial W}{\partial \lambda_3^I} \tag{19}$$

3.2.3 Electromechanical coupling

The Cauchy-stress t_3^{II} corresponds to the (negative) electrostatic pressure p_{el} acting across the electrodes [1],

$$p_{el} = \varepsilon_r \cdot \varepsilon_0 \cdot \left(\frac{U}{d^{II}} \right)^2 = -t_3^{II} \tag{20}$$

Thereby, ε_o is the free-space permittivity ($8.85 \cdot 10^{-12}$ As/Vm), ε_r is the elastomer specific relative permittivity, U is the electrical voltage applied to the electrodes and d^{II} is the thickness of the polymer film in the activated configuration. The thickness d^{II} is related to the original thickness d_0:

$$d^{II} = \lambda_3^{II} \cdot d_0 = \left(\frac{1}{\lambda_p^{\,2}} - k \right) \cdot d_0 \tag{21}$$

The combination of eq. (19), (20) and (21) yields an expression for the voltage U in function of the kinematic quantities and derivatives of the strain energy function W:

$$U^2 = -\frac{d_0^{\,2}}{\varepsilon_r \cdot \varepsilon_0} \cdot \left(\frac{1}{\lambda_p^{\,2}} - k\right)^2 \cdot t_3^{\,II}$$
$$= -\frac{d_0^{\,2}}{\varepsilon_r \cdot \varepsilon_0} \cdot \left(\frac{1}{\lambda_p^{\,2}} - k\right)^2 \cdot \left(\lambda_3^{II} \frac{\partial W}{\partial \lambda_3^{II}} - \lambda_1^{II} \frac{\partial W}{\partial \lambda_1^{II}} + \lambda_1^{I} \frac{\partial W}{\partial \lambda_1^{I}} - \lambda_3^{I} \frac{\partial W}{\partial \lambda_3^{I}} \right) \tag{22}$$

The expressions for the different strain energy potentials (eq. (11)) are inserted in eq. (22). Eq. (16) is used to express the out-of-plane elongation parameter k in function of the measured in-plane strain s_1. In this way a relation between the applied voltage U, the pre-strain of the elastomeric film λ_p and the 'activated' strain s_1 is obtained.

4 Calculation results for VHB 4910

4.1 Material parameters from uniaxial tests

The dielectric elastomer used in the present work is an acrylic polymer, VHB 4910 (3M). Uniaxial tests were performed in order to characterize the mechanical behavior of this material [16]. Uniaxial relaxation experiments were performed at room temperature by stretching the samples to a predefined elongation and measuring the force decrease over a time period of approximately 0.5 hour. Fourteen experiments have been performed, the nominal strain being between 20% and 500%. Uniaxial tensile tests have been performed for two samples with a Zwick (Z010) machine at room temperature. The time history of the elongation consisted of three steps: the sample was first loaded up to 300% nominal strain linearly over a time period of 900 s, the strain was hold fix for 900 s, and the sample was than unloaded with a negative strain rate of -0.33 %/s. Testpieces had undeformed dimensions of 150 x 10 x 1 mm^3 (length x width x thickness). A finite element model was created and the material modeled as quasi-linear viscoelastic using different strain energy formulations. Material parameters were obtained from the experimental data using an optimization algorithm with iterative finite element simulations. The corresponding results for the instantaneous uniaxial response of the Yeoh, Ogden and Mooney-Rivlin strain energy forms are shown in Figure 3 and, in terms of material parameters, in Table 1. For all strain energy formulations good fitting of the experimental data up to a stretch ratio of 5 can be obtained.

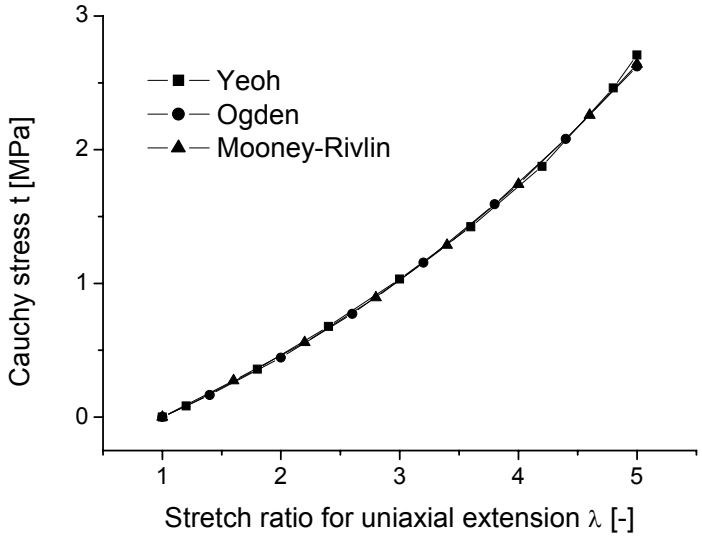

Figure 3. Uniaxial instantaneous hyperelastic response: Yeoh, Ogden and Mooney-Rivlin model from uniaxial experiments. The Cauchy stress $t = t_1$ is obtained from eq. 8 a, b and c, with $\lambda = \lambda_1$.

Table 1. Material parameters for the Yeoh, Ogden and the Mooney-Rivlin form

Yeoh		
C_{10}	[MPa]	0.0693
C_{20}	[MPa]	-8.88×10^{-4}
C_{30}	[MPa]	16.7×10^{-6}
Ogden		
α_1	[-]	1.76
μ_1	[MPa]	0.156
Mooney-Rivlin		
C_{10}	[MPa]	0.0450
C_{01}	[MPa]	0.0412

4.2 Results for the circular actuator

The principal Cauchy stresses for the pre-strained and activated configurations were calculated using the material parameters of Table 1. The in-plane Cauchy stress t_p (principal stress in direction 1 and 2 in the pre-strained configuration) is plotted in Figure 4 for all three forms in function of the in-plane stretch ratio λ_p.

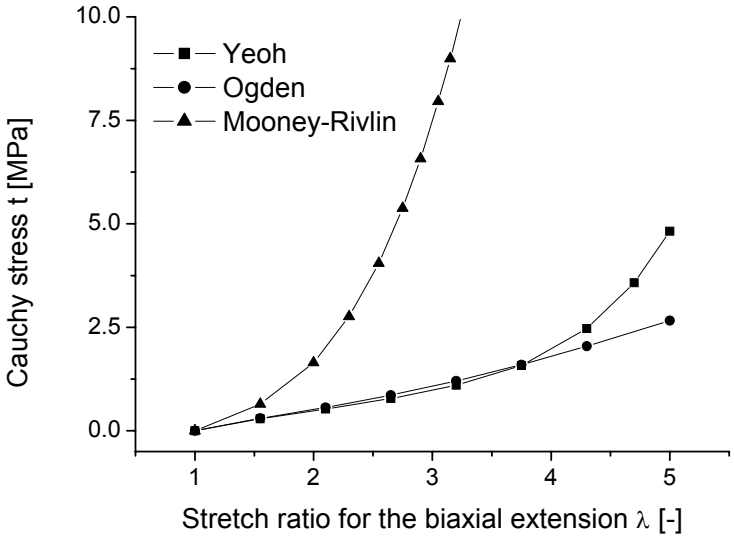

Figure 4. Pre-strained configuration: in-plane Cauchy stress $t = t_p$ vs. pre-strain stretch ratio $\lambda = \lambda_p$ for the three strain energy forms calculated from eq. (10) and (11).

The results for the Ogden and the Yeoh model are similar, whereas the pre-stress t_p of the Mooney-Rivlin model is about one order of magnitude higher.

The results of the activated configuration for a pre-strain with $\lambda_p = 4.08$ are presented in Figure 5. The pre-strain with $\lambda_p = 4.08$ corresponds to the measured film thickness change from 1 mm (undeformed configuration) to 0.06 mm (pre-strained configuration) in the experiment. The nominal strain in the radial direction (s_1, eq. (16)) is plotted against activation voltage, using the results of section 3. For VHB 4910, a relative permittivity $\varepsilon_r = 4.7$ has been used, [17]. The analytical results are compared with the strain-voltage curves obtained with a FE calculation of the whole circular actuator (see section 5). In order to enable a direct comparison with the analytical results, for this particular numerical analysis time dependent material properties have been neglected.

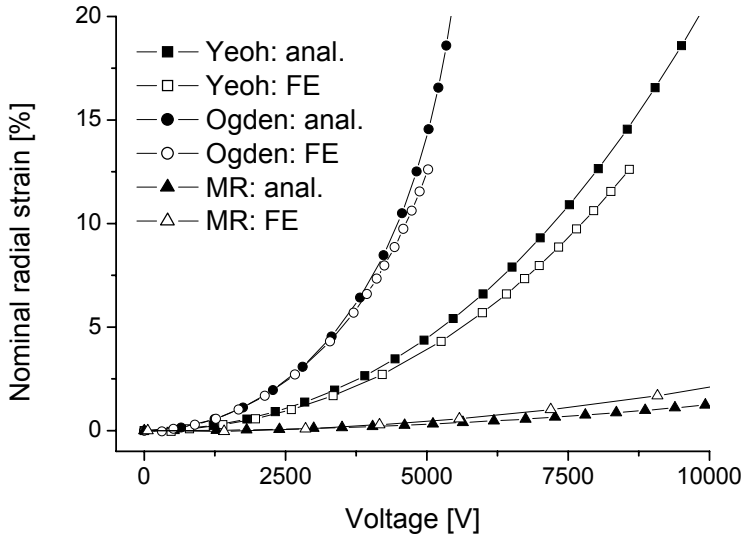

Figure 5. Activation: instantaneous nominal radial strain vs. voltage. Comparison of analytical (anal.) and numerical (FE) results for the different strain energy forms. Yeoh, Ogden and Mooney-Rivlin (MR).

5 Finite Element modeling of the circular actuator

For the calculations of the circular planar actuators the general purpose FE program ABAQUS [18] has been used. The FE model of the circular actuator is shown in Figure 6 and consists of 140 solid hybrid elements (8-node linear brick).

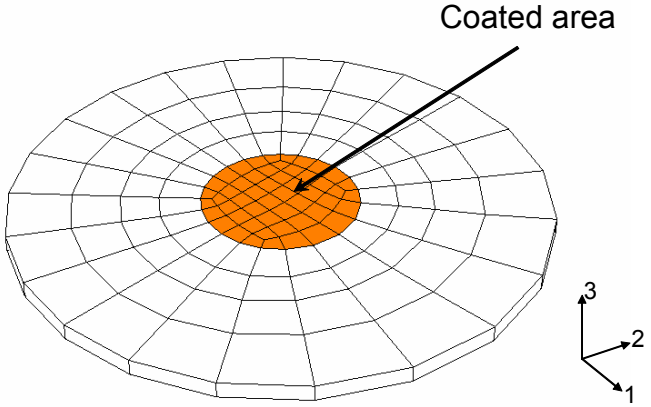

Figure 6. FE-model for the circular actuator. The coated area is indicated.

Time dependent material behavior is described by a quasi-linear viscoelastic model, [19]. The time functions for the parameters of the strain energy functions were determined from uniaxial relaxation and tensile tests, [16].

The circular actuator simulation included three steps: (i) pre-strain ($\lambda_p = 4.08$) in radial direction, by imposing the displacement of the nodes at the model boundary, (ii) relaxation over a time period of one hour, and (iii) activation by imposing a thickness reduction in the activated region. The time history of thickness reduction corresponds to the radial strain history measured in the experiment (assuming incompressibility). The measured deformation represents therefore the input of the finite element analysis, whereas the voltage needed to realize this deformation history is the output of the calculation, and allows comparison with the experimental values and validation of the model. The required voltage is determined from the calculated stresses in thickness direction in the activated region: the electrostatic pressure p_{el} corresponds to the negative Cauchy stress t_3 in the direction of the electric field, eq. (20); with eq. (20) the voltage can be calculated from the current values of film thickness and stress t_3. Further details on the simulation of EAP actuators by FE are given in [16].

The measured time dependent in-plane elongation history of the actuator that has been used as the input for the FE simulation is shown in Figure 7. The result of the calculation is the time history of the required activation voltage. A constant voltage of 3500 V has been applied in the experiment. The results of the FE-modeling for the three strain energy potentials are presented in Figure 8.

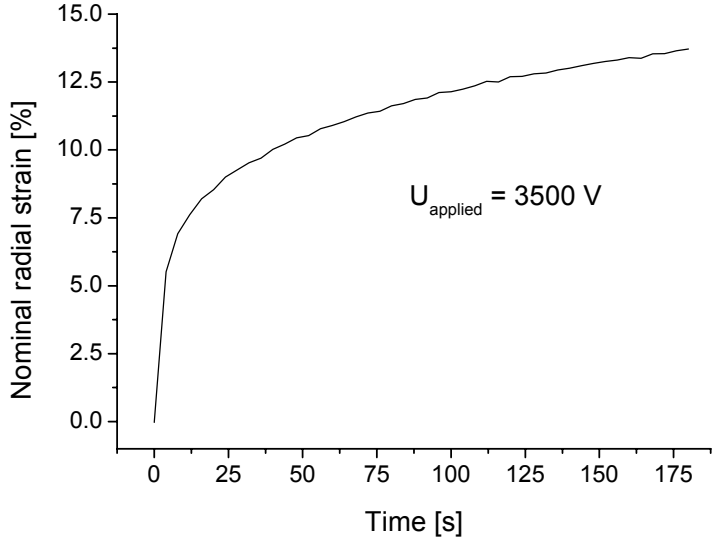

Figure 7. Nominal radial strain (s_1, eq. (16)) history measured in the circular actuator experiment.

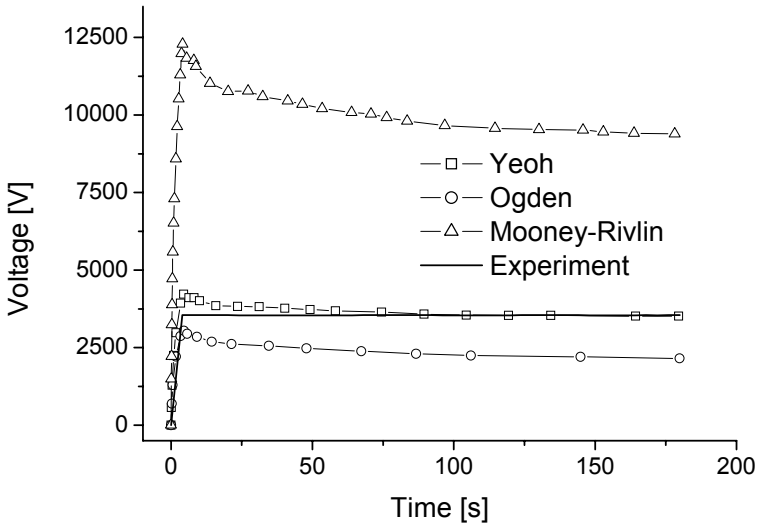

Figure 8. FE-calculation: time history of the voltage required to obtain the observed radial elongation history for the Yeoh-, Ogden- and Mooney-Rivlin-form. Constant voltage (3500 V) was applied in the experiment.

6 Discussion

Fitting of the hyperelastic parameters for the instantaneous response to the uniaxial experimental data yields good results for all three strain energy formulations. This is in contrast with the results presented in [5] for the same dielectric elastomer, for which only the Ogden form allowed the stress-stretch data to be reproduced over a large range of elongation.

As expected, major differences in the biaxial (pre-straining) and three-axial (activation) response are obtained from the different strain energy forms. In particular, the results for Ogden and Yeoh are similar for uniaxial and for equibiaxial loading, but differ considerably for the three-axial deformation of the activated phase. This highlights the importance of performing multi-axial tests for characterizing the mechanical behavior of EAP materials. Experiments with the pre-strained circular actuator can serve for this purpose.

The circular actuator can be studied with analytical models. Figure 5 compares analytical and numerical calculations of the instantaneous behavior in the activation phase. The discrepancies between numerical and analytical calculations are due to the simplified kinetic boundary conditions of the analytical model. The curves of Figure 5 show that neglecting the reduction of in-plane stresses due to the radial elongation of

the film does not affect the results to a significant extent for nominal radial strains in the order of up to 10%.

The calculation of the time-dependent behavior of the circular actuator was performed here by FE, due to the difficulties in evaluating the hereditary integrals of the viscoelastic model in the analytical framework. This FE simulation allowed comparing the strain energy functions in their predictive capabilities. The results of Figure 8 demonstrate that the Yeoh form performs best for the present application. Some mismatching is visible for the initial part of the activation phase.

The analytical model allows studying the instantaneous response of the circular actuator. This is useful for design and optimization of EAP actuators. For instance, the occurrence of "electromechanical instability" can be investigated with this model. Instability occurs due to the fact that the electrostatic pressure increases when the film thickness decreases. If the increase in out-of-plane stiffness of the film does not compensate for the increased electrostatic forces, thickness will decrease in an unstable manner (mechanical collapse). This phenomenon is evident from the curves shown in Figure 9: the nominal radial strain is plotted against the required voltage for the three strain energy forms ($\lambda_p = 4.08$). Instability occurs when the slope of the curve is vertical: increase in lateral expansion (i.e. decrease in thickness) occurs without increase of applied voltage. Instability occurs here for approximately 5000 V and 45000 V for the Ogden and Mooney-Rivlin models, whereas no instability is found for the Yeoh model (for the present level of pre-stretching). It must be underlined that for EAP actuators instability is not expected to represent the failure mechanism when the so called electrical breakdown [17] occurs at a lower voltage. Indeed voltage of 45000 V over a film thickness < 0.1 mm cannot realistically be expected to occur without prior electrical breakdown.

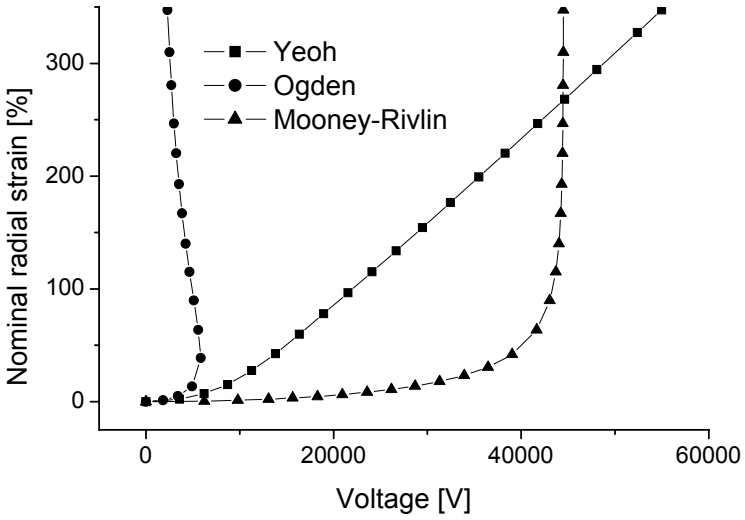

Figure 9. Electromechanical instability occurs when the strain vs. voltage curve has an infinite slope.

Instability and more in general the relationship between in-plane strain and applied voltage strongly depends on the pre-strain level. This relation can be studied with the analytical model. Calculations were performed for the Yeoh form. Nominal radial strain curves vs. applied voltages were calculated for different values of the pre-strain stretch ratio λ_p. The results are shown in Figure 10.

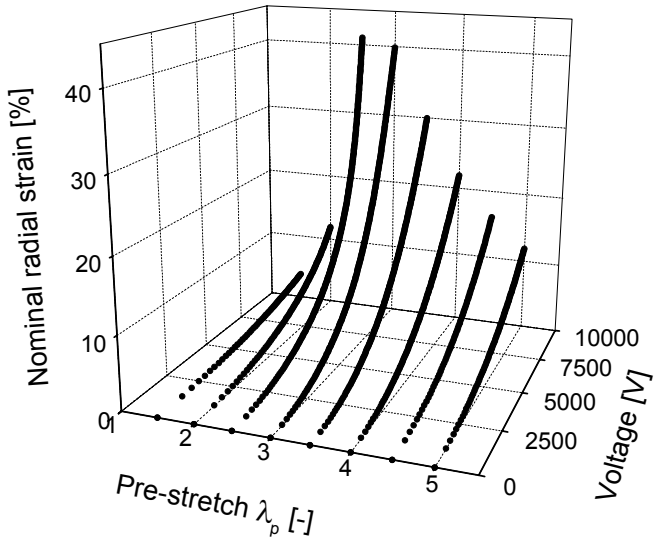

Fig 10. Dependence of the instantaneous strain-voltage curves on pre-strain for the Yeoh strain energy potential.

For a given voltage, the lateral elongation increase with increasing pre-stretch level up to about $\lambda_p = 2.5$, and than decreases. These curves along with the information of

maximum allowable voltage for each pre-strain level (given by the breakdown strength) can be used for selecting appropriate pre-straining of EAP actuators.

7 Conclusions

The results of the analytical and numerical calculations show that the selection of an appropriate strain energy form is essential to a reliable characterization of the behavior of dielectric elastomer actuators. In particular, it was demonstrated that no conclusions can be drawn from uniaxial test data alone.

The model system proposed in this paper for the evaluation of electromechanical models of EAP actuators offers several advantages:

(i) Important characteristics of the actuator can be studied with analytical calculations. Qualitative analyses can be easily performed on the influence of specific design parameters. Use of (time independent) long term moduli (in place of the instantaneous moduli applied in the present work) would yield quantitative results on the long term response of the actuator to a given voltage.

(ii) The multi-axial stress and deformation state of the pre-strained circular actuator is representative for the working conditions of EAP actuators. Models that are validated on a circular actuator arrangement are expected to usefully describe the behavior of other arrangements.

(iii) The circular actuator can be easily realized and used for laboratory tests. In-plane elongation, undeformed and pre-strained thickness, and voltage are the data required for model fitting and can be easily determined in the experiment.

The Yeoh strain energy form with parameters determined from uniaxial tests led to an excellent prediction of the observed electromechanical behavior. The agreement between experiment and numerical calculations confirms (i) the constitutive model (including the time dependent behavior) and (ii) the modeling approach adopted for electromechanical coupling.

Further experiments with the circular actuator set-up will be performed in order to confirm the validity of the present constitutive model. In particular, the influence of the pre-strain level will be investigated. Future work on the characterization of dielectric EAP actuators includes: (i) realization of multi-axial relaxation and creep tests; (ii) verification of the viscoelastic model with cyclic experiments, in order to study the evolution of the hysteretic behavior; and (iii) investigation of the role of the electrodes compliance [20].

8 References

[1] R.E. Pelrine, R.D. Kornbluh, J.P. Joseph, Electrostriction of polymer dielectrics with compliant electrodes as a means of actuation, Sens. Actuators, A 64 (1998) 77-85

[2] R. Pelrine, P. Sommer-Larsen, R. Kornbluh, R. Heydt, G. Kofod, Q. Pei, P. Gravesen, Applications of dielectric elastomer actuators, Proc. SPIE, 4329 (2001) 335-349

[3] R. Pelrine, R. Kornbluh, Q. Pei, J. Joseph, High-speed electrically actuated elastomers with strain greater than 100%, Science, 287 (2000) 836-839

[4] Y. Bar-Cohen, Electroactive Polymer (EAP) Actuators as Artificial Muscles - Reality, Potential and Challenges, vol. PM98, SPIE Press, Washington, 2001, p. 309

[5] G. Kofod, Dielectric elastomer actuators, PhD Thesis, Riso-R-1286(EN), Denmark, 2001, p. 13

[6] R.W. Odgen, Large deformation isotropic elasticity – on the correlation of theory and experiment for incompressible rubberlike solids, Proc. R. Soc. Lond., A 326 (1972) 565-584

[7] H. Kim, S. Oh, K. Hwang, H. Choi, J.W. Jeon, J.D. Nam, Actuator model of electrostrictive polymers (EPs) for microactuators, Proc. SPIE, 4329 (2001) 482-490

[8] P. Sommer-Larsen, G. Kofod, M. Shridhar, M. Benslimane, P. Gravesen, Performance of dielectric elastomer actuators and materials, Proc. SPIE, 4695 (2002) 158-166

[9] R.S. Rivlin, K.N. Sawyers, Nonlinear continuum mechanics of viscoelastic fluids, Ann. Rev. Fluid Mech, 3 (1971) 117-146

[10] F. Carpi, D. De Rossi, Dielectric elastomer cylindrical actuators: electromechanical modeling and experimental evaluation, Mat. Sci. Eng., C 24 (2004) 555-562

[11] O.H. Yeoh, Some forms of the strain energy function for rubber Rubber, Chem. Technol., 66 (1993) 754-771

[12] O.H. Yeoh, Characterization of elastic properties of carbon-black-filled rubber vulcanizates, Rubber Chem. Technol., 63 (1990) 792-805

[13] M. Mooney, A theory of large elastic deformation, J. Appl. Phys., 11 (1940) 582-592

[14] R. Pelrine, R. Kornbluh, G. Kofod, High-strain actuator materials based on dielectric elastomers, Adv. Mater., 12 (16) (2000) 1223-1225

[15] R. Zhang, A. Kunz, G. Kovacs, S. Michel, A. Mazzone, Dielectric elastomer actuators for a portable force feedback device, The 4th European Conference on EuroHaptics 2004, Munich Germany, June 2004, 300-307

[16] M. Wissler, E. Mazza, Modeling and simulation of dielectric elastomer actuators, submitted to Smart Mater. Struct.

[17] G. Kofod, P. Sommer-Larsen, R. Kornbluh, R. Pelrine, Actuation response of polyacrylate dielectric elastomers, J. Intel. Mat. Syst. Str., 14 (2003) 787-793

[18] ABAQUS/Standard Manual, 2003. Version 6.4.1, Hibbitt, Karlsson & Sorensen, Inc.

[19] Y.C. Fung, Biomechanics. Mechanical properties of living tissues, 2nd edn., Springer-Verlag, New York, 1993, p. 277

[20] F. Carpi, P. Chiarelli, A. Mazzoldi and D. De Rossi, Electromechanical characterisation of dielectric elastomer planar actuators: comparative evaluation of different electrode materials and different counterloads, Sens. Actuators, A 107 (2003) 85-95

3.3 Article 3

This section contains a reprint of the article:

M. Wissler and E. Mazza, Mechanical behavior of an acrylic elastomer used in dielectric elastomer actuators, Sensors and Actuators A, 2007, vol. 134, pp. 494-504

Background motivation: In article 1 and 2 the circular actuator was identified as a valuable modeling system, including a constitutive model and an electromechanical coupling. The simulation at prestrain $\lambda_p = 4$ and voltage U = 3.5 kV with the Yeoh strain energy form showed a good agreement between simulation and experiment. In order to characterize a larger strain range, more experiments are required at different prestrains and voltages. Several experiments have to be carried out for each condition in order to verify the experimental data statistically. Furthermore, an actuator simulation is required where the voltage and not the strain history is the input. In article 2 it was shown that the selection of an appropriate strain energy form is essential. Alternative strain energy forms are also investigated here.

Summary of methods: A large experimental study investigating circular actuators was performed at three different prestrains and four different voltage levels. A total number of 40 actuators was tested. Each experiment was carried out 3-4 times for statistical aspects. A novel approach is proposed for finite element analysis. The material parameters were calibrated for the three different prestrains at 2 kV. Different strain energy functions were investigated, viz. the Yeoh form, the Ogden form (with 6 parameters) and the Arruda-Boyce form. Uniaxial experiments and corresponding finite element simulations were carried out for verification. Further, the mechanical model was evaluated by considering a cyclic actuation.

Summary of results: The comparison between experiments and simulations for the circular actuators shows a reasonable agreement for all three strain energy forms. By contrast, a discrepancy between experimental data and simulations is evidenced for the uniaxial behavior. The novel finite element approach successfully simulates the actuator behavior in nearly all cases, including those with large prestrains and large active strains. The quasilinear visco-hyperelastic model fails to describe the cyclic actuator behavior.

Main conclusions, link to the next article: A large effort was made for the experimental characterization of circular actuators. These experiments are also important for the whole research community for model verification purposes. The 'global' actuator behavior is described well by the constitutive model and the applied simulation techniques. The reason for the discrepancy between experimental data and simulations for the uniaxial behavior lies in the electromechanical coupling which is investigated in article 4.

Mechanical behavior of an acrylic elastomer used in dielectric elastomer actuators

Michael Wissler[1,2] and Edoardo Mazza[2,1]

[1] Swiss Federal Laboratories for Materials Testing and Research (EMPA), 8600 Dübendorf, Switzerland
[2] Swiss Federal Institute of Technology (ETH), Dept. of Mechanical Engineering, 8092 Zürich, Switzerland

Abstract

The paper reports on extensive experimental work for the characterization of a dielectric elastomer used as base material for electroactive polymer (EAP) actuators. The mechanical behavior of the acrylic elastomer VHB 4910 is characterized using large strain experiments (uniaxial and equibiaxial deformation) under force and displacement controlled loading conditions. Next to tensile and relaxation tests, experiments were conducted also using so called circular actuators. Over 40 actuators were produced (with different in-plane prestrain levels) and activated with voltages between 2000 and 3500 V. The experimental data are useful for determining constitutive model parameters as well as for validating models and simulation procedures for electromechanical coupling in EAP actuators. A novel approach is proposed for finite element analysis of dielectric elastomer actuator, which has been used in the present work for the evaluation of the experimental observations from circular actuators. Material parameters of different visco-hyperelastic models have been determined from a subset of the experimental data and the predictive capabilities of the models evaluated through comparisons with the remaining data. The prediction of the circular actuator behavior was satisfactory so that the proposed models might be useful for actuator design and optimization purposes. Limitations of the proposed constitutive model formulation are presented.

Keywords: Modeling, EAP, dielectric elastomer, simulation, actuator

1 Introduction

Dielectric elastomers (DE) are materials that are used as actuators in adaptive structures, in particular when large deformations are required. DE actuators belong to the category of so called “electro active polymer actuators”: they transform electric energy directly into mechanical work and produce large strains, in the order of 10% to 30%. They were first proposed in 1998 for use as actuators [1]. Important progresses in this emerging field were achieved in the selection of suitable elastomers and actuator configurations (e.g. [2], [3]), in the development of technologies for the realization of the actuators (e.g. [4]), in the evaluation of potential applications and the characterization of simple actuators (e.g. [5]). The present work focuses on modeling, which represents a fundamental task for the development of optimized actuators, for simulating and predicting the efficiency, functionality and reliability of DE actuators. Account of previous work on DE modeling is provided in our recent papers [6], [7].

Dielectric elastomer actuators were shown to provide good overall performance [5], combining large elongation, high energy density, good efficiency and high speed of response. In particular an acrylic elastomer is investigated here, VHB4910 (3M), which is widely used for the realization of DE actuators.

The actuators consist basically of a compliant capacitor, with a thin passive elastomer film sandwiched between two compliant electrodes. The electrostatic pressure acting on the insulating elastomer film can be calculated for a given applied voltage and film thickness [1]. Due to the mechanical compression, the elastomer film contracts in the thickness direction and expands in the film plane directions. This in-plane expansion is exploited to generate motion or forces. In order to improve their performance dielectric elastomers are pre-stretched, typically up to five times of their in-plane dimensions.

Characterization of the constitutive behavior of the elastomer is essential for modeling purposes. Fitting of large strain constitutive models using the results of conventional uniaxial tests is not sufficient for this purpose. In fact, in DE actuators the material is subjected to cyclic loading and unloading in a multiaxial stress state with finite deformations. Suitable material laws must be developed in order to describe the multiaxial large deformation behavior of the material and to reproduce the time and history dependence of its mechanical response.

A systematic and comprehensive experimental characterization has been carried out at the DE laboratory of EMPA, with large strain uniaxial displacement controlled tests and multi-axial experiments using a circular actuator [6]. A total number of 40 circular actuators were built and tested in order to characterize the electro-mechanical response

at several pre-strain levels and with different activation voltages. One of the main objectives of the present paper is to share the experimental data with the DE research community so that other researchers might use these data for model development and validation purposes. The experimental details are presented in section 2.

Section 3 describes our evaluation of the experimental data: a quasi-linear viscoelastic constitutive model (with three different strain energy formulations) is applied and the corresponding material parameters are determined from the experimental data. This section describes also the calculation procedure applied for the solution of the inverse problem. In particular a novel approach is proposed for simulation of the active DE behavior by finite element (FE) calculations.

The proposed constitutive models are discussed and their predictive capabilities are evaluated in section 4. The results of a multi-cycle experiment with the circular actuator (up to 75 activation-deactivation cycles) are shown in order to demonstrate the limitations of a quasi-linear viscoelastic constitutive model formulation.

2 Experiments

2.1 Material details

VHB 4910 is an acrylic elastomer produced by 3M. The chemical composition is not declared by the manufacturer. The material is commercially available in form of a membrane with 1 mm thickness, 23 mm width and arbitrary length. Testing was performed at room temperature (23° C).

2.2 Uniaxial displacement controlled experiments

Uniaxial tensile tests were performed with a Zwick (Z010) machine (tensile testing equipment) and relaxation tests with a hand-operated setup under displacement control conditions (see Figure 1 for the control profiles). For the tensile test the probe dimensions in the undeformed state were: 1 mm thickness, 10 mm width and 150 mm length in axial direction. The strain was monitored with an elongation sensor (Zwick multisens) in the middle of the sample, over an undeformed gauge length of 50 mm. For the relaxation test the undeformed sample geometry was set to a ratio between length and width of 10:1, in order to ensure uniaxial stress conditions, with thickness of 1mm. Several experiments (figure 1) were carried out: (i) relaxation tests (Rel50, Rel200 and Rel500), (ii) tensile tests at fixed deformation rate (Ten500), (iii) tensile tests with a deformation history comprising a loading ramp, hold time, and unloading

(Ten300). Experimental results (force history for each test) are reported in figure 2. The nominal stress, the force divided by the initial cross section, is plotted against the time. Each curve corresponds to the average of two experiments, whereby the scatter between experiments with identical control profiles was very low. Analysis of the relaxation curves led to the conclusion that this material might be modeled as quasilinear viscoelastic [6].

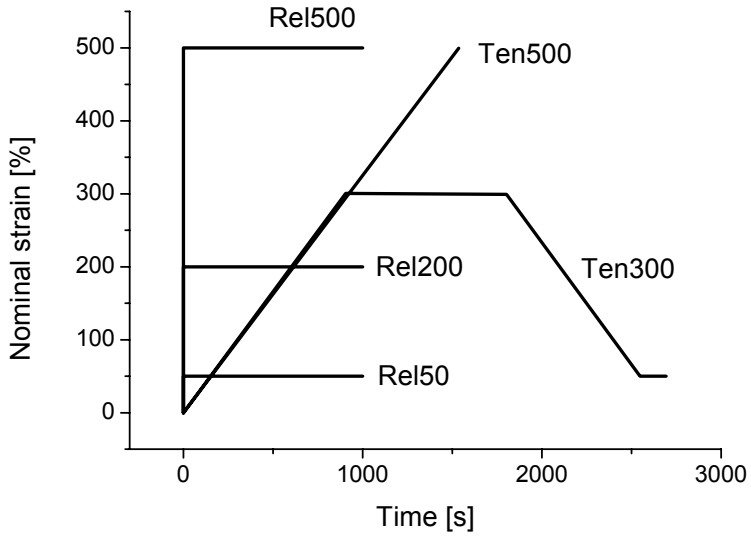

Figure 1. Control profile for the uniaxial tests.

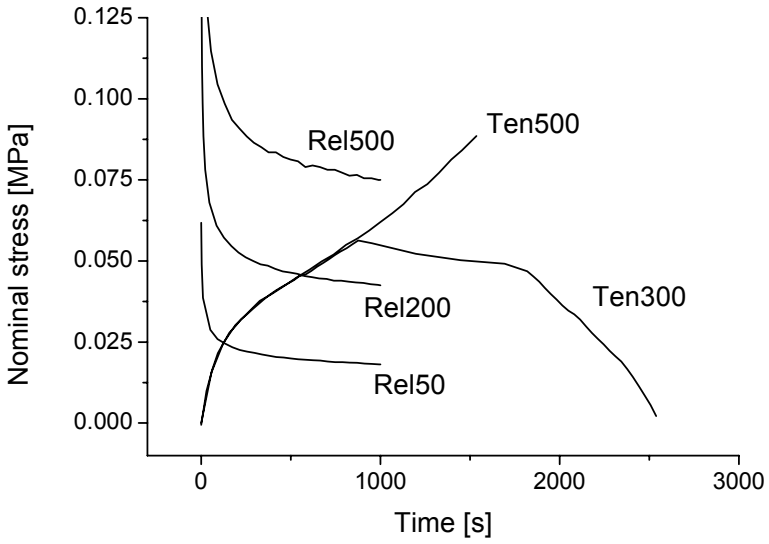

Figure 2. Nominal stress vs. time for the uniaxial experiments

2.3 Experiments with circular actuators

2.3.1 Description of the tests

Multi-axial electromechanical experiments were performed using biaxially prestrained circular actuators (in a so called circular strain test [8]) at room temperature (23° C), see figure 3. The actuators consist of a VHB4910 membrane radially pre-strained and fixed on a circular frame with radius R= 75 mm. A circular area (radius r_0 = 7.5 mm) at the center of the membrane is coated with a mixture of graphite powder (TIMREX SP30, 11 g) and silicone oil (DC 200 / 100 cs, 10 ml) for the electrodes.

Radial pre-straining was realized by a special device developed at the DE laboratory of EMPA for biaxial stretching of elastomeric films. With this machine the pre-stretch ratio λ_p (for the circular actuator: the deformed radial length divided by the undeformed radial length of the membrane) can be arbitrarily prescribed. Three families of actuators were realized with prestretch ratios λ_p = 3, 4 and 5. After radial stretching, the film was fixed uniformly along a circular frame. The circular area at the center of the film was coated with the graphite / silicone electrode on the upper and lower side (electrode thickness: approximately 40 μm). The electrodes were connected to a high voltage supplier through a thin metal wire.

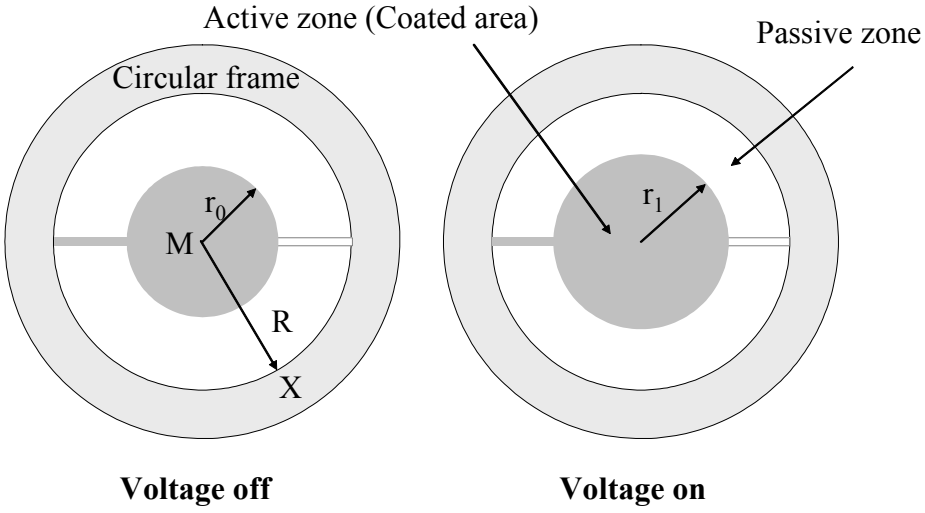

Figure 3. Arrangement of the circular actuator for electromechanical measurements (r_0 = 7.5 mm and R = 75 mm).

The experiment consisted of one single activation cycle in which a constant voltage of 2, 2.5, 3 or 3.5 kV was applied for 900 s. The nominal radial strain $s_r = r_1/r_0 - 1$ of the coated area was measured with a video-extensometer (Ovex ME-46) connected to a PC LabView system for data acquisition and analysis.

A total number of about 40 actuators were used for the present experimental work, with identical conditions of pre-strain and voltage applied to 3 or 4 actuators, in order to evaluate the repeatability of the test results.

2.4 Experimental results

Measurement results are presented in Figure 4, 5 and 6. For each test, the time history of nominal radial strain s_r is reported. For each actuator group with same testing conditions an average strain history curve is calculated which is then used for material modeling, section 3.

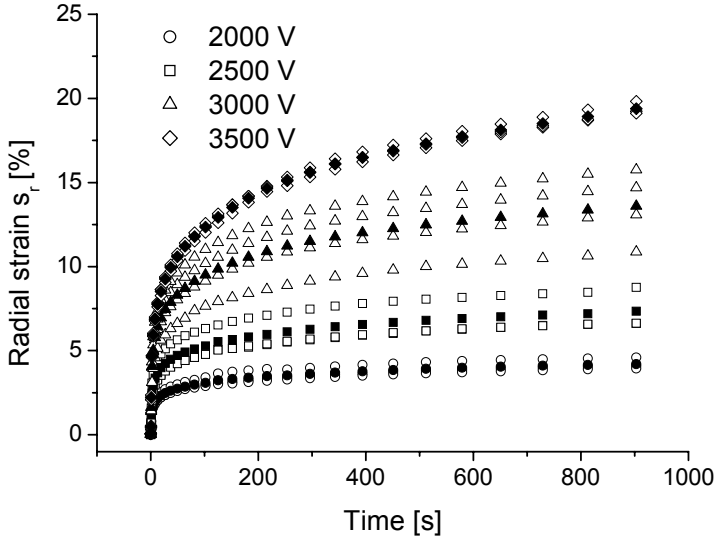

Figure 4. Circular actuator tests at $\lambda_p = 3$. The filled symbols represent the average

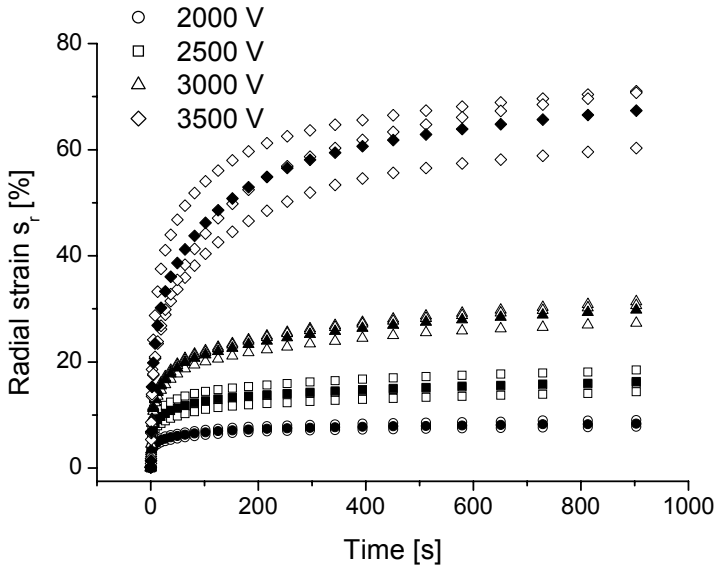

Figure 5. Circular actuator tests at $\lambda_p = 4$. The filled symbols represent the average

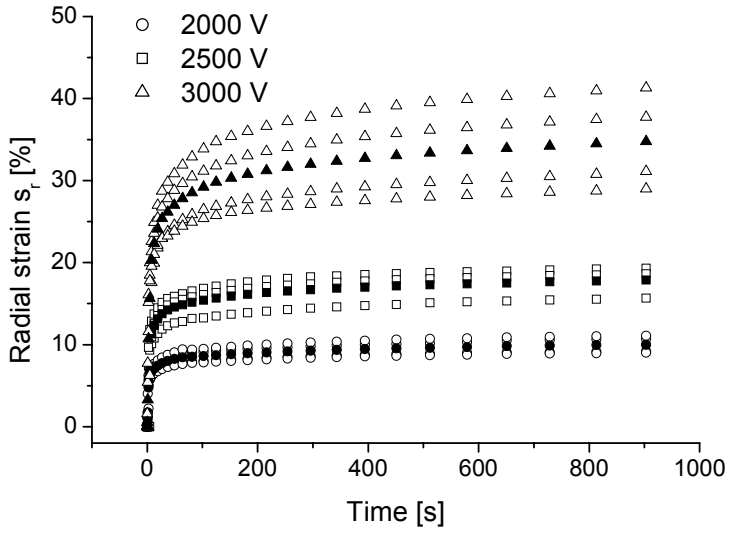

Figure 6. Circular actuator tests at $\lambda_p = 5$. The filled symbols represent the average

Generally, larger scatter is observed for higher activation voltage, with the exception of the three tests at $\lambda_p = 3$, 3500 V. This might be attributed to the in-homogeneity of the electrodes, which is expected to increase at larger deformations. At $\lambda_p = 5$, 3500V the actuators consistently experienced an electric breakdown (no data points available). The largest radial strain values (up to 70%) were measured for $\lambda_p = 4$, 3500V.

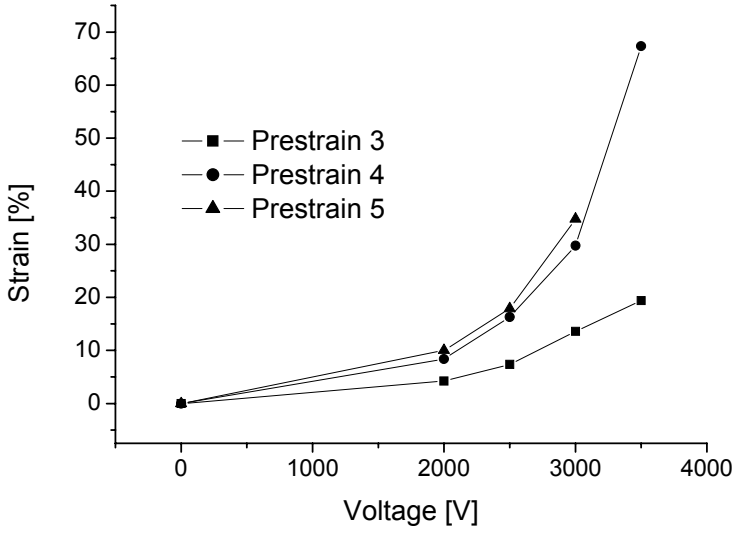

Figure 7. Time vs. strain at the time 900 s

In Figure 7 the average strains measured at the end of the experiment (900 seconds) are plotted as a function of activation voltage. The difference between strains at $\lambda_p = 3$ and $\lambda_p = 4$ is considerably larger than the strain difference between $\lambda_p = 4$ and $\lambda_p = 5$.

This is the consequence of two concurrent effects: The radial deformation depends on (i) the applied electrostatic pressure in thickness direction, and (ii) the stiffness of the membrane. The electrostatic pressure is assumed here to follow eq. (1) (see [1]):

$$p_{el} = \varepsilon_r \cdot \varepsilon_0 \cdot \left(\frac{U}{d}\right)^2 \tag{1}$$

d: membrane thickness, U: voltage, ε_r (4.7 for VHB 4910, [9]): the dielectric constant and ε_0: the vacuum permittivity (8.5×10^{-12} As/Vm). Larger pre-strain leads to a reduction in d, and therefore to a larger electrostatic pressure, for the same activation voltage. On the other hand the material becomes stiffer (larger tangent modulus) at higher values of λ_p so that lower radial strains are obtained for the same electrostatic pressure.

3 Material modeling

The demands on a constitutive model describing the mechanical response of the elastomer in the experiments of section 2 are challenging. Non-linear three dimensional constitutive models have to be formulated and material parameters determined in order to describe the time dependent mechanical response over a wide deformation range: uniaxial stretch up to $\lambda = 6$, biaxial deformation (from a kinematical point of view, a circular DE actuator is akin to a biaxial test) at different pre-strain and voltage levels.

These challenges correspond to two classical problems of material modeling: (i) the model must be capable to describe the large strain response in uniaxial as well as multiaxial loading conditions; (ii) the time dependent component of the model must be capable to describe the deformation history in force controlled experiments as well as the stress history under displacement controlled loading conditions.

Further challenges are related to the electromechanical coupling in DE: (i) prediction of the mechanical loading as function of the applied voltage; (ii) influence of the electrodes on the electromechanical performance; (iii) simulation of the active behavior by numerical methods (finite elements).

3.1 Constitutive models

The quasilinear viscoelastic model proposed by Fung [10] and applied already for DE modeling in [6] is used here. It comprises hyperelastic equations (for the large strain elastic response) and a viscoelastic dissipative component (describing the time

dependence of the mechanical response). For the hyperelastic part three different model formulations are investigated: the strain energy potentials of Yeoh [11], Ogden [12] and Arruda-Boyce [13]. Incompressible material behavior is assumed for all three formulations.

The Yeoh form describes the strain energy function W as:

$$W = C_{10}(I_1 - 3) + C_{20}(I_1 - 3)^2 + C_{30}(I_1 - 3)^3 \tag{2}$$

C_{10}, C_{20} and C_{30} are material parameters. I_1 can be calculated from the eigenvalues of the deformation gradient tensor, i.e. the so called principal stretch ratios λ_i (i=1,2 and 3) as

$$I_1 = \lambda_1^{\,2} + \lambda_2^{\,2} + \lambda_3^{\,2} \tag{3}$$

The Ogden model is characterized through the following strain energy potential with material parameters μ_i and α_i:

$$W = \sum_{i=1}^{n} \frac{\mu_i}{\alpha_i}(\lambda_1^{\,\alpha_i} + \lambda_2^{\,\alpha_i} + \lambda_3^{\,\alpha_i}) \tag{4}$$

A strain energy function with three terms (n=3) is used here.

The strain energy form of Arruda-Boyce is based on statistical mechanics and includes only two material parameters (A and N), which can be related to properties of the elastomer microstructure:

$$\begin{aligned} W = A \cdot \Bigg[& \frac{1}{2}(I_1 - 3) + \frac{1}{20N}(I_1^{\,2} - 9) + \frac{11}{1050N^2}(I_1^{\,3} - 27) \\ & + \frac{19}{7000N^3}(I_1^{\,4} - 81) + \frac{519}{673750N^4}(I_1^{\,5} - 243) \Bigg] \end{aligned} \tag{5}$$

The time dependence of the mechanical response is described by assuming time dependent coefficients in the strain energy functions. The corresponding time functions are defined through the relaxation function g(t):

$$g(t) = 1 - \sum_{k=1}^{K} g_k \cdot (1 - \exp(-\frac{t}{t_k})) \tag{6}$$

where g_k and t_k characterize the relaxation behavior. Here K is chosen as 4. For a specific material the quasi-linear viscoelastic model is appropriate when the relaxation function g(t) is independent of the applied strain. The uniaxial relaxation tests (section 2) were used to confirm the validity of this assumption for VHB 4910 [6]. The stress - deformation behavior for arbitrary loading histories is calculated through so called

hereditary integrals. Further details on the quasi-linear viscoelastic model are described in [6].

3.2 Finite element calculations and constitutive model parameters

Material parameters (the parameters of the strain energy functions and of the relaxation function) were determined by fitting the experimental results of the circular actuator experiments with activation voltage of 2 kV, at λ_p = 3, 4 and 5. The resulting constitutive models were then applied for predicting the response of the other circular actuator tests (with higher voltages) and uniaxial tests.

In [7] an analytical model is presented for analyzing the circular actuator test in case of purely elastic material behavior. The problem cannot be solved analytically when the time dependence of the material response is considered. For this reason, a finite element simulation of the experiment has been used for the determination of the material parameters from the circular actuator tests.

The software ABAQUS 6.5.1 [14] has been used for the calculations. The axisymmetric model consists of 4-node elements (CAX4H: 4-node bilinear axisymmetric quadrilateral, hybrid, constant pressure). Subsequent mesh refinement was introduced (with higher mesh density at the extremity of the active zone) in order to avoid artifacts due to discretization errors. The model considers a symmetry plane in the horizontal direction (Figure 8). The axis of rotational symmetry is perpendicular to the membrane plane and passes through the centre of the coated area, see Figure 3. The electromechanical pressure p_{el} acts on the active zone and depends on the current membrane thickness and the activation voltage, according to eq. 1.

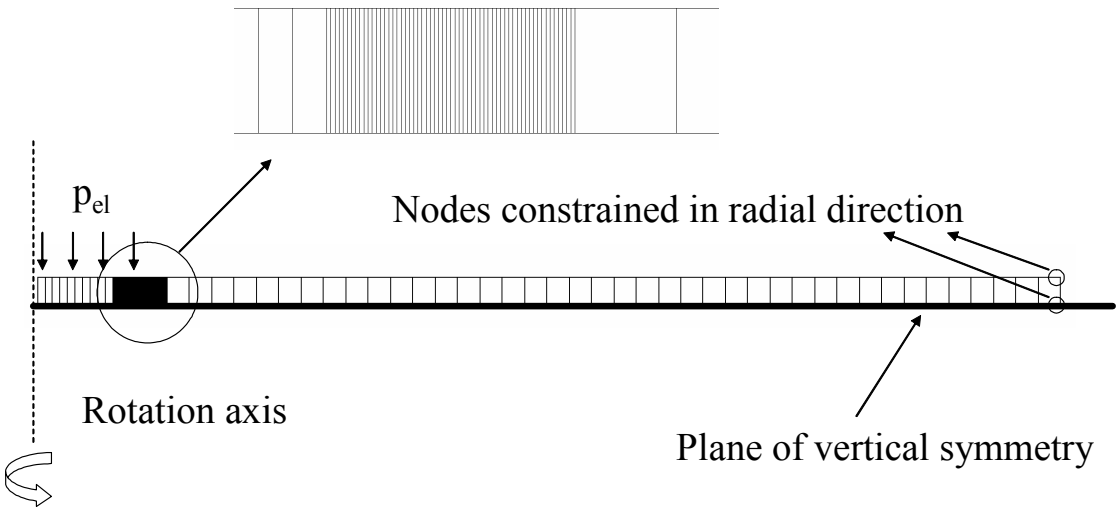

Figure 8. Finite element model of a circular dielectric elastomer actuator

In [6] a finite element calculation of the circular actuator behavior was proposed in which the measured radial displacement of the active zone is imposed as kinematic boundary condition (by prescribing the membrane thickness variation); in those simulations the corresponding "required" activation voltage represent the result of the calculation, to be compared with the experimental activation voltage. Here a novel approach is proposed in which the activation voltage is the input and the time history of the radial strain the output of the calculation. Two approaches were implemented to this end:

a) the straight forward approach consists of applying the electromechanical pressure p_{el} as a 'surface pressure'. Due to thickness reduction during the activation process, the amplitude of the pressure (for a given activation voltage) changes according to eq. 1. The corresponding evolution of the amplitude of p_{el} is defined by a Fortran code (in a so called "user subroutine") which calculates the current pressure as a function of the current thickness d and the activation voltage U (which is constant for each experiment). The main disadvantage of this approach is that a large displacement analysis with kinetic (force) boundary conditions requires considerably larger number of iterations (and in certain cases does not converge) as compared with a calculation with kinematic (displacement) boundary conditions.

b) this approach aims at realizing the same loading history by applying kinematic boundary conditions: the vertical displacement u_v of the nodes at the upper border of the active zone is prescribed in order to achieve (at the upper face of the coated zone) a stress component in vertical direction equal to current value of p_{el} (depending on the activation voltage and the current membrane thickness). The vertical displacement u_v is controlled using a Fortran code (embedded in a user subroutine): the velocity change Δv for the current calculation increment is defined as

$$\Delta v = 0.2 \cdot \frac{U_{pres} - U_{calc}}{abs(U_{pres} - U_{calc})} \cdot v \tag{7}$$

where v: velocity in the previous increment, U_{pres} is the prescribed activation voltage (e.g. 2 kV), and U_{calc} is the calculated activation voltage of the previous increment, based on the values of vertical stress and thickness according to eq. 1. In this way, the vertical displacement u_v is continuously adjusted in order to minimize the discrepancy between the prescribed activation voltage and the current voltage level.

Procedure (b) provides considerable advantages in terms of calculation times and convergence. However, this control procedure leads to an unstable behavior when dealing with the sudden (stepwise) change of the activation voltage at the beginning of

the test: for this reason procedure (a) was applied in the initial phase (20 sec.) and procedure (b) for the remaining duration of the active phase (880 sec.).

In Figure 9 an example is shown of the performance of the proposed procedure (Yeoh model, λ_p=4) The applied voltage is compared with the constant prescribed activation voltage during the active phase. The discrepancy is larger for higher voltage level, but overall the agreement is satisfactory.

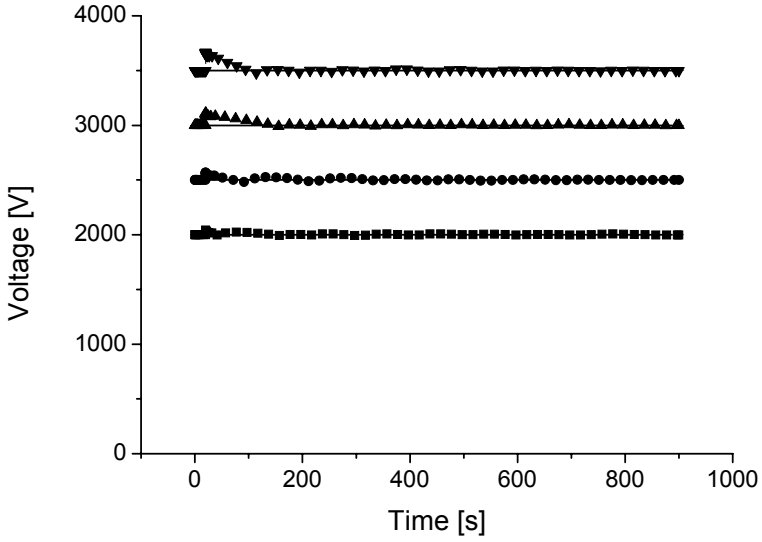

Figure 9. Comparison of realized (symbols) and experimentally prescribed (horizontal line) activation voltages for the finite element calculation of the circular actuator (example with λ_p=4).

The simulation of one experiment consists of four steps: (i) radial pre-strain; (ii) hold time of 1 h (with stress relaxation, corresponding to the experiments); (iii) application of the activation voltage step according to procedure (a); (iv) control of the constant voltage level according to procedure (b).

The material parameters for the quasilinear visco-hyperelastic behavior are determined using an optimization procedure (described schematically in Figure 10) which is programmed to run automatically in Matlab [15]. Starting with initial material parameters as a vector X_0 Matlab writes an ABAQUS input file with these material parameters. The components of X_0 are the material parameters of the strain energy function (C_{ij} for Yeoh, μ_i, α_i for Ogden and A, N for Arruda-Boyce) and the relaxation function parameters (t_k and g_k). Matlab calls ABAQUS to run the simulation with the material parameters X_0. When the simulation is completed the ABAQUS results (calculated strain history) are extracted and compared with the experimental strain history. Next, the error function f (eq. 8) is calculated.

$$f(X) = \sum f_i^{\,2} = \sum (s_c(X) - s_e)_i^{\,2} \tag{8}$$

f depends on the material parameters (vector X) and is defined as the sum of the squares of the differences f_i between the calculated strains s_c and the experimental strains s_e. The optimization function fminsearch (in Matlab) is based on the Nelder-Mead-Simplex algorithm and changes the material parameters (vector X) in order to find a minimum of f. The whole procedure is repeated until the minimum of f is found.

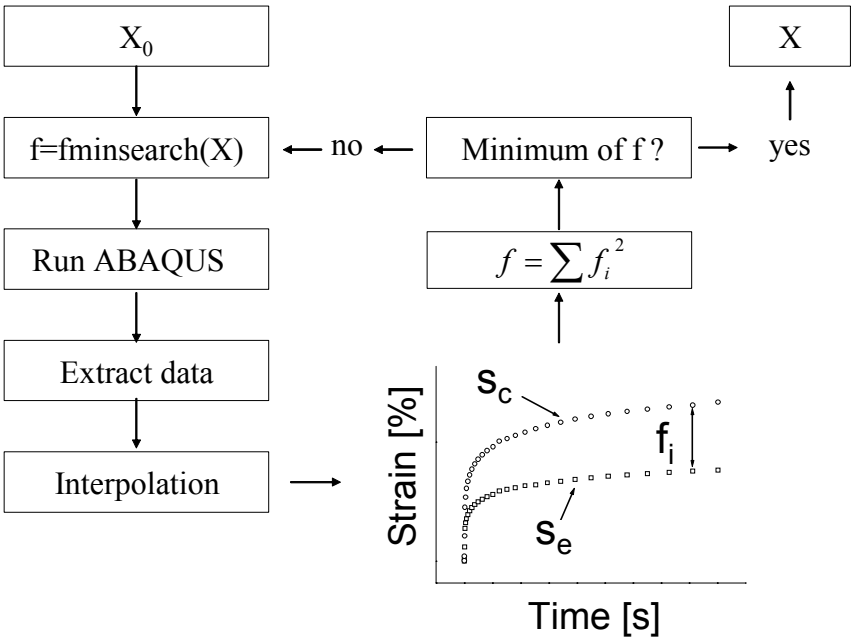

Figure 10. Optimization procedure for evaluation of the material parameters

The results of the combined optimization for the circular actuator tests at 2 kV, with λ_p = 3, 4 and 5 are given in Figure 11.

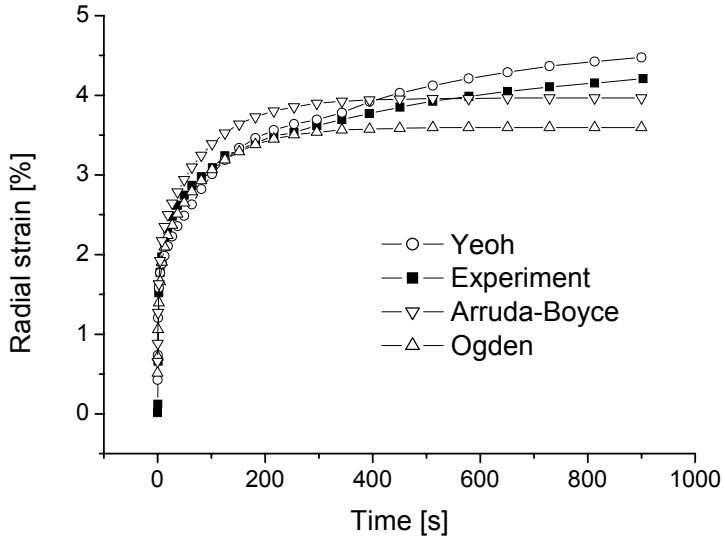
Radial strain [%]
Time [s]
Yeoh
Experiment
Arruda-Boyce
Ogden

(i)

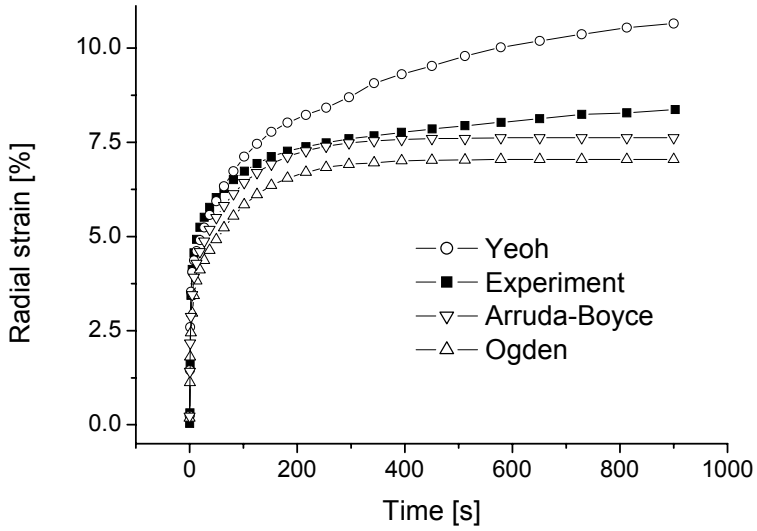
Radial strain [%]
Time [s]
Yeoh
Experiment
Arruda-Boyce
Ogden

(ii)

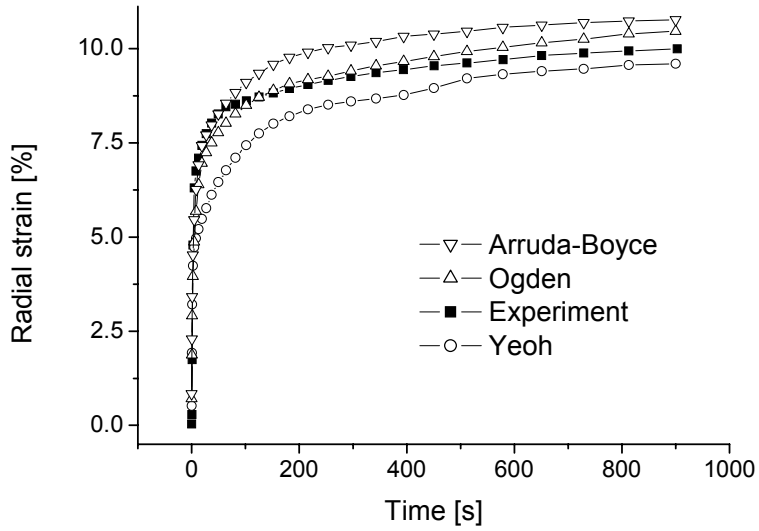

(iii)

Figure 11. Optimization of the three models (Yeoh, Ogden and Arruda-Boyce) for 2 kV: (i) $\lambda_p = 3$; (ii) $\lambda_p = 4$; (iii) $\lambda_p = 5$.

The material parameters obtained through the optimization procedure are reported in Tables 1 and 2.

Table 1. Optimized hyperelastic material parameters

Yeoh	C_{10} [MPa]	C_{20} [MPa]	C_{30} [MPa]			
	0.0827	-0.000747	5.86e-6			
Ogden	μ_1 [MPa]	α_1 [-]	μ_2 [MPa]	α_2 [-]	μ_3 [MPa]	α_3 [-]
	0.00858	1.293	0.0843	2.3252	-0.0233	2.561
Arruda-Boyce	A [MPa]	N [-]				
	0.0686	124.88				

Table 2. Optimized parameters of the relaxation function

	g_1 [-]	t_1 [s]	g_2 [-]	t_2 [s]	g_3 [-]	t_3 [s]	g_4 [-]	t_4 [s]
Yeoh	0.478	0.153	0.205	0.464	0.0727	32.021	0.0492	215.85
Ogden	0.534	0.357	0.134	3.254	0.0495	46.11	0.0290	476.75
Arruda-Boyce	0.452	0.341	0.144	2.326	0.0746	33.07	0.0215	313.8

3.3 Comparison of simulations and experimental results

The radial strain histories calculated with the parameters of Tables 1 and 2 for the whole experimental range of circular actuator tests are reported in Figures 12 to 14 for the different constitutive model formulations.

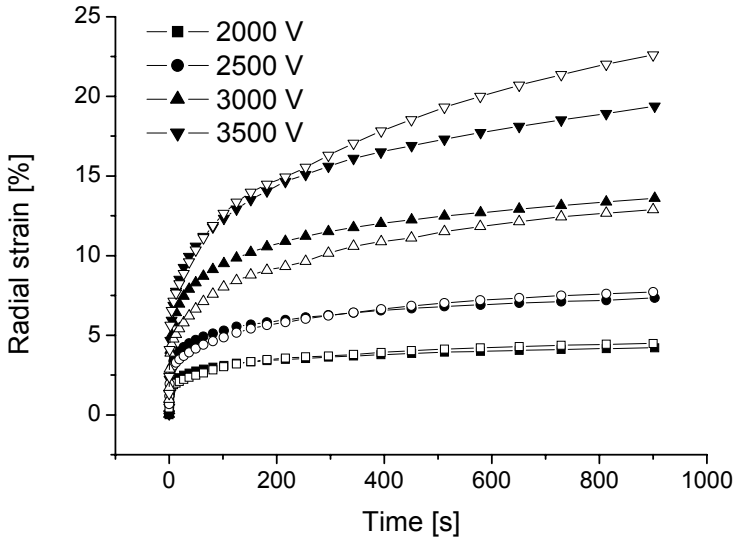

(i)

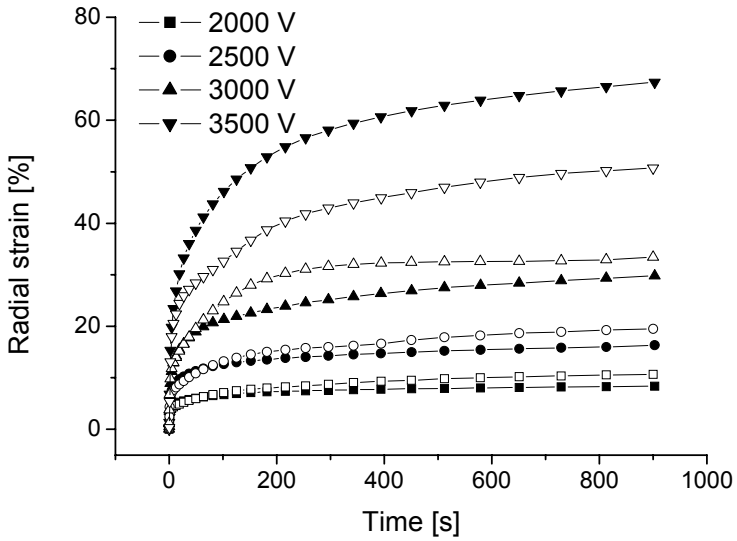

(ii)

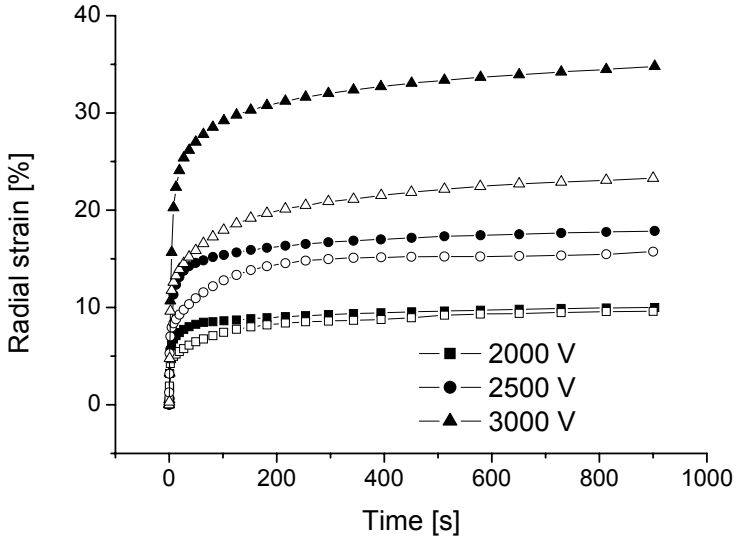

(iii)

Figure 12. Comparison between experimental data and simulation for the Yeoh model for prestrain $\lambda_p = 3$ (i), $\lambda_p = 4$ (ii) and $\lambda_p = 5$ (iii). The filled symbols represent the experimental data and the open symbols the corresponding simulation.

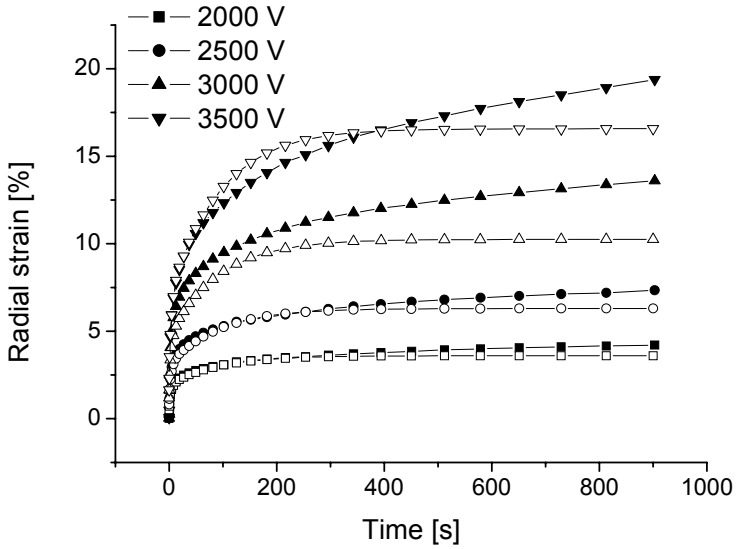

(i)

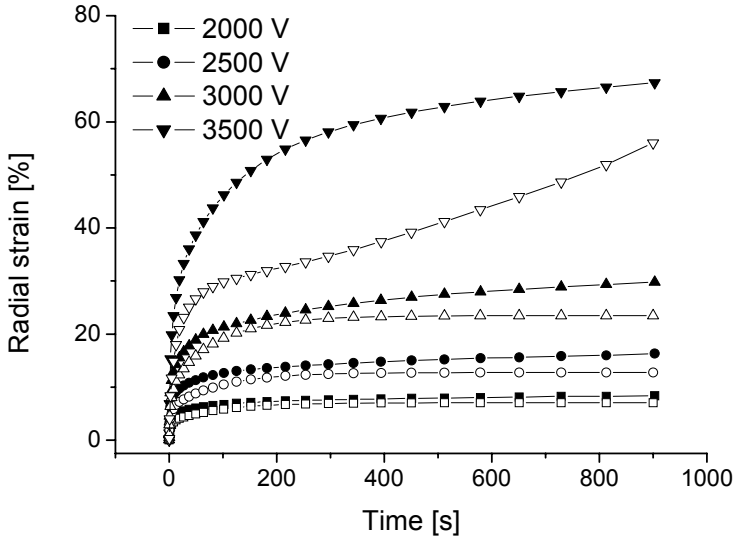

(ii)

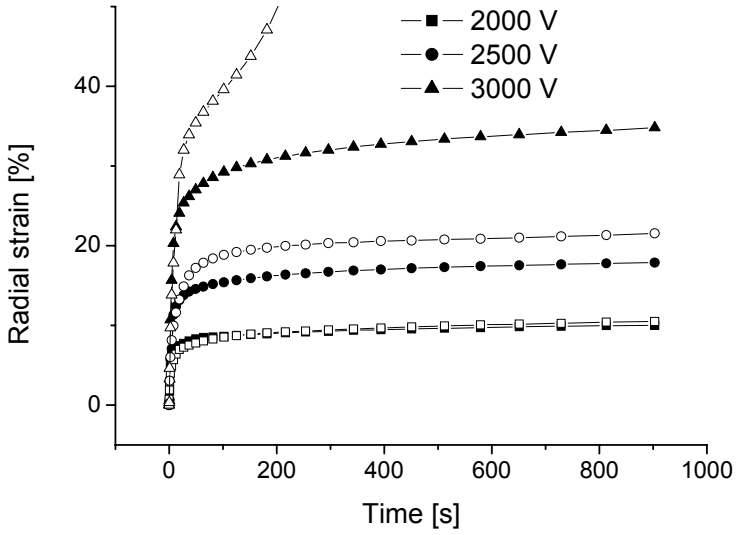

(iii)

Figure 13. Comparison between experimental data and simulation for the Ogden model for prestrain $\lambda_p = 3$ (i), $\lambda_p = 4$ (ii) and $\lambda_p = 5$ (iii). The filled symbols represent the experimental data and the open symbols the corresponding simulation.

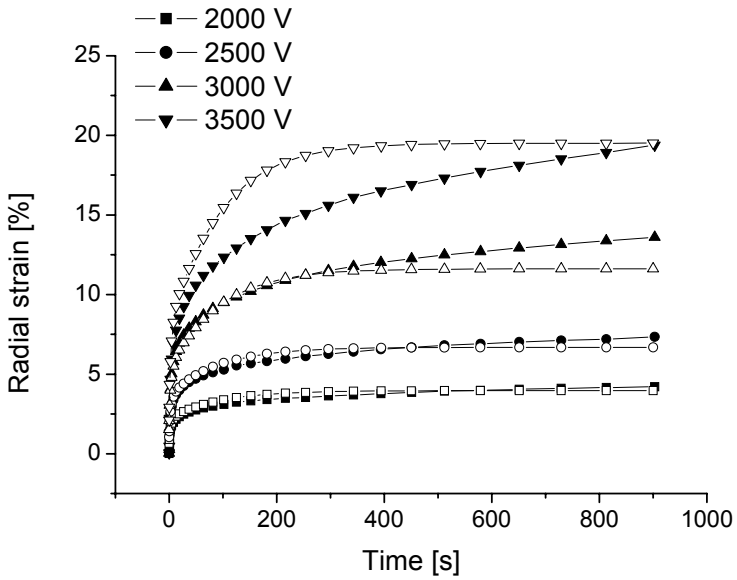
2000 V
2500 V
3000 V
3500 V
Radial strain [%]
Time [s]
0
5
10
15
20
25
0
200
400
600
800
1000

(i)

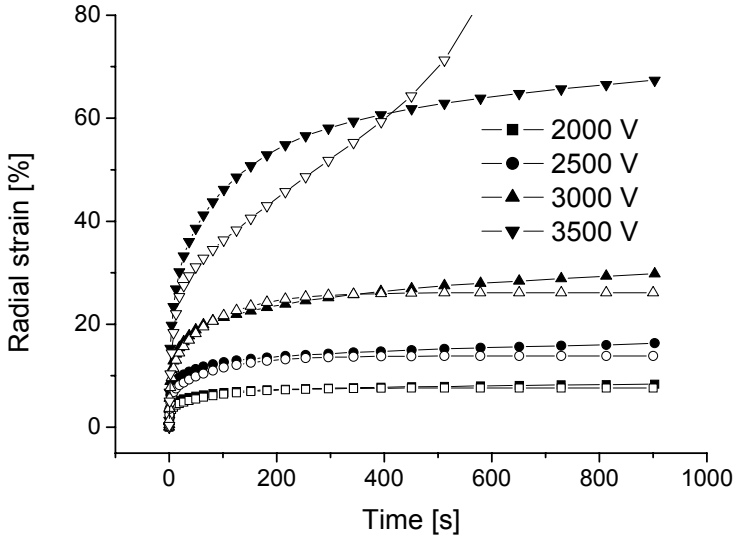
2000 V
2500 V
3000 V
3500 V
Radial strain [%]
Time [s]
0
20
40
60
80
0
200
400
600
800
1000

(ii)

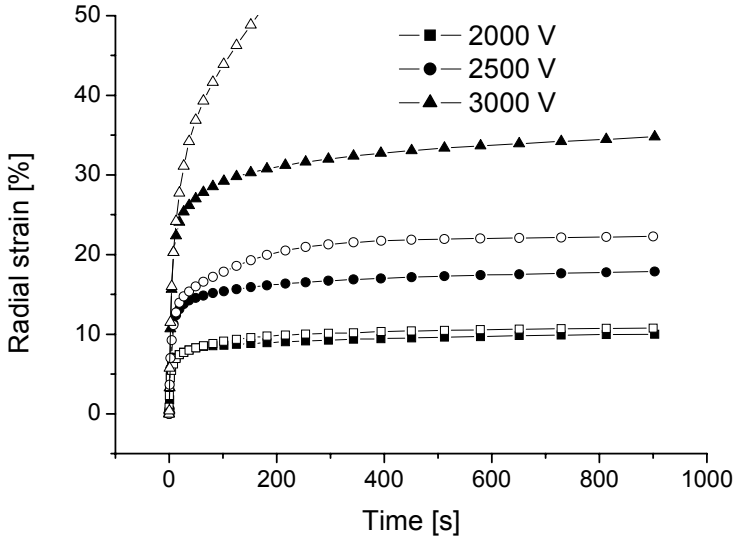

(iii)

Figure 14. Comparison between experimental data and simulation for the Arruda-Boyce model for prestrain $\lambda_p = 3$ (i), $\lambda_p = 4$ (ii) and $\lambda_p = 5$ (iii). The filled symbols represent the experimental data and the open symbols the corresponding simulation.

The corresponding predicted uniaxial behavior for the different models are compared with the experimental data in Figures 15 to 17. The uniaxial test simulation was performed according to the procedure described in [6].

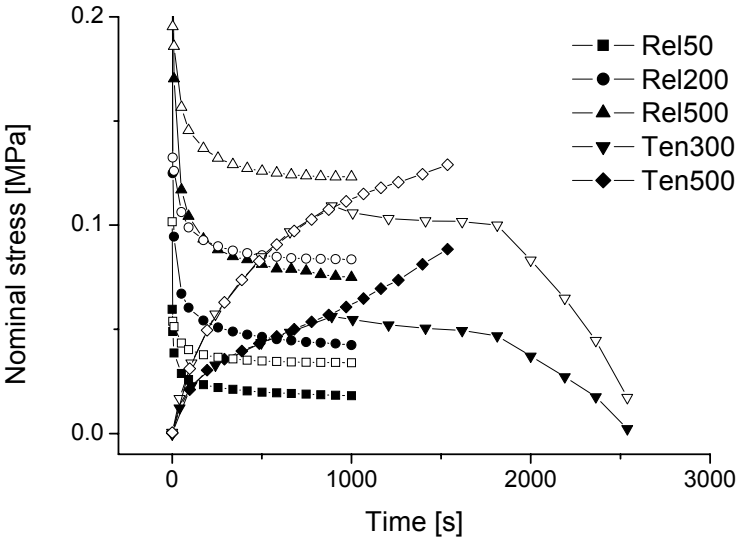

Figure 15. Uniaxial behavior: experimental data (filled symbols) compared to the Yeoh model simulation (open symbols).

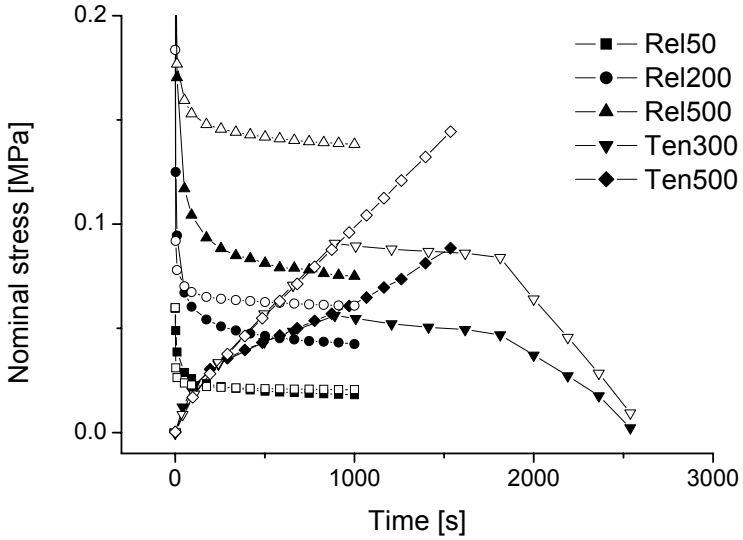

Figure 16. Uniaxial behavior: experimental data (filled symbols) compared to the Ogden model simulation (open symbols).

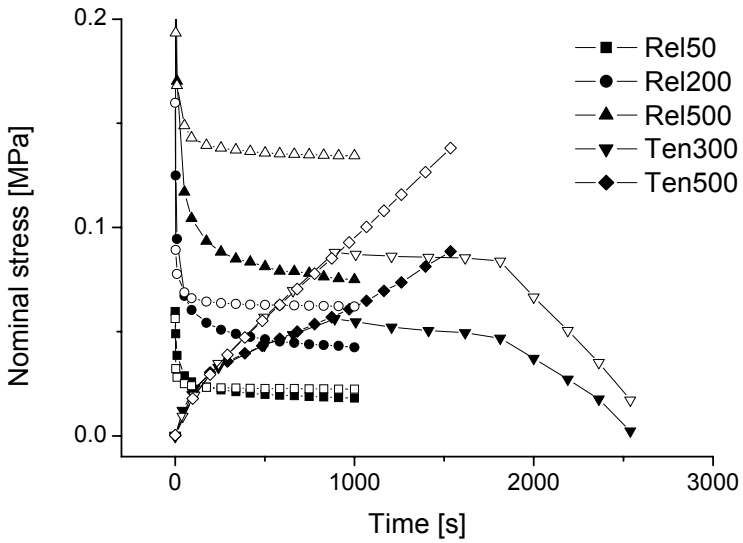

Figure 17. Uniaxial behavior: experimental data (filled symbols) compared to the Arruda-Boyce model simulation (open symbols).

4 Discussion

The predictive capabilities of the three different models used in the present work can be evaluated from the results of section 3.3. All three models show reasonable agreement with respect to the actuator behavior, whereas the correspondence between experiment and simulation for the uniaxial test is not satisfactory. Obviously, an

optimization procedure that would include all the uniaxial tests could lead to improved correspondence for these experiments (but probably to worse predictive capabilities in the biaxial tests).

A comparison of the radial strain predicted by the different models at the end of the active phase (900 sec) and the corresponding scatter band of the experimental values is reported in Figures 18.

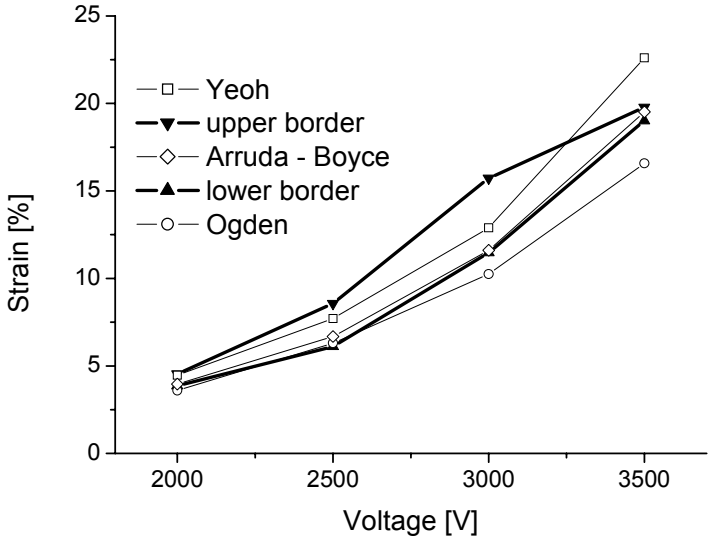

(i)

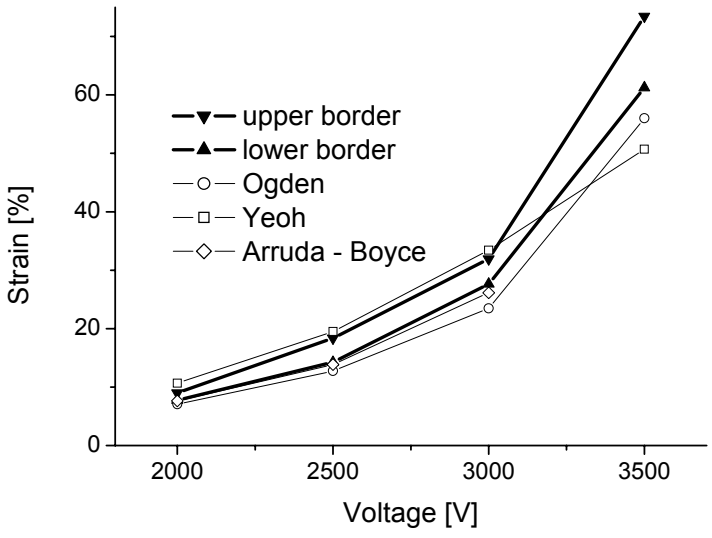

(ii)

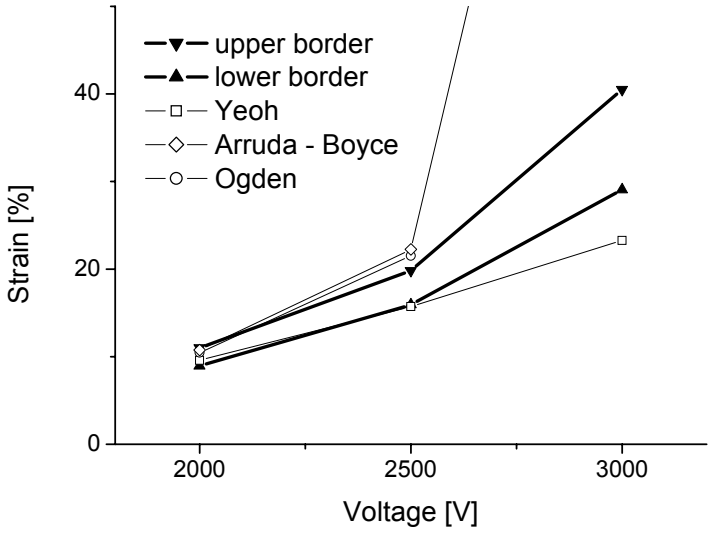

(iii)

Figure 18. Comparison between simulation and experimental values (with scatter band) for the strain at 900 s for λ_p= 3 (i), λ_p= 4 (ii) and λ_p= 5 (iii)

In case of λ_p=4 and 5, at higher activation voltages the discrepancy between simulation and experimental data is larger. This might be considered as a limitation of the proposed constitutive model. At this deformation level, however, the scatter in the test data is quite large and in certain cases electric breakdown occurred. It is possible that in-homogeneities in the electrodes or in the thickness distribution influence the actuator behavior to such extent that the electromechanical coupling might not be correctly described by eq. 1.

Mechanical instability (one possible failure mode of DE actuators, see [7]) is predicted in certain calculations (Arruda-Boyce-model at λ_p=4, 3.5 kV, Ogden model at λ_p=5, 3. kV). The Arruda-Boyce-model at prestrain λ_p=5, 3 kV converges, but the radial strain reaches a value of 120 %.

It is noteworthy that the Arruda-Boyce model shows good predictive capabilities despite the lower number of material parameters available as degree of freedom for the optimization procedure.

4.1.1 Cyclic behavior

An additional experiment with a circular actuator has been performed in order to evaluate the predictive capabilities of the proposed quasi-linear viscoelastic model in case of cyclic behavior. The actuator was activated with a voltage of 3 kV over a time

period of 240 seconds and then deactivated for 60 seconds. The cycle was repeated 75 times.

The quasi-linear viscoelastic model leads to excellent predictions when fitted to one specific pre-strain and voltage level, as demonstrated by the comparison between simulation (here a Yeoh model) and measured radial strain history for the first cycle of this experiment, Figure 19.

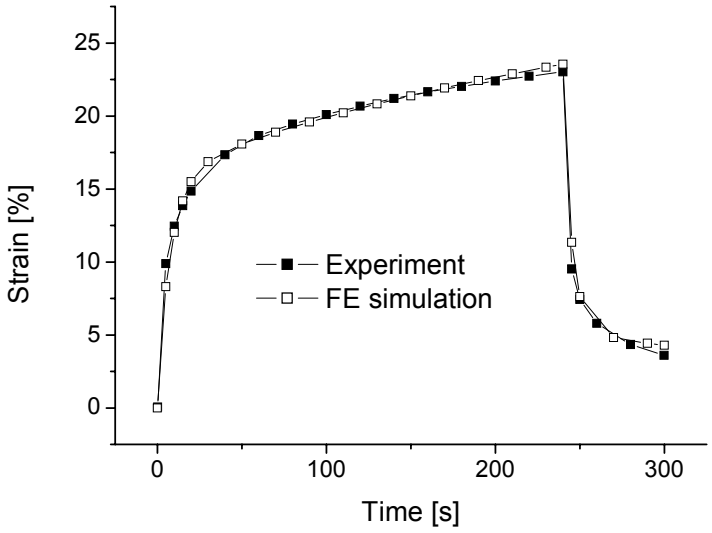

Figure 19. Calculated and measured radial strain history of the first cycle (Yeoh model)

Simulation of the radial strain for the whole cyclic history of the experiments shows an increasing discrepancy with respect to the measurements, Figure 20.

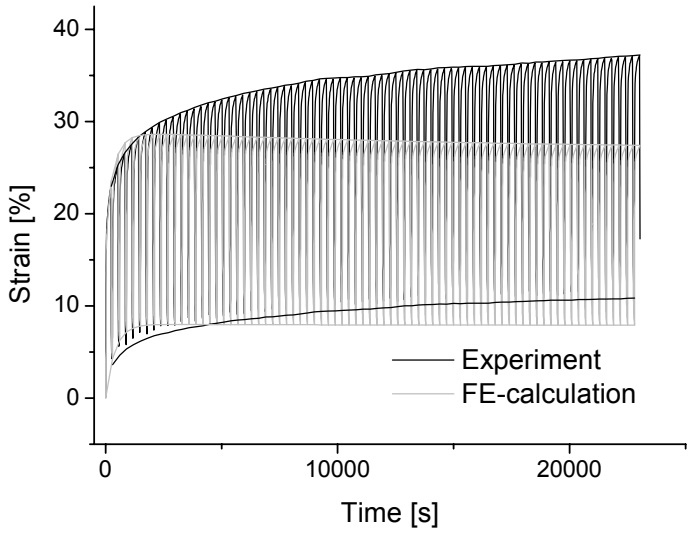

Figure 20. Cyclic behavior: experiment and simulation of 75 cycles

The progressive increase in the maximum radial strain observed in the experiments cannot be reproduced by the simulation with the quasi-linear viscoelastic model. This increase might be attributed to changes in the mechanical response of the elastomer due to the loading history, which could be described with a viscoplastic constitutive model with internal variables (and corresponding evolution equations). Further experiments (with different voltage range, frequencies and pre-strain level) will help understanding whether this observation is related to material degradation or to temperature effects influencing the material response and the electromechanical behavior.

5 Conclusions

The mechanical behavior of the acrylic elastomer VHB 4910 used in DE actuators has been investigated. Next to force and displacement controlled uniaxial data, experimental observations from tests with 40 circular actuators are reported. The activation behavior for different prestrain levels and at different activation voltages is presented. Multiple tests at same prestrain and voltage levels allow evaluating the scatter of the electromechanical response obtained from virtually identical actuators. The experimental data presented in section 2 represent a unique collection that can be used for material and actuator modeling purposes.

The numerical procedure adopted for simulating the electromechanical behavior of the circular actuator allowed determining material model parameters from the experimental data through an optimization algorithm. The novel approach proposed for electromechanical coupling might be generally useful for finite element simulations of DE actuators.

Three different constitutive model formulations were used and compared in their predictive capabilities. It is noteworthy that the Arruda-Boyce model, having only 2 parameters for describing the three dimensional hyperelastic response, leads to comparable matching as the Yeoh and Ogden models. Model parameters were determined from a subset of circular actuator tests and then applied for simulating the whole range of experiments performed. Since the prediction of the circular actuator behavior was satisfactory, the proposed models might provide useful results for actuator design and optimization purposes.

On the other hand, large discrepancies were obtained between the uniaxial data and the corresponding simulations for all three model formulations. This mismatch represents a limitation of the proposed models, which is related to the problem of describing the time dependent material response over a wide range of uniaxial and multiaxial

deformation states and with force or displacement controlled experiments. Further limitations of the proposed quasi-linear viscoelastic constitutive models have been demonstrated when applied for predicting the multicycle actuator behavior.

Acknowledgements

Financial support from the Swiss National Science Foundation (Project 200021-107661/1) is gratefully acknowledged.

6 References

[1] R.E. Pelrine, R.D. Kornbluh, J.P. Joseph, Electrostriction of polymer dielectrics with compliant electrodes as a means of actuation, Sens. Actuators, A 64 (1998) 77-85

[2] R. Kornbluh, R. Pelrine, Q. Pei, S. Oh, J. Joseph, Ultrahigh strain response of field-actuated elastomeric polymers, Proc. SPIE, 3987 (2000) 51-64

[3] R. Pelrine, P. Sommer-Larsen, R. Kornbluh, R. Heydt, G. Kofod, Q. Pei, P. Gravesen, Applications of dielectric elastomer actuators, Proc. SPIE, 4329 (2001) 335-349

[4] X. Zhang, C. Löwe, M. Wissler, B. Jähne, G. Kovacs, Dielectric elastomers in actuator technologies, Advanced Materials Engineering, 7, No.5, (2005) 361-367

[5] Y. Bar-Cohen, Electroactive Polymer (EAP) Actuators as Artificial Muscles - Reality, Potential and Challenges, vol. PM98, SPIE Press, Washington, 2001

[6] M. Wissler, E. Mazza, Modeling and simulation of dielectric elastomer actuators, Smart Materials and Structures, 14 (2005) 1396 - 1402

[7] M. Wissler, E. Mazza, Modeling of a prestrained circular actuator made of dielectric elastomers, Sens. Actuators, A 120 (2005), 184-192

[8] R. Pelrine, R. Kornbluh, Q. Pei, J. Joseph, High-speed electrically actuated elastomers with strain greater than 100%, Science, 287 (2000) 836-839

[9] G. Kofod, P. Sommer-Larsen, R. Kornbluh, R. Pelrine, Actuation response of polyacrylate dielectric elastomers, J. Intel. Mat. Syst. Str., 14 (2003) 787-793

[10] Y.C. Fung, Biomechanics. Mechanical properties of living tissues, 2nd edn., Springer-Verlag, New York, 1993, p. 277

[11] O.H. Yeoh, Characterization of elastic properties of carbon-black-filled rubber vulcanizates, Rubber Chem. Technol., 63 (1990) 792-805

[12] R.W. Odgen, Large deformation isotropic elasticity – on the correlation of theory and experiment for incompressible rubberlike solids, Proc. R. Soc. Lond., A 326 (1972) 565-584

[13] E.M. Arruda, M.C. Boyce, A three-dimensional constitutive model for the large stretch behavior of rubber elastic materials, J. Mech. Phys. Solids, 41, No.2 (1993) 389 - 412

[14] ABAQUS/Standard Manual, 2003. Version 6.4.1, Hibbitt, Karlsson & Sorensen, Inc.

[15] Matlab 7.0, 2004, The MathWorks, Inc.

3.4 Article 4

This section contains a reprint of the article:

M. Wissler and E. Mazza, Electromechanical coupling in dielectric elastomer actuators, submitted to Sensors and Actuators A

Background motivation: In article 3, the agreement between experiments and simulations was shown to be reasonable for the actuator behavior but not for the uniaxial behavior. This might be the consequence of the electromechanical coupling not being adequately described by Pelrine's equation (eq. (1.1)). Therefore, the electromechanical coupling was evaluated both analytically and numerically. Further, the dielectric constant was measured at different prestrains and spring roll experiments were carried out for an overall verification.

Summary of methods: Energy considerations were performed analytically and numerically for a circular actuator. For the analytical investigation, an energy balance was used for determining the electrostatic pressure. An electrostatic analysis which also took into account the electrodes was performed with COMSOL Multiphysics. The capacity and the thickness of the film were measured at different prestrain levels and the dielectric constant was determined. Six spring rolls were fabricated. The force difference was measured in an experiment where the elongation of the spring roll was constrained.

Summary of results: Results show that analytical and numerical considerations are consistent. The latter provide a new physical interpretation of the electrostatic forces acting on the DE film, with contributions from in-plane and out-of-plane stresses. Pelrine's equation is confirmed by superposition of a hydrostatic stress state. The value of the dielectric constant decreases with increasing pre-stretch ratio, from 4.7 for the un-stretched film, down to 2.6 for an equi-biaxial prestrain with λ_p=5. Spring roll measurements confirm a value of 3.2 at prestrain λ_p=4.

Main conclusions, link to the next section: The equation proposed by Pelrine was verified theoretically and experimentally. The dielectric constant is about 3.2 and not 4.7 for a relevant prestrain of 4. With the modified dielectric constant, uniaxial simulations agree to a great extent to the corresponding experiments without loss of predictability of the actuator behavior (see article 3).

Electromechanical coupling in dielectric elastomer actuators

Michael Wissler[1,2] and Edoardo Mazza[2,1]

[1] Swiss Federal Laboratories for Materials Testing and Research (EMPA), 8600 Dübendorf, Switzerland
[2] Swiss Federal Institute of Technology (ETH), Dept. of Mechanical Engineering, 8092 Zürich, Switzerland

Abstract

In this paper the electromechanical coupling in dielectric elastomer actuators is investigated. An equation proposed by Pelrine et al. (Sensors and Actuators, A 64, 1998) is commonly used for the calculation of the electrostatic forces in dielectric elastomer systems. This equation is analyzed here with (i) energy consideration and (ii) numerical calculations of charge and force distribution. A new physical interpretation of the electrostatic forces acting on the dielectric elastomer film is proposed, with contributions from in-plane and out-of-plane stresses. Representation of this force distribution using Pelrine's equation is valid for an incompressible material, such as the acrylic elastomer VHB 4910. Experiments are performed for the measurement of the dielectric constant ε_r of the acrylic elastomer VHB 4910 for different film deformations. The values of ε_r are shown to decrease with increasing pre-stretch ratio λ_p, from 4.7 for the un-stretched film, down to 2.6 for equi-biaxial deformation with λ_p=5. This result is important in that it corrects the constant value of 4.7 largely applied in literature for pre-stretched dielectric elastomer actuator modeling. With the results of this work the predictive capabilities of a model describing the three-dimensional passive and active actuator behavior are remarkably improved.

Keywords: Electromechanical coupling, dielectric elastomer, dielectric constant, actuator, modeling.

1 Introduction

Actuators made of dielectric elastomers (DE) consist of a compliant capacitor, with a thin soft elastomer film sandwiched between two compliant electrodes [1, 2]. Application of a voltage leads to electrostatic forces that deform the elastomer membrane, which contracts in the thickness direction and expands in the film plane. This in-plane expansion is exploited to generate motion or forces. Dielectric elastomers actuators transform electrical energy directly into mechanical work and are able to generate in-plane deformations of up to 30% with respect to the un-activated configuration. They belong to the group of so called electroactive polymers (EAP).

Modeling and simulation of DE systems are key steps in the design and optimization of DE actuators. Challenges thereby are represented by the description of (i) the passive mechanical behavior of the elastomers (with large strains, time and history dependence of the mechanical response) and (ii) the mechanical forces generated by the electric field, i.e. what is often referred to as "electromechanical coupling". Significant work has been performed for the mechanical characterization of the elastomers [3-8], whereas only few papers exist on electromechanical coupling.

Electromechanical coupling is commonly described using a model proposed by Pelrine et al. [1]. In this model electrostatic forces are assumed to act in the direction perpendicular to the insulating elastomer film, and their magnitude is characterized by p_{el}, the so called "electrostatic pressure". p_{el} is calculated for a given applied voltage U and film thickness z as

$$p_{el} = \varepsilon_0 \cdot \varepsilon_r \cdot \frac{U^2}{z^2} = \varepsilon_0 \cdot \varepsilon_r \cdot E^2 \tag{1}$$

Thereby, ε_0 is the free-space permittivity ($8.854 \cdot 10^{-12}$ As/Vm), ε_r is the elastomer dielectric constant and E is the electric field.

Eq. 1, which will be referred to as "Pelrine's equation" in this paper, has been derived for free boundary conditions and is generally accepted as representing the electromechanical coupling in dielectric elastomer systems. Kofod et al. [4] validated the equation for silicone experimentally. To our knowledge, no comprehensive analysis of this expression has been presented so far.

The present investigations on electromechanical coupling are mainly motivated by inconsistent results obtained from uniaxial mechanical tests and DE actuator experiments recently presented in [8]. We reported there on an extensive experimental characterization of so called "circular actuators" made of VHB 4910 (an acrylic elastomer produced by 3M) with tests over a wide pre-strain and voltage range. Visco-

hyperelastic constitutive equations were used to describe the response of the elastomer. The parameters of the mechanical model were determined from the results of circular actuators experiments with radial pre-stretch ratios λ_p = 3, 4 and 5 (the pre-stretch ratio λ_p is defined as the ratio between radius of the circular actuator after and before stretching) at a constant voltage of 2 kV. Figure 1a shows the comparison between simulation and experimental results for the model using the Arruda-Boyce strain energy formulation [9]. Electromechanical coupling was thereby described by eq. (1) and a value of 4.7 was used for the dielectric constant of VHB 4910, according to [10, 11]. Despite the good predictive capabilities of the model for the circular actuator test, the constitutive equations failed to describe the passive uniaxial response, with significant discrepancy between data points from tensile and relaxation experiments and the corresponding simulations, Figure 1b.

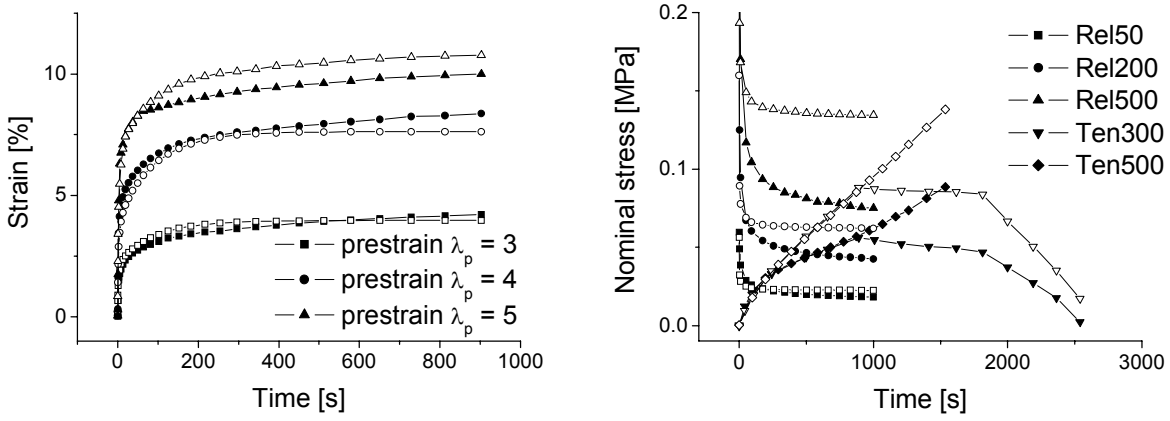

(a) (b)

Figure 1. Experiment vs. simulation for (a) circular actuator tests at λ_p = 3, 4 and 5, and (b) uniaxial experiments with three relaxation tests (Rel50, Rel200 and Rel500) and two tensile tests (Ten300 and Ten500) [8]. The filled symbols represent the experimental data and the open symbols the corresponding simulations.

Describing the mechanical behavior over a wide range of stress and deformation states represents a common challenge for three-dimensional constitutive equations. We therefore concentrated first on the mechanical model formulation when searching for the causes of this inconsistency. The corresponding exercises using different strain energy formulations (with the strain energy functions of Yeoh [12] and Ogden [13] in addition to that of Arruda-Boyce) failed to overcome the inconsistency. We then focused our attention on the electromechanical coupling model, thereby questioning (i) the general validity of eq. (1), and more specifically (ii) the adopted value of 4.7 for the dielectric constant ε_r. The results of these investigations are reported in this paper.

In section 2 we analyze Pelrine's equation for the case of a circular actuator. In a first step an energy balance is formulated which includes the energy from the power source, the energy of the electrical field and the mechanical energy. In a second step, the charge and the forces distributions on a circular actuator are calculated numerically. In section 3 the dielectric constant is determined for VHB 4910 with two different approaches: (i) the dielectric constant is measured using a capacitor set-up, at different pre-strain levels (λ_p = 1, 3, 4 and 5) and frequencies (100 Hz and 10 kHz); (ii) the electromechanical forces and thus the corresponding dielectric constant are measured in experiments with a spring roll actuator. This test is similar to an experiment ('blocking force experiment') proposed by Kofod et al. [4, 11] for measuring the dielectric constant. The results of these investigation and their implications for DE actuator models (in particular concerning the inconsistency illustrated in Figure 1) are discussed in Section 4.

2 Electromechanical coupling

A circular actuator consisting of a dielectrica (elastomer) and two electrodes (Figure 2) is selected as electromechanical system. The following assumptions hold for this analysis: (i) electrostrictive effects are negligible [11], (ii) the electrodes are assumed to be ideally compliant (they do not constrain the elastomer mechanically) and (iii) the elastomer is incompressible.

2.1 Energy considerations

A closed system including the circular actuator is considered (Figure 2). Application of a voltage U leads to a charge Q on the electrodes. The time rate of change of Q correspond to the current I. Charge Q on the electrodes and voltage U are linked. Most energy considerations in literature are formulated by either a constant voltage or a constant charge [1]. This corresponds to a usual approach to calculate forces of plate capacitors. In the present analysis charge and voltage are described as variables dependent on the deformation of the elastomer film. For the present configuration the deformation consists in equi-biaxial in-plane extension and the corresponding out-of-plane contraction. For an incompressible material (volume is constant) this deformation can be described by the film thickness z. U and Q are therefore handled as functions of z.

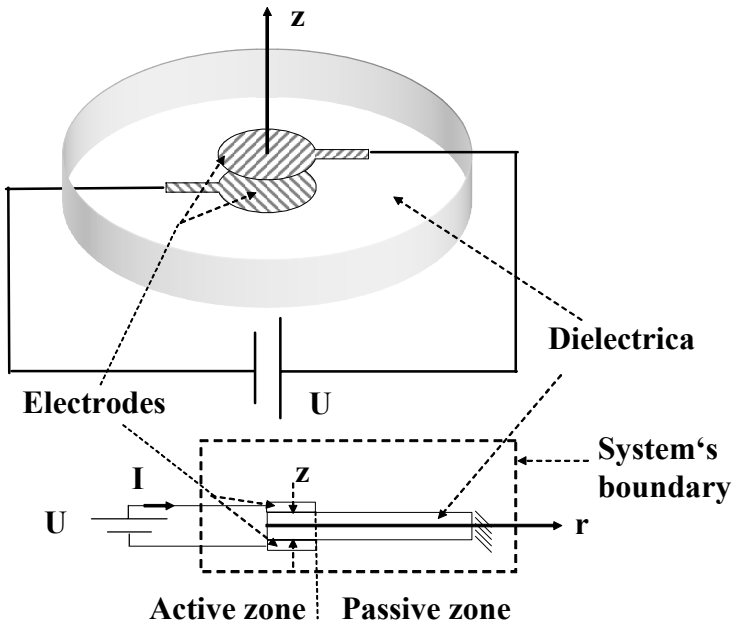

Figure 2. Sketch of the considered electromechanical system. The film thickness z is indicated.

Three energy forms are considered for the energy balance: the energy from the electrical power source W_{ext}, the energy of the electric field W_{el} and the mechanical energy W_m. All three energies are dependent on the thickness z. The energy balance for the closed electromechanical system for an incremental deformation dz is given by eq. (2).

$$\frac{dW_{ext}(z)}{dz} = \frac{dW_{el}(z)}{dz} + \frac{dW_m(z)}{dz} \tag{2}$$

In the following W_{ext}, W_{el} and W_m are determined. The time derivative of the energy from the power source is related to current I and voltage U, as

$$\frac{dW_{ext}}{dt} = U \cdot I = U \cdot \frac{dQ}{dt} \tag{3}$$

where t is the time. Considering z(t) and applying the chain rule leads to

$$\frac{dW_{ext}}{dz} = U(z) \cdot \frac{dQ(z)}{dz} \tag{4}$$

Q and U are linked as $Q(z) = C(z) \cdot U(z)$ with the capacitance C defined here as

$$C = \frac{\varepsilon_0 \cdot \varepsilon_r \cdot A}{z} = \frac{\varepsilon_0 \cdot \varepsilon_r \cdot V_0}{z^2} \tag{5}$$

where A is the area coated by the electrodes and V_0 is the elastomer volume (A·z) of the active zone, which remains constant during deformation. dQ/dz can thus be expressed as:

$$\frac{dQ(z)}{dz} = \varepsilon_0 \cdot \varepsilon_r \cdot V_0 \cdot \frac{d}{dz}\left(\frac{U(z)}{z^2}\right) = \frac{\varepsilon_0 \cdot \varepsilon_r \cdot V_0}{z^2} \cdot \left(\frac{dU}{dz} - 2 \cdot \frac{U}{z}\right) \tag{6}$$

dW_{ext}/dz is given by the combination of eqs. (4) and (6):

$$\frac{dW_{ext}}{dz} = \frac{\varepsilon_0 \cdot \varepsilon_r \cdot V_0 \cdot U}{z^2} \cdot \left(\frac{dU}{dz} - 2 \cdot \frac{U}{z}\right) \tag{7}$$

The rate of change of the energy of the power source depends on the rate of change of the voltage. The energy W_{el} stored by the electric field in a capacitor is

$$W_{el} = \frac{1}{2} C \cdot U^2 \tag{8}$$

by inserting C from eq. (5) the derivative dW_{el}/dz results:

$$\frac{dW_{el}}{dz} = \frac{1}{2}\varepsilon_0 \cdot \varepsilon_r \cdot V_0 \cdot \frac{d}{dz}\left(\frac{U(z)^2}{z^2}\right) = \frac{\varepsilon_0 \cdot \varepsilon_r \cdot V_0 \cdot U}{z^2} \cdot \left(\frac{dU}{dz} - \frac{U}{z}\right) \tag{9}$$

Note that also dW_{el}/dz depends on dU/dz. Equations (9), (7) and (2) lead to the following result for the derivative of the mechanical energy dW_m/dz:

$$\frac{dW_m}{dz} = -\frac{\varepsilon_0 \cdot \varepsilon_r \cdot V_0 \cdot U^2}{z^3} \tag{10}$$

The basic assumption of Pelrine's model is that electrostatic forces are homogeneously distributed over the coated area $A = V_0/z$ and act in z direction. The mechanical energy represents the work of the external (electrostatic) forces on the film. With the assumption that dW_m/dz is the total external force, the corresponding pressure p_z is obtained as:

$$p_z = -\frac{dW_m}{dz} \cdot \frac{1}{A} = \varepsilon_0 \cdot \varepsilon_r \cdot \left(\frac{U}{z}\right)^2 \tag{11}$$

This result confirms Pelrine's equation, when comparing p_z with p_{el} from eq. (1). Pelrine et al. refer to the contribution of lateral and out-of-plane effects, included in eq. (3) in [1]. By the definition of the pressure p_z (eq. (5) in [1] and eq. (11) in this work) the presence of forces acting only in z-direction is assumed. The influence of radial ("lateral") electrostatic forces [1, 14] can be determined with a direct calculation of charge and electrostatic force distributions. To this end, for the configuration shown in

Figure 2, a corresponding numerical calculation has been carried out and is described in the next section.

2.2 Charge and force distributions

The simulation program COMSOL Multiphysics [15] has been used for the present calculations. An axisymmetric model of a circular actuator (element type: 'Lagrange-quadratic') including a dielectrica and two electrodes has been created, Figures 3 and 4. The electrodes are assumed to have straight edges. The following geometrical parameters are used, Figure 3: the thickness of the dielectrica is z_d = 60µm, this corresponds to a VHB 4910 actuator pre-stretched by a factor of approximately λ_p=4. The radius of the dielectrica is r_d = 14 mm. The radius of the electrode is r_{el} = 7 mm and the thickness of the electrode is z_{el} = 20µm. Microscopic investigations showed that z_{el} = 20µm is a reasonable value for a hand-applied graphite powder / silicone oil electrode.

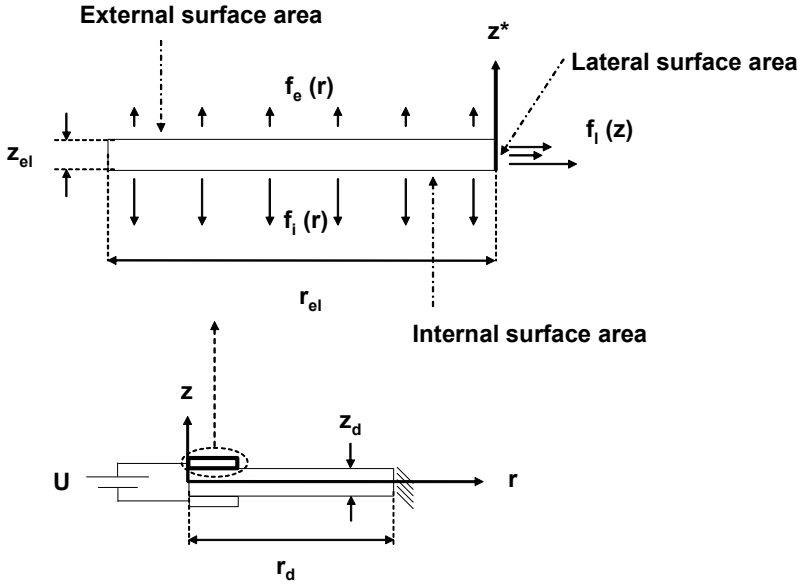

Figure 3. Sketch of the COMSOL Mulitphysics model. For the electrode, the coordinates r, z and z* are introduced for later reference

The dielectric constant of the dielectrica was chosen as ε_r = 4.7. For the bordering empty space the dielectric constant of vacuum ε_r = 1 was used. As boundary condition a potential difference of U = 3 kV has been applied between the electrodes. Since the electrodes are conductive, all the charges are on the surface area of the electrodes: the so called internal surface area, lateral surface area and external surface area, indicated in Figure 3. The mesh is shown in Figure 4. Singularities at corners have been closely investigated at the upper electrode with a strong mesh refinement at the corresponding locations.

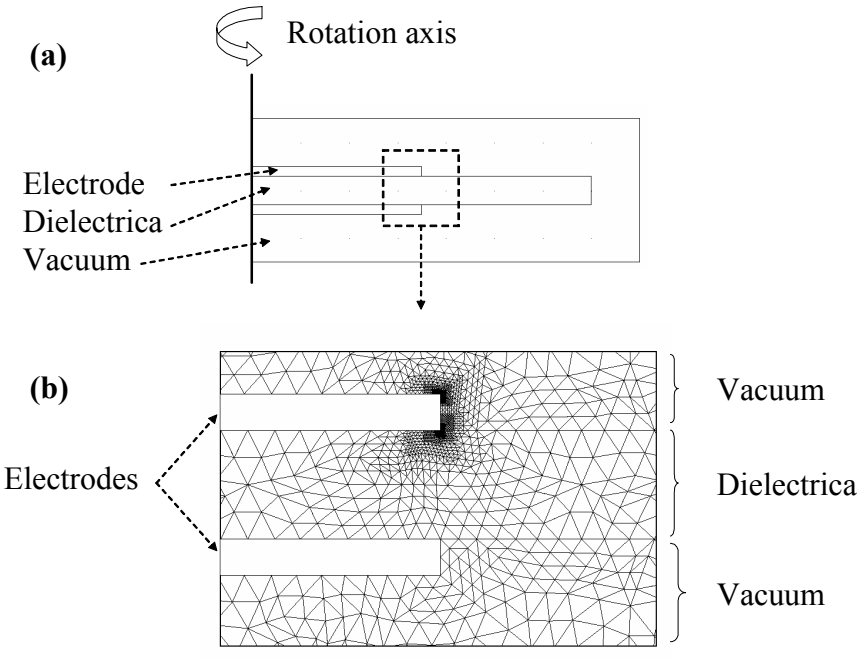

Figure 4. (a) Sketch of the COMSOL Multiphysics model and (b) meshing of the part indicated in (a)

All electric field variables (electric potential, electric field, surface charge density ρ_s) are calculated by solving Poisson's equation numerically. On the rotational axis a suitable symmetry boundary condition is applied. Further information on the numerical calculation can be found in [15].

The surface charge density of the internal surface area $\rho_i(r)$ and the surface charge density of the lateral surface area $\rho_l(z^*)$ are shown in Figure 5. The surface charge density of the external surface area is neglected because there is no charge on this surface except at the right corner, with a singularity which does not influence the electromechanical behavior.

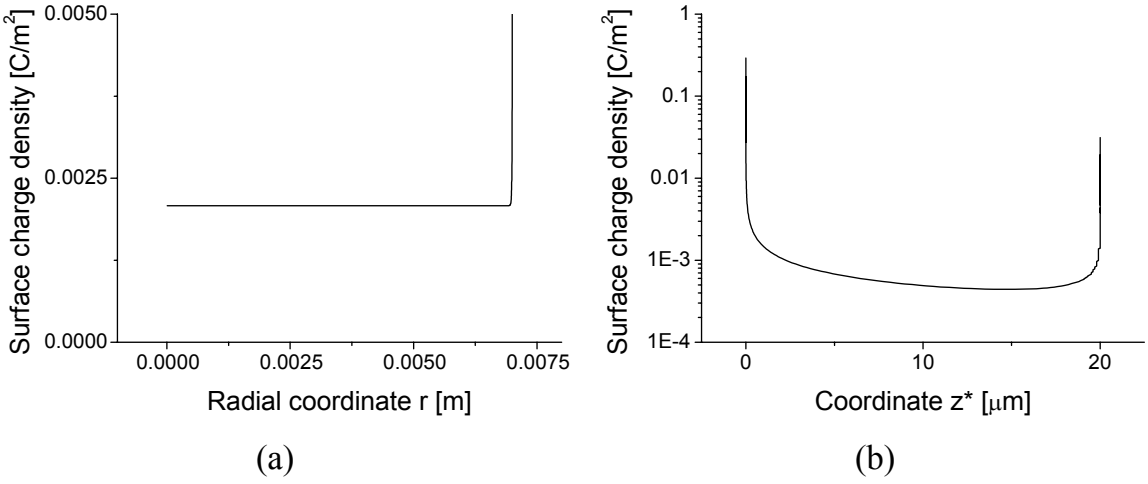

Figure 5. Charge distributions on the electrode for (a) the internal surface area and (b) the lateral surface area

The charges on the electrodes cause electrostatic forces. These forces are parallel to the electric field. Both forces and electric field vectors are perpendicular to the electrode's surface area. The calculated electric field distribution is qualitatively represented in Figure 6.

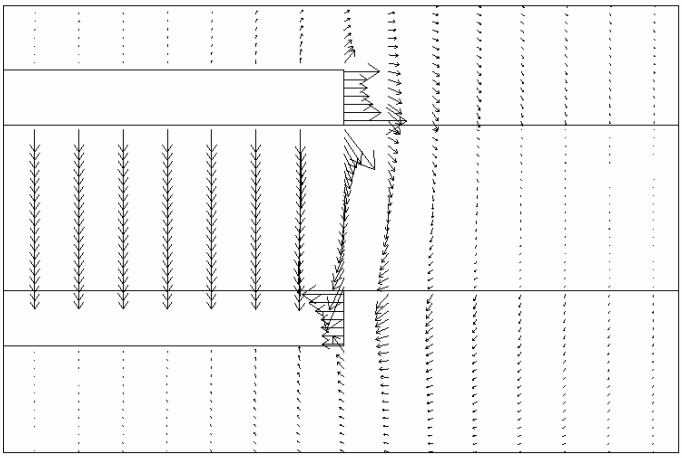

Figure 6. Electric field distribution: arrows length is proportional to field intensity.

The electrostatic forces are described by Maxwell's stress tensor t^{M}_{ij} [16]. The stress vectors at the electrode surface are parallel to the electric field vectors and their magnitude t_M is calculated from the electric field magnitude E or alternatively from the surface charge density ρ_s, see [3].

$$t_M = \frac{1}{2}\varepsilon_0 \cdot \varepsilon_r \cdot E^2 = \frac{\rho_s^{\,2}}{2 \cdot \varepsilon_0 \cdot \varepsilon_r} \tag{12}$$

In Figure 7 the electrostatic stress distribution for the internal surface area $t_{M,i}$ and the lateral surface area $t_{M,l}$ are shown. For the calculation of $t_{M,l}$ the dielectric constant of vacuum (ε_r=1) was used because the lateral surface area borders the empty space.

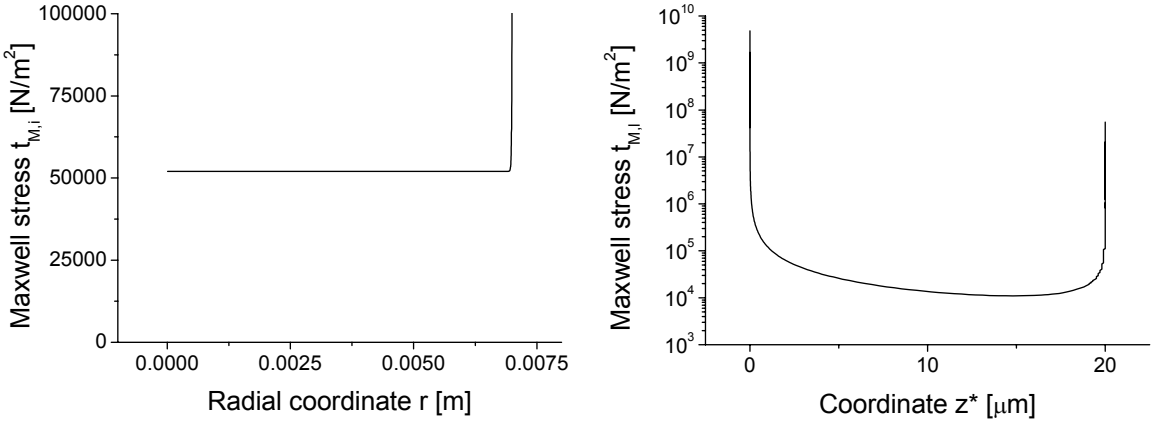

(a) (b)

Figure 7. Electrostatic stress distribution for (a) the internal surface area and (b) the lateral surface area

The stress for the internal surface area $t_{M,i}$ is constant with a singularity at the edge of the electrode. Singularities occur also at the extremities of the lateral surface. Subsequent mesh refinement have shown that (i) the singularity for $t_{M,i}$ has no influence on the electromechanical behavior, and (ii) the value of the total radial force F_r from integration of $t_{M,l}$ over the thickness converges to a finite value.

The mechanical pressure p_z transmitted from the electrode to the dielectrica in (negative) z-direction (see Figure 8) is constant over the coated area and has a value of $p_z = 52018$ N/m^2.

The total force F_r caused by the Maxwell stress $t_{M,l}$ of the lateral surface area (see Figure 3) is given by

$$F_r = \int_0^{z_{el}} 2 \cdot \pi \cdot r_{el} \cdot t_{M,l}(z^*) \cdot dz^* \tag{13}$$

F_r converges after mesh refinement to a value of 0.06784 N. As a simplification, $t_{M,l}$ can be replaced by a statically equivalent constant stress distribution in radial direction acting over the thickness of the elastomer film, see Figure 8. The corresponding "lateral pressure" value (p_r, Figure 8) is calculated taking into account the contribution of both electrodes (factor 2 in eq. 14):

$$p_r = 2 \cdot \frac{F_r}{2 \cdot \pi \cdot r_{el} \cdot z_d} = \frac{F_r}{\pi \cdot r_{el} \cdot z_d} \tag{14}$$

The calculated value of p_r for the applied mesh refinement is 51415 N/m^2.

The electromechanical pressure p_{el} calculated with eq. 1 is, for the present case, p_{el} =104036 N/m^2. This value is double as much as the calculated value of p_z and, with a slight approximation due to numerical errors, p_r.

$$p_z = p_r = \frac{1}{2} \cdot p_{el} = \frac{1}{2} \cdot \varepsilon_r \cdot \varepsilon_0 \cdot \frac{U^2}{z_d^{\,2}} \tag{15}$$

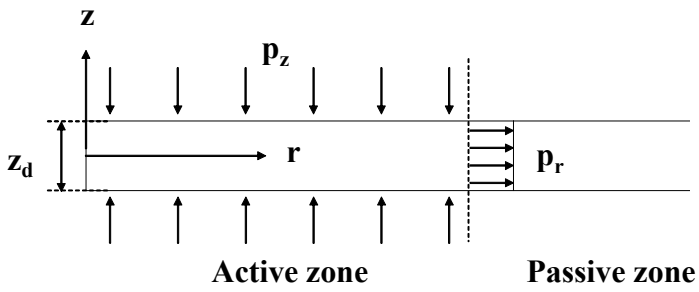

Figure 8. Out-of-plane pressure p_z and lateral stress p_r acting on the dielectrica in a circular actuator, axisymmetric view.

This result shows that (i) the electrostatic forces act in out-of-plane and in-plane direction, and (ii) the out-of-plane component is half the value predicted with Pelrine's equation.

For an incompressible material, however, Pelrine's model can be shown to provide a suitable description of electromechanical coupling. In fact, a superimposed hydrostatic stress state does not affect, by definition, the deformation of the incompressible elastomer. For the present case a hydrostatic stress with negative sign and magnitude of $0.5p_{el}$ is superimposed to the vertical and radial components p_z and p_r. The resulting kinetic boundary condition is a homogeneous out-of-plane compression with p_{el}, i.e. the loading conditions predicted with Pelrine's model.

3 Dielectric constant

The analysis presented in section 2 has confirmed that eq. 1 can be used for modeling electromechanical coupling in DE systems. The value of the dielectric constant for VHB 4910 is investigated in this section. Several researchers, [3, 5, 8, 17, 18], adopted a deformation independent value of about 4.7, originally proposed by Kofod [10]. Different techniques were used here to measure ε_r for un-deformed and pre-stretched elastomer films.

3.1 Capacitor set-up

A capacitor set-up has been used to measure the dielectric constant of VHB 4910 at room temperature (23 °C). ε_r has been determined for different in-plane pre-stretch ratios (λ_p = 1, 3, 4 and 5) at the frequencies 100 Hz and 10 kHz. The dielectric constant can be obtained from measurements of capacitance and geometry of a capacitor:

$$\varepsilon_r = \frac{C \cdot z}{A \cdot \varepsilon_0} \tag{16}$$

The elastomeric film is pre-deformed by a pre-stretching machine [8, 19] and glued on a circular frame (radius 15 mm), Figure 9. For each pre-stretch ratio five samples have been created for multiple measurements. Each sample is inserted between two gold plungers with a radius of 12.5 mm (Figure 9). The capacitance is measured by a LCR-meter (an instrument for measuring the inductance (L), capacitance (C) and resistance (R), 4263B from Agilent) connected to two gold tubes (Figure 9).

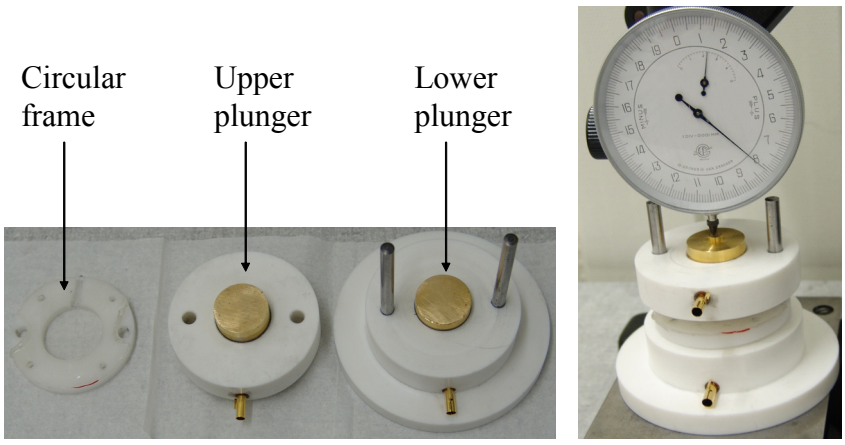

(a) (b)

Figure 9. Device for measuring the dielectric constant: (a) disassembled and (b) assembled device under the mechanical dial gage for thickness measurement.

The thickness is measured by a mechanical dial gage (Compac, Switzerland, measurement range: 5 mm, resolution: 0.001 mm). The displacement of the upper capacitor plate is measured with and without the elastomer sample. The thickness corresponds to the displacement difference. The results of the dielectric constant are presented in Table 1 and Figure 10.

Table 1. Dielectric constant (mean value ± standard deviation) for VHB 4910 at different frequencies and pre-strain levels

Pre-strain λ_p [-]	ε_r [-] at 100 Hz	ε_r [-] at 10 kHz
1	4.68 ± 0.029	4.30 ± 0.025
3	3.71 ± 0.088	3.41 ± 0.098
4	3.34 ± 0.152	3.08 ± 0.184
5	2.62 ± 0.378	2.40 ± 0.410

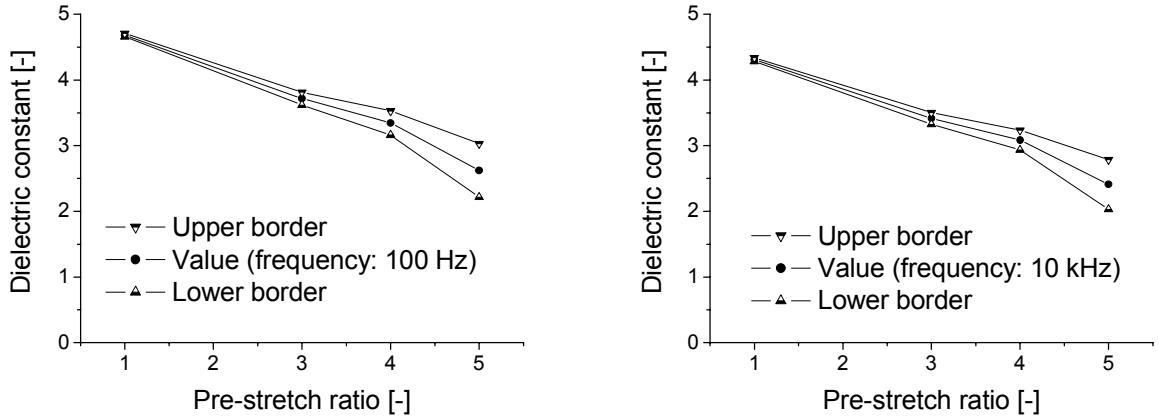

(a) (b)

Figure 10. Dielectric constant in dependence of the pre-stretch ratio (with scatter band) for (a) 100 Hz and (b) 10 kHz

3.2 "Spring roll" set-up

Dielectric constant measurements have been carried out using DE actuators in a cylindrical configuration, called "spring roll". Six spring rolls were manufactured and tested. The VHB 4910 membrane was coated with a mixture of graphite powder (Superior Graphite, ABG1005, 20 g) and silicone oil (Dow Corning, DC 200/50 cs, 45 g) as electrodes. A brief account on the actuator configuration is given below and detailed information can be found in [19].

The elastomer film is pre-strained biaxially (using the pre-stretching device, [8, 19]) with the pre-stretch ratios $\lambda_x = 4$ and $\lambda_y = 4$, see Figure 11a. The pre-strained film is fixed to a rigid frame and one electrode is applied on one side (Figure 11). The geometrical parameters after pre-straining are $x_1 = 143$ mm, $y_1 = 445$ mm and $z_1 = 62.5$ µm. The coated (active) zone is in the middle of the actuator with $x_a = 110$ mm. The ratio r of the coated area divided by the whole area is $r = x_a/x_1 = 77$ %. A second layer consisting of the pre-stretched elastomer film and a second electrode is glued

over the first layer at the uncoated side. Then, both layers are wrapped around an elastic core, Figure 11.

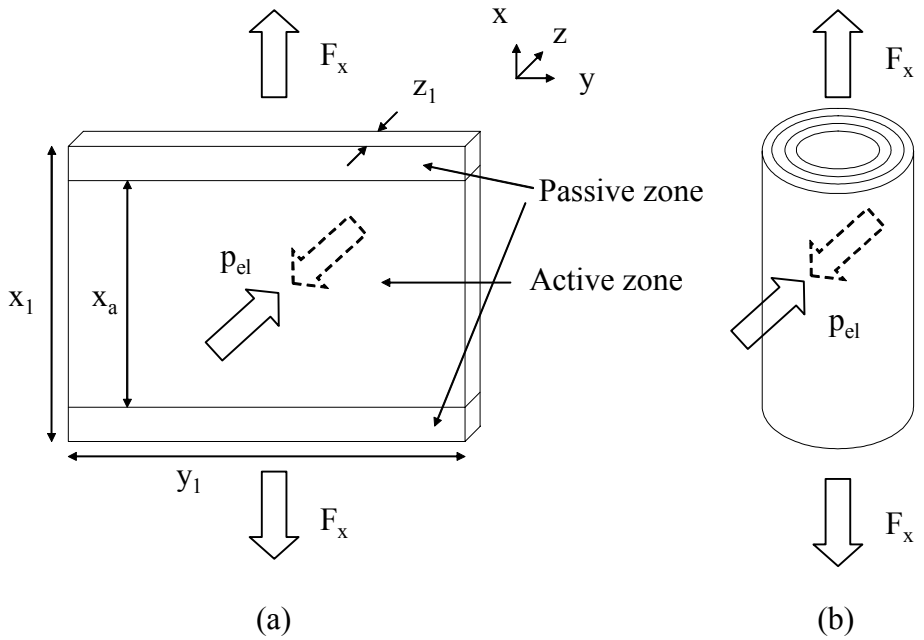

Figure 11. (a) One layer (coated, pre-strained elastomer film) and (b) complete spring roll actuator

The spring roll is hold at the extremities in x-direction by the force F_x. The experiment is performed at room temperature (23 °C). A voltage U is applied with a high voltage amplifier (Trek, Model 5/80) linearly increasing from 0 to 3 kV in 2 minutes. The force F_x required to keep the length of the actuator constant is continuously measured with a force transducer (HBM type S2). The experiment is controlled with a PC LabView system. The measured force difference ΔF is defined as

$$\Delta F(U) = F_x(U) - F_x(U=0) \tag{17}$$

The actuators length remains unchanged despite the application of the voltage (and thus application of electrostatic forces). This means that the electrostatic forces together with the variation of axial stresses correspond to a hydrostatic stress state. As a consequence, measurement of the axial force (or the corresponding stress component) provides a direct measurement of the electrostatic stress:

$$p_{el} = \frac{\Delta F_i}{2 \cdot x_1 \cdot y_1} = \varepsilon_0 \cdot \varepsilon_r \cdot E^2 \tag{18}$$

This equation allows determining the dielectric constant from the measurement of the force difference of an 'ideal' spring roll ΔF_i where the whole film is coated, r=100%. The present spring rolls have r=77%. The presence of passive parts (the remaining

23%) causes a deformation of the film with elongation in the coated and contraction in the uncoated area, Figure 12. As a consequence, the change in axial force is somewhat lower with respect to the prediction according to eq. (18). For describing the change in axial force the ratio k is introduced which is defined as $k=\Delta F / \Delta F_i$. The ratio k between force reduction with r=77% and r=100% has been evaluated analytically and numerically (finite element). The result of this analysis is that a constant value corresponding to the geometrical ratio (i.e. k= r=0.77) represents a valid approximation for the present case. By using this result, eq. (18) can be rewritten as:

$$p_{el} = \frac{\Delta F_i}{2 \cdot x_1 \cdot y_1} = \frac{\Delta F}{2 \cdot x_1 \cdot y_1 \cdot k} = \frac{\Delta F}{2 \cdot x_1 \cdot y_1 \cdot r} = \varepsilon_0 \cdot \varepsilon_r \cdot E^2 \qquad (19)$$

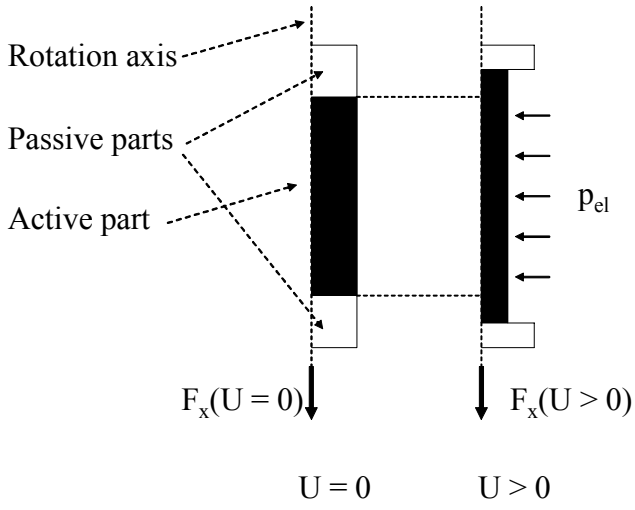

Figure 12. Sketch to illustrate the influence of the passive parts on the spring roll behavior.

ε_r is evaluated by using eq. (19). The electromechanical pressure $p_{el}=\Delta F/(2x_1y_1r)$ as a function of the electric field E is presented in Figure 13. By fitting the experimental curve of p_{el} with eq. (1), a dielectric constant of 3.24 is obtained. This result agrees to a great extent with the values reported in Table 1 for λ_p=4.

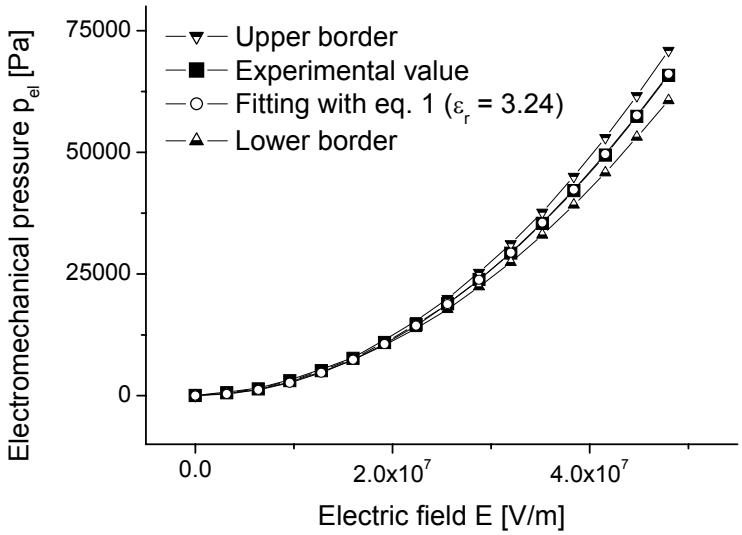

Figure 13. Electromechanical pressure (with scatter band) evaluated by spring roll experiments compared to a fit with eq. (1). The fitting parameter ε_r is 3.24.

4 Discussion

The analysis presented in Section 2 provides a validation of the Pelrine's equation for modeling electromechanical coupling in a circular actuator and a new interpretation of the electromechanical forces distribution. Energy and force considerations are consistent.

The energy balance considered here leads to the same result as in Pelrine et al. although the derivation is different. In fact, we considered the dependence of Q and U on the deformation. As a consequence the derivatives dW_{ext}/dz and dW_{el}/dz depends on the voltage derivative dU/dz.

Electrostatic charge and force distribution calculations showed that half of the electromechanical pressure acts as out-of-plane compression and the other half as in-plane tension. The out-of-plane force corresponds to the one calculated for a standard parallel plate capacitor. Due to the incompressibility of the material, electromechanical coupling can be modeled with an out-of-plane pressure with magnitude p_{el} according to eq. (1). This approach is advantageous in actuator modeling since only out-of plane forces have to be considered.

Note, the validity of Pelrine's equation for modeling dielectric elastomer actuators is not an implicitness. Consider for instance a spheric configuration ('ballon actuator', Figure 14) with the radius of the elastomer r_s and the thickness of the elastomer z_s,

$z_s << r_s$. The elastomer is prestrained and is coated at the inner and the outer surface. The inner pressure of a gas (e.g. helium) maintains the prestrain. The capacity is $C=\varepsilon_0\varepsilon_r A_s/z_s$ where A_s is the surface area of the sphere. The charge is $Q=C\cdot U$ and the uniform surface charge density at the electrode is $\rho_s=Q/A_s=CU/A_s=\varepsilon_0\varepsilon_r U/z_s$. Eq. (12) for the Maxwell stress gives $t_m=0.5\varepsilon_0\varepsilon_r(U/z_s)^2$. This is the half of the pressure that one would obtain by direct application of Pelrine's equation.

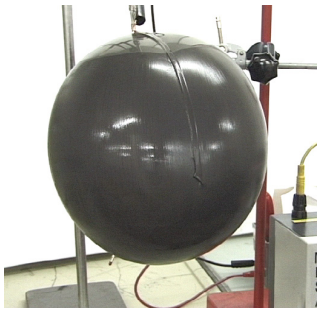

Figure 14. Ballon actuator, taken from [20]

The results of the dielectric constant measurements show a remarkable dependence on the pre-strain and a weak dependence on the frequency. In the undeformed state (pre-strain $\lambda_p = 1$) the value of the dielectric constant is around 4.7 which is the commonly used value [10, 11]. An increase of the pre-strain causes a significant decrease of the dielectric constant. For a relevant actuator pre-strain range (around $\lambda_p= 4$) the dielectric constant is close to 3.

The present results are in contrast to the findings in [10, 11] where it is shown experimentally that the dielectric constant of VHB 4910 has a negligible dependence on pre-strain and frequency. A reason for the different outcome of the present tests might be in the material composition, which might have changed recently. Interestingly, in a 3M data sheet [21] of November 2005 the dielectric constant of VHB 4910 is given as 3.21 for 1 kHz and 2.68 at 1 MHz.

The measurements with the capacitor set-up are confirmed by the experiment with the spring roll actuator. An evaluation of the dielectric constant for a biaxially pre-strained actuator ($\lambda_p=4$) gives a value of 3.24, in agreement with the results of section 3.1 where the dielectric constant at a pre-strain of $\lambda_p=4$ was measured as 3.34 for 100 Hz and 3.08 for 10 kHz.

The results of the spring roll experiments confirm the validity of Pelrine's equation for DE actuator modeling. This is consistent with the experimental validation of electromechanical coupling by Kofod et al. [4].

The stretching of the elastomer might cause an anisotropy of the dielectric constant. The fact that the dielectric constant decreases in thickness direction by stretching might cause a change of the dielectric constant in planar direction. Since the molecules align in planar direction by stretching, it is expected that the polarizability increases in planar direction and decreases in thickness direction. As a consequence an increase of the dielectric constant in planar direction is expected. With our set-up it is not possible to measure the dielectric constant in planar direction. In order to evaluate the influence of an anisotropic dielectric constant with respect to the electromechanical coupling, the numerical analysis has been repeated. Four calculations with COMSOL Multiphysics were carried out using the dielectric constant in a tensor form. Thereby, the dielectric constant in thickness direction $\varepsilon_{r,z}$ was set to $\varepsilon_{r,z} = 4.7$ in each calculation. The dielectric constant in radial direction $\varepsilon_{r,r}$ was varied with values of 4.7 (isotropic case), 6, 8 and 10. Results shows, that the surface charge distribution of the internal surface area and therefore the mechanical pressure p_z remains unchanged. In contrast, the surface charge distribution at the lateral surface area changes, which has an influence on the radial pressure p_r. In Figure 15, the ratio p_r/p_z is plotted against the dielectric constant in radial direction, $\varepsilon_{r,r}$.

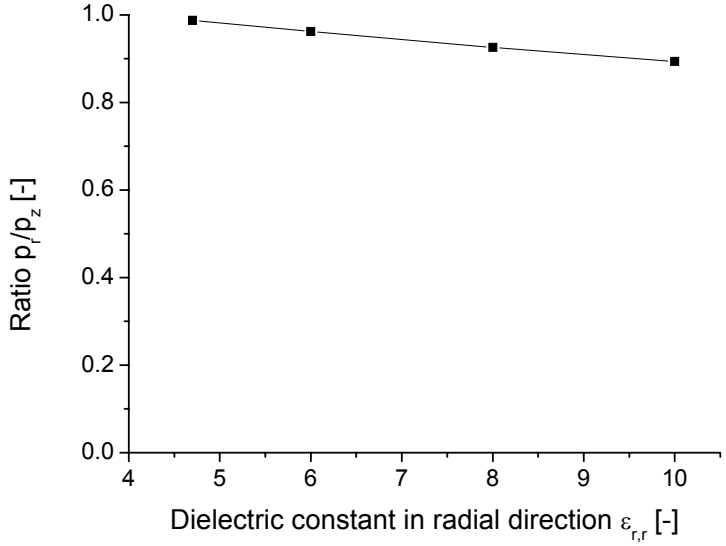

Figure 15. The dielectric constant in radial direction $\varepsilon_{r,r}$ is plotted against the ratio p_r/p_z

These results show that contributions of out-of-plane and radial pressure are equal only for the case of isotropic dielectric behavior. With $\varepsilon_{r,r} = 10$ (more than double as $\varepsilon_{r,z} = 4.7$), the radial pressure p_r is 10% less as compared to the isotropic case. It can

however be stated that the anisotropy of the dielectric constant has a small influence on the overall electromechanical behavior.

The results of section 2 and 3 showed that the Pelrine's equation can be used for circular actuator modeling but the dielectric constant has to be changed with respect to the value used in [8]. As a consequence, the results of the circular actuator experiments have been revisited and the constitutive model parameter identification corrected.

The circular actuators had pre-stretch ratios of λ_p= 3, 4 and 5. As a simplification, ε_r is not considered as pre-strain dependent for the present analysis, and a constant value of ε_r = 3.24 has been selected, according to the value obtained for the spring roll actuator, see Figure 12.

The new constitutive model parameters have been determined for the Arruda-Boyce strain energy form. In particular, the initial shear modulus (parameter A) is corrected with respect to [8], with A = 0.0473 MPa instead of 0.0686 MPa. Figure 16 summarizes the new results for simulations of circulator tests and uniaxial response. The circular test fit is identical to the one reported in Figure 1, and a significant improvement is obtained for the prediction of the uniaxial behavior.

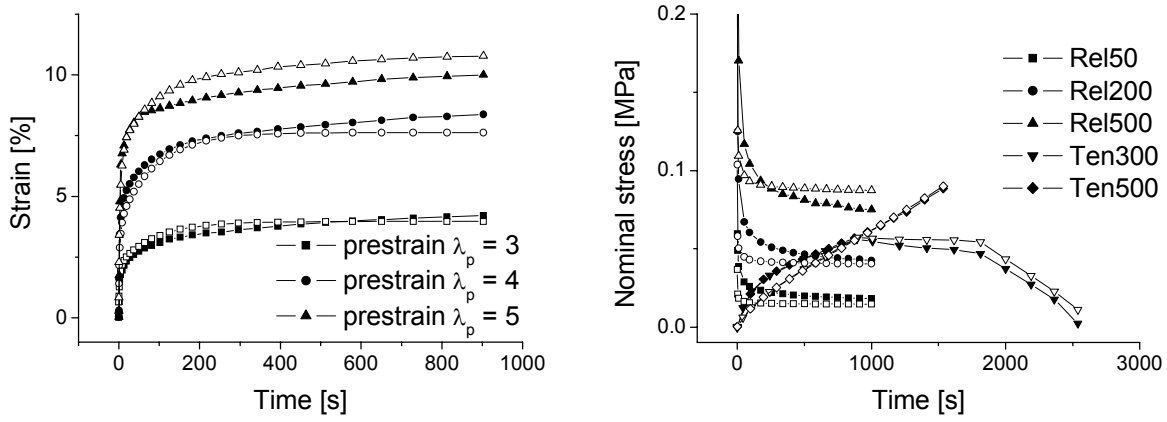

(a) (b)

Figure 16. Experiment vs. simulation for the same testing data points shown in Figure 1: (a) circular actuator tests; and (b) uniaxial experiments. The filled symbols represent the experimental data and the open symbols the corresponding simulations, based on ε_r = 3.24.

5 Conclusions

Electromechanical coupling in DE actuator has been investigated. Validation of Pelrine's equation for modeling electromechanical coupling in circular actuators has been provided through (i) energy consideration and (ii) numerical calculation of charge and force distribution. The latter provided a new physical interpretation of the electrostatic forces acting on the DE film, with contributions from in-plane and out-of-plane stresses. Representation of this force distribution using Pelrine's equation is valid for an incompressible material, such as VHB 4910.

The value of the dielectric constant has been measured for different pre-stretched VHB 4910 membranes. The values are shown to decrease with increasing pre-stretch ratio, from 4.7 for the un-stretched film, down to 2.6 for a equi-biaxial deformation with λ_p=5. This result is important in that it corrects the constant value of about 4.7 originally proposed in [10] and, since then, largely applied for pre-stretched DE actuator modeling, see e.g. [3, 5, 8, 17, 18]. The present values were obtained from a capacitor set-up and confirmed by the analysis of spring roll and circular actuator experiments.

Correction of the dielectric constant leads to a change in the VHB 4910 constitutive model parameters with respect to the values proposed in [8]. The new model is capable of describing the active and passive material behavior over a large range of loading conditions and deformation histories.

Acknowledgment

Financial support from the Swiss National Science Foundation (Project 200021-107661/1) is gratefully acknowledged.

6 References

[1] R.E. Pelrine, R.D. Kornbluh, J.P. Joseph, Electrostriction of polymer dielectrics with compliant electrodes as a means of actuation, Sens. Actuators, A 64 (1998) 77-85

[2] R. Pelrine, R. Kornbluh, Q. Pei, J. Joseph, High-speed electrically actuated elastomers with strain greater than 100%, Science, 287 (2000) 836-839

[3] N. Goulbourne, E. Mockensturm, M. Frecker, A nonlinear model for dielectric elastomer membranes, Journal of Applied Mechanics, 72 (2005) 899 – 906

[4] G. Kofod, P. Sommer-Larsen, Silicone dielectric elastomer actuators: Finite-elasticity model of actuation, Sens. Actuators, A 122 (2005), 273-283

[5] J. Plante, S. Dubowsky, Large-Scale Failure Modes of Dielectric Elastomer Actuators, International Journal of Solids and Structures, in press (available online)

[6] M. Wissler, E. Mazza, Modeling and simulation of dielectric elastomer actuators, Smart Materials and Structures, 14 (2005) 1396 - 1402

[7] M. Wissler, E. Mazza, Modeling of a prestrained circular actuator made of dielectric elastomers, Sens. Actuators, A 120 (2005), 184-192

[8] M. Wissler, E. Mazza, Mechanical behavior of an acrylic elastomer used in dielectric elastomer actuators, Sens. Actuators, in press (available online)

[9] E.M. Arruda, M.C. Boyce, A three-dimensional constitutive model for the large stretch behavior of rubber elastic materials, J. Mech. Phys. Solids, 41, No.2 (1993) 389 – 412

[10] G. Kofod, R. Kornbluh, R. Pelrine, P. Sommer-Larsen, Actuation response of polyacrylate dielectric elastomers, Proc. SPIE 4329 (2001) 141 – 147

[11] G. Kofod, P. Sommer-Larsen, R. Kornbluh, R. Pelrine, Actuation response of polyacrylate dielectric elastomers, J. Intel. Mat. Syst. Str., 14 (2003) 787-793

[12] O.H. Yeoh, Characterization of elastic properties of carbon-black-filled rubber vulcanizates, Rubber Chem. Technol., 63 (1990) 792-805

[13] R.W. Odgen, Large deformation isotropic elasticity – on the correlation of theory and experiment for incompressible rubberlike solids, Proc. R. Soc. Lond., A 326 (1972) 565-584

[14] R. McMeeking, C. Landis, Electrostatic forces and stored energy for deformable dielectric materials, Journal of Applied Mechanics, 72 (2005) 581 – 590

[15] COMSOL Multiphysics, User's Guide, 2005, version 3.2, COMSOL, Inc.

[16] J. C. Maxwell, A treatise on electricity and magnetism, Dover, Oxford, 1954

[17] P. Lochmatter, S. Michel, G. Kovacs, Electromechanical model for static and dynamic activation of elementary dielectric elastomer actuators, Proc. SPIE 6168 (2006) 61680F-1 - 61680F-13

[18] E. Yang, M. Frecker, E. Mockensturm, Viscoelastic model of dielectric elastomer membranes, Proc. SPIE 5759 (2005) 82 – 92

[19] G. Kovacs, P. Lochmatter, Arm wrestling robot driven by dielectric elastomer actuators, Proc. SPIE, vol. 6168 (2006) pp. 616807-1 - 616807-12

[20] P. Lochmatter, Develompent of a shell-like electroactive polymer (EAP) actuator, ETH dissertation, in preparation

[21] www.mmm.com

4 Further Verification of the Actuator Model

4.1 Introduction

The results of section 3 are verified further and completed in this chapter. Four main points are considered:

(i) In article 3 the agreement between experiments and simulations is good for the circular strain test data, but the model fails to correctly describe the uniaxial tensile tests. The reason for this is the dielectric constant which is about 3.2 and not 4.7, see article 4. Identical to the Arruda-Boyce strain energy form in article 4, the material parameters of the Yeoh and the Ogden strain energy form are adapted considering the correct value of the dielectric constant of VHB 4910. This results in a modification of the predicted uniaxial behavior which is presented in section 4.2.

(ii) In order to evaluate the predictive capability of the constitutive model, aspiration and compression tests are performed. The aspiration test method is based on the pipette aspiration technique [Aoki 1997] and is commonly used for testing the biaxial behavior of biological soft tissues. The tests have been performed for prestrained VHB-films with a radial pre-stretch ratio of λ_p = 3, 4 and 5. Furthermore, compression tests are performed on un-stretched elastomer films. Finite element models are created for both tests, the aspiration test in section 4.3 and the compression test in section 4.4. The simulations are compared to the experiments in order to verify the mechanical model. The material parameters listed in section 4.2 are used here.

(iii) Models in continuum mechanics are phenomenological. The model validity is usually limited to a certain deformation range. An effective way of illustrating the deformation range of a certain test for an incompressible material is to plot the first invariant against the second invariant of the left Cauchy-Green deformation tensor [Bird 1977 and Treloar 1975]. This results in a ‘map’ of the deformation range which is presented in section 4.5. Each experiment represents a curve on the map.

(iv) In article 4 spring rolls are used for the determination of the dielectric constant. The evaluation of the dielectric constant for VHB 4910 yielded a value of 3.2 which is in agreement with LCR-meter experiments (article 4). One important assumption was that the ratio k (section 3.2, article 4) is equal to the ratio r

(section 3.2, article 4). This relationship is important for the design of spring rolls and is analyzed in section 4.6.

4.2 Correction of material parameters

In order to consider the fact that the dielectric constant is about 3.2 and not 4.7 (article 4), the constitutive material parameters for the Yeoh and the Ogden strain energy forms presented in article 3 are adapted as for the Arruda-Boyce strain energy form (article 4).

The optimization procedure presented in article 3 has been carried out again for the Yeoh and the Ogden strain energy form with a dielectric constant of 3.2 instead of 4.7. The actuator behavior did not vary by using the new material parameters. By contrast, the simulations of the uniaxial tensile and relaxation tests change. The new material parameters for the Ogden, the Yeoh and the Arruda Boyce strain energy forms are presented in Table 4.1 (hyperelastic parameters). The appropriate viscoelastic parameters are listed in article 3, Table 2.

Table 4.1. New hyperelastic material parameters

Yeoh	C_{10} [MPa]	C_{20} [MPa]	C_{30} [MPa]			
	0.05374	-4.86e-04	3.809e-06			
Ogden	μ_1 [MPa]	α_1 [-]	μ_2 [MPa]	α_2 [-]	μ_3 [MPa]	α_3 [-]
	0.00592	1.293	0.0582	2.325	-0.0161	2.561
Arruda-Boyce	A [MPa]	N [-]				
	0.0473	124.88				

The comparison between experiments and simulations for the uniaxial tensile and relaxation tests is illustrated in Figure 4.1 for all three strain energy forms.

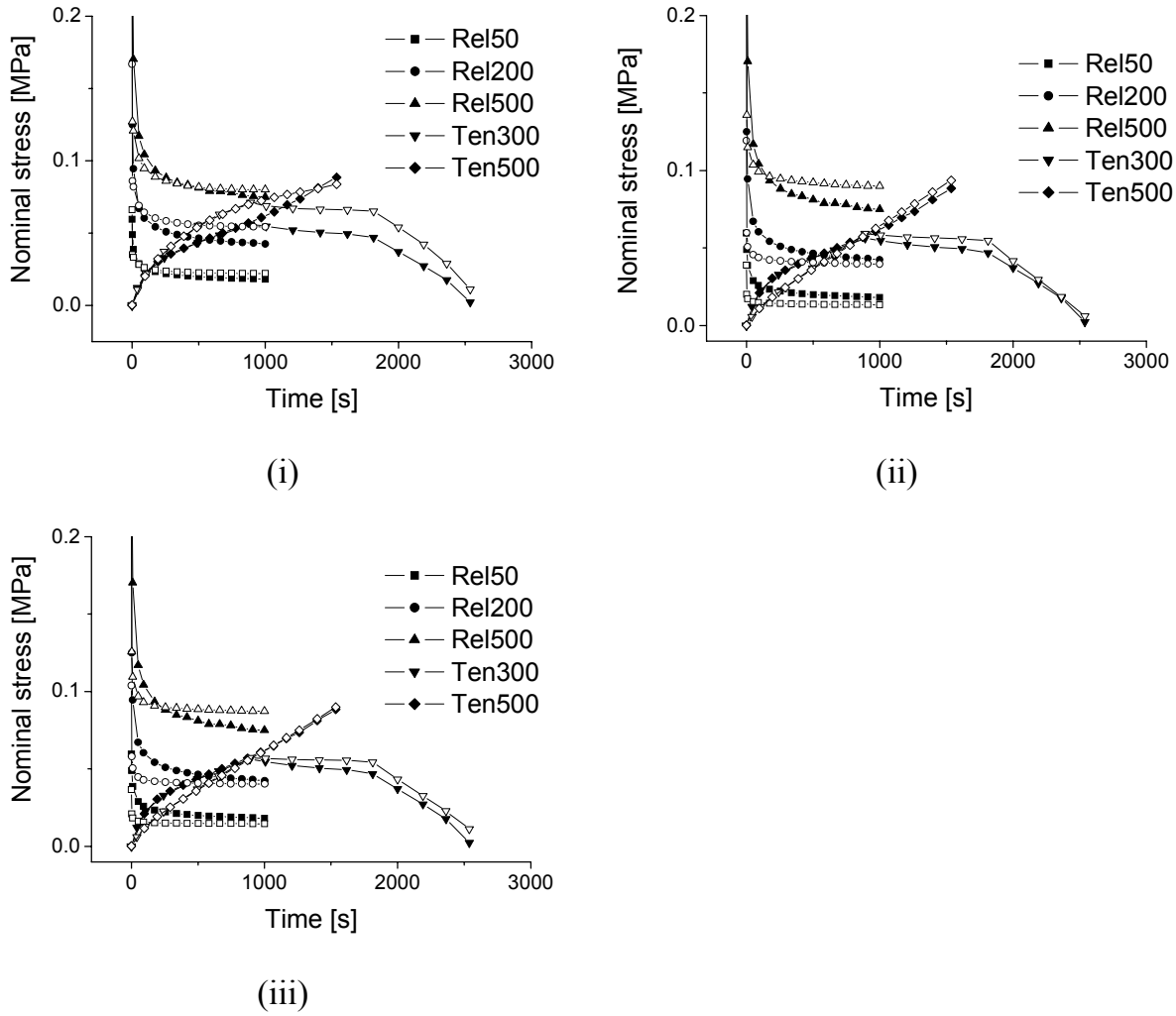

Figure 4.1. Uniaxial behavior for the adapted material parameters: experimental data (filled symbols) compared to the simulations (open symbols) for (i) the Yeoh, (ii) the Ogden and (iii) the Arruda-Boyce strain energy forms

The results of the uniaxial behavior show that this modification leads to an improvement in the predictive capabilities of the constitutive model. Both the actuator and the uniaxial behavior are described reasonably by all three strain energy forms.

In article 1, the Yeoh model provided good predictive capability. The dielectric constant was 4.7 and the material parameters were different from Table 4.1. These facts are in disagreement with the results of article 3, article 4 and this section. The reason for this are that (i) the gold electrodes (article 1) cause a mechanical resistance in the activation and (ii) the material parameter determination was verified solely on one single prestrain and voltage level.

(i) The actuation strain (article 1, Figure 8) at 180 s is 14% at prestrain 4.08. By contrast, actuators with silicone/graphite electrodes at prestrain 4 (article 3, Figure 5) show a strain value of about 50% after 180 s. The silicone/graphite

electrode is more compliant than the gold electrode. Therefore, graphite powder/silicone electrodes were used in article 3. For investigating whether the silicone/graphite electrode constrains the active strain, experiments have been performed with two different silicone/graphite mixtures but identical conditions [Wyrsch 2006]. Mixture 1 contained 11 g graphite powder (TIMREX SP30) and 10 ml silicone oil (DC 200/100 cs) and mixture 2 contained 13.5 g graphite powder (TIMREX SP30) and 10 ml silicone oil (DC 200/100 cs). There was almost no difference in the strain response between the two actuator types. Thus, the used graphite/silicone electrode does not constrain the active strain.

(ii) A total number of 11 parameters (three for the Yeoh strain energy form and eight for the Prony series) were determined in article 1 on the basis of uniaxial tests. The modeling system had too many free parameters, which led to imprecise results in the actuator behavior. By contrast, the parameter determination in article 3 was more restricted. Three multiaxial tests (at various prestrain levels) were involved in the fitting procedure. The detailed considerations of article 3, article 4 and this chapter resulted in an improved model and a better understanding.

4.3 Aspiration tests

4.3.1 Introduction

The aspiration device [Vuskovic 2001] is based on the pipette aspiration technique [Aoki 1997] and is commonly used for testing the biaxial behavior of biological soft tissues. In order to characterize the biaxial passive mechanical properties, the aspiration test was used for the VHB 4910 membrane under different prestrain levels. A finite element model was created and the constitutive model (with the material parameters presented in section 4.2) was applied. The comparison between experiments and simulations yields a further verification of the mechanical model.

4.3.2 Working principle of the aspiration device

The aspiration test device was originally developed by Vuskovic [Vuskovic 2001] and further improved by Nava [Nava 2004 and Nava 2007]. The working principle of the aspiration device [Nava 2007] is illustrated in Figures 4.2 and 4.3. The device consists of a tube (outer radius: 13 mm, inner radius: 5 mm) in which the internal pressure can be controlled according to a desired pressure law.

The experiment is performed by (i) gently pushing a tube against the tissue to ensure a good initial contact and (ii) creating a vacuum (variable over time) inside the tube so that the tissue is sucked through the aspiration area, Figure 4.2.

For an isotropic and homogenous film, a complete description of the deformation field can be obtained by monitoring the side-view profile of the tissue during the vacuum change. An optical fibre, which is connected to an external source of light, provides the necessary illumination in the inner part of the tube.

The images of the side-view (see Figure 4.2, b) are reflected by a mirror and are captured at a frequency of 25 Hz by a digital camera mounted on the upper part of the device. The grabbed images are analyzed off-line in order to extract the profiles of the deformed tissue. The present image acquisition and analysis technique allows the tissue's vertical displacement, d, (Figure 4.2, b) to be measured with an accuracy of 0.05 mm. A standard personal computer (running NI LabView Version 6.1) controls the pressure inside the device by means of a pump, an air reservoir and two valves. Time histories of measured pressure and deformation profiles represent the input data used to evaluate the mechanical properties and to determine the constitutive model. Further information is given in [Nava 2007].

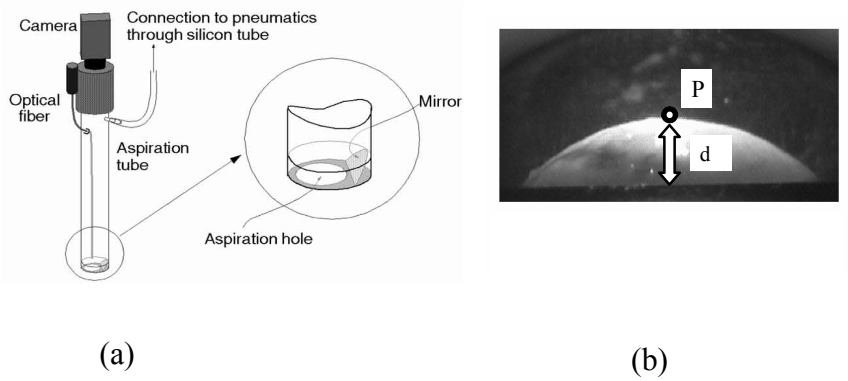

Figure 4.2. (a) Sketch of the aspiration device and (b) image of the side view. The light half-bubble is the part of the tissue that is aspirated inside the device. The point P and the distance d are indicated for reference. The pictures are from [Nava 2007].

4.3.3 Description of the experiments

The samples (VHB 4910) for the aspiration tests were bi-axially pre-strained (see also article 3). Radial pre-straining was realized by the pre-straining machine [Kovacs 2006] developed at EMPA's DE laboratory for biaxial stretching of elastomeric films. Three types of samples were realized with prestretch ratios λ_p = 3, 4 and 5. After radial stretching, the film was fixed uniformly along a circular frame.

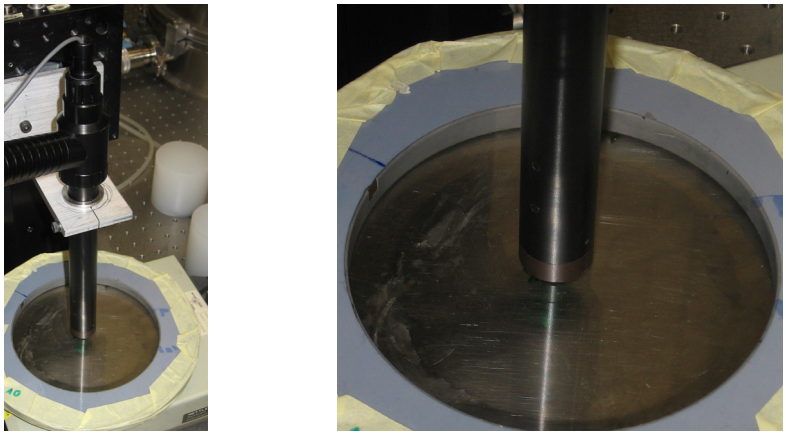

(a) (b)

Figure 4.3. (a) Aspiration test device with a prestrained VHB 4910 membrane and (b) close-up of the device.

Two different aspiration cycles with a pressure of 40 or 55 mbar were applied for 100 s, Figure 4.4. Each experiment consisted of one single aspiration cycle. The displacement d (Figure 4.2 b) was measured.

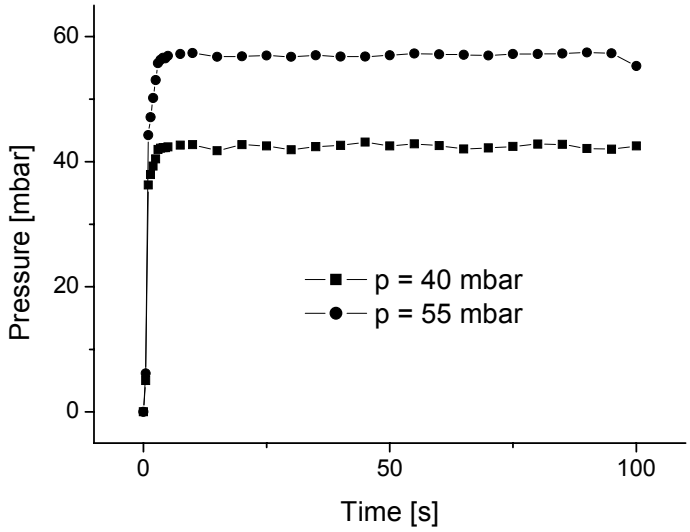

Figure 4.4. Imposed pressure history for the aspiration test

A total number of twelve samples was used for the experimental work. Two experiments were performed for each prestrain and pressure history.

4.3.4 Experimental results

Measurement results are presented in Figure 4.5. The displacement, d, is plotted against time. Each curve corresponds to the average of two experiments, whereby the scatter between experiments was low (the relative variability was less than 7%).

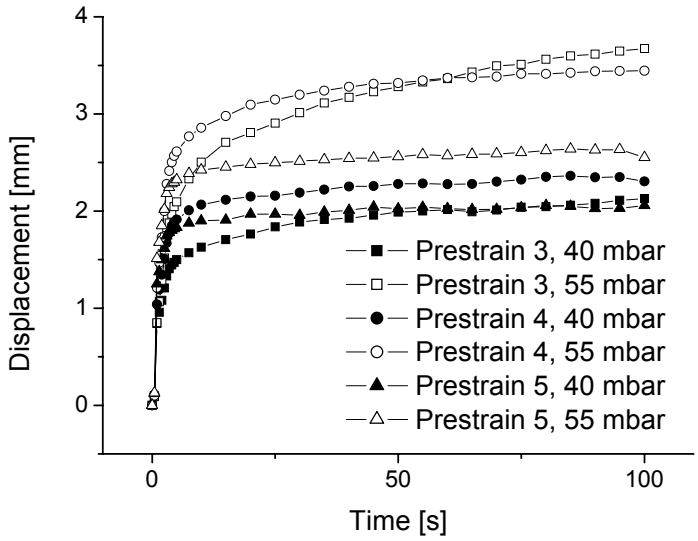

Figure 4.5. Experimental results for the aspiration test device

4.3.5 Finite element calculations

The software ABAQUS 6.5.1 [ABAQUS 2004] has been used for the present calculations of the aspiration test. The axially symmetrical model (Figure 4.6) consists of 4-node elements (CAX4H: 4-node bilinear axisymmetric quadrilateral, hybrid, constant pressure). The homogeneous pressure, p_{as}, corresponds to the imposed pressure history in Figure 4.4 and acts on the aspiration area as a 'surface pressure'.

The simulation of one experiment consists of three steps:

(i) pre-strain in the radial direction, by imposing the displacement of the nodes at the model boundary (Figure 4.6)

(ii) hold time of 1 h. In the time span of 1h, the material is supposed to relax completely (see also relaxation tests, article 1). This corresponds to the experimental conditions of the aspiration test (at least 1 h elapsed between prestretching and aspiration of the elastomer)

(iii) aspiration by imposing the pressure history (Figure 4.4) to the aspiration area. Since VHB 4910 is very sticky, the area with contact to the tube is assumed to be

fixed. Therefore, the nodes of this area were constrained in radial and vertical direction.

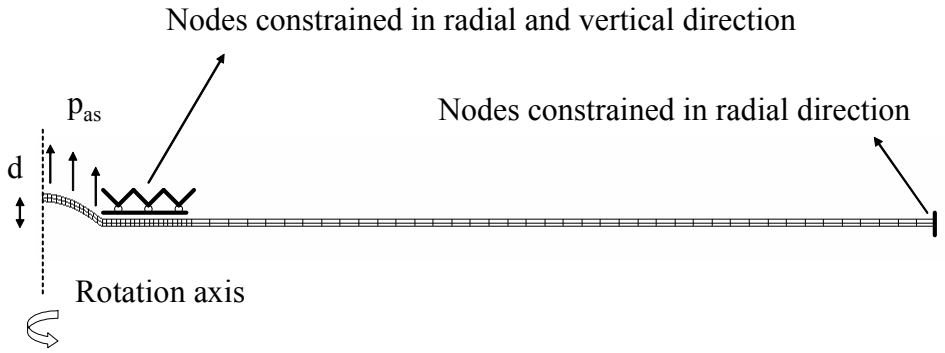

Figure 4.6. Finite element model of the aspiration test

The quasilinear visco-hyperelastic model with the material parameters presented in Table 4.1 and Table 2 in article 3 was applied for the simulations.

4.3.6 Results

Figures 4.7, 4.8 and 4.9 show the comparison between experiments and simulations for the Yeoh, the Ogden and the Arruda-Boyce models respectively.

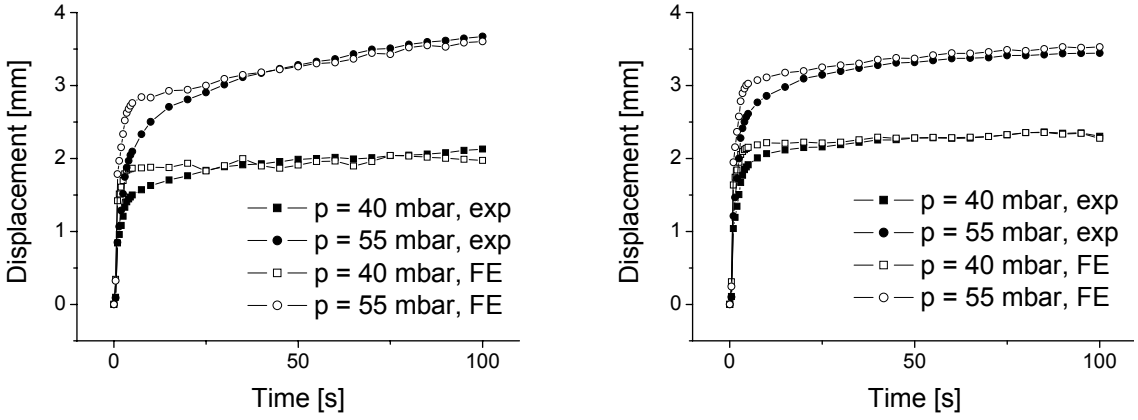

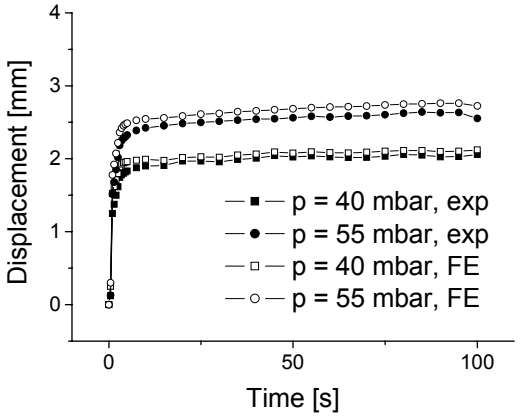

(iii)

Figure 4.7. Comparison between experimental data and simulation for the Yeoh model for pre-strain $\lambda_p = 3$ (i), $\lambda_p = 4$ (ii) and $\lambda_p = 5$ (iii). The abbreviation 'exp' is used for experimental data and 'FE' is used for finite element simulation.

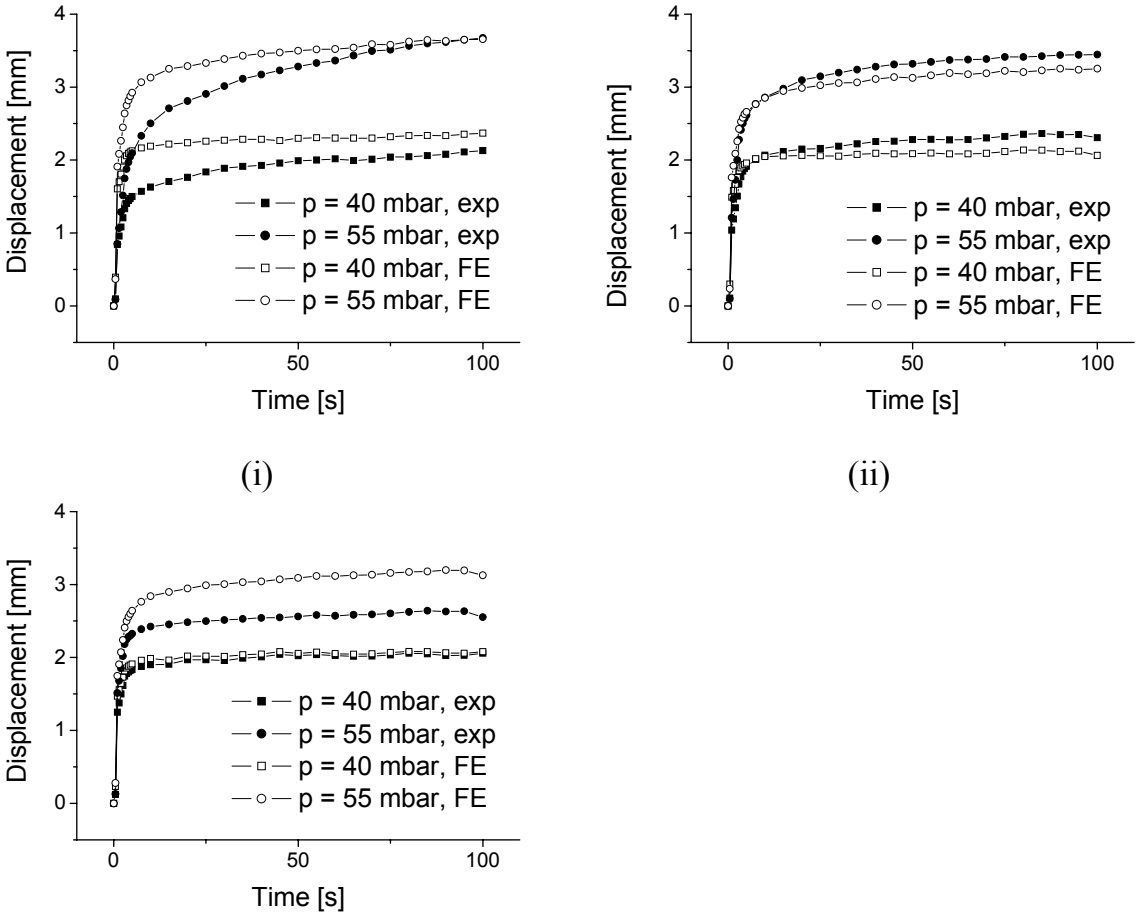

(i) (ii)

(iii)

Figure 4.8. Comparison between experimental data and simulation for the Ogden model for pre-strain $\lambda_p = 3$ (i), $\lambda_p = 4$ (ii) and $\lambda_p = 5$ (iii). The abbreviation 'exp' is used for experimental data and 'FE' is used for finite element simulation.

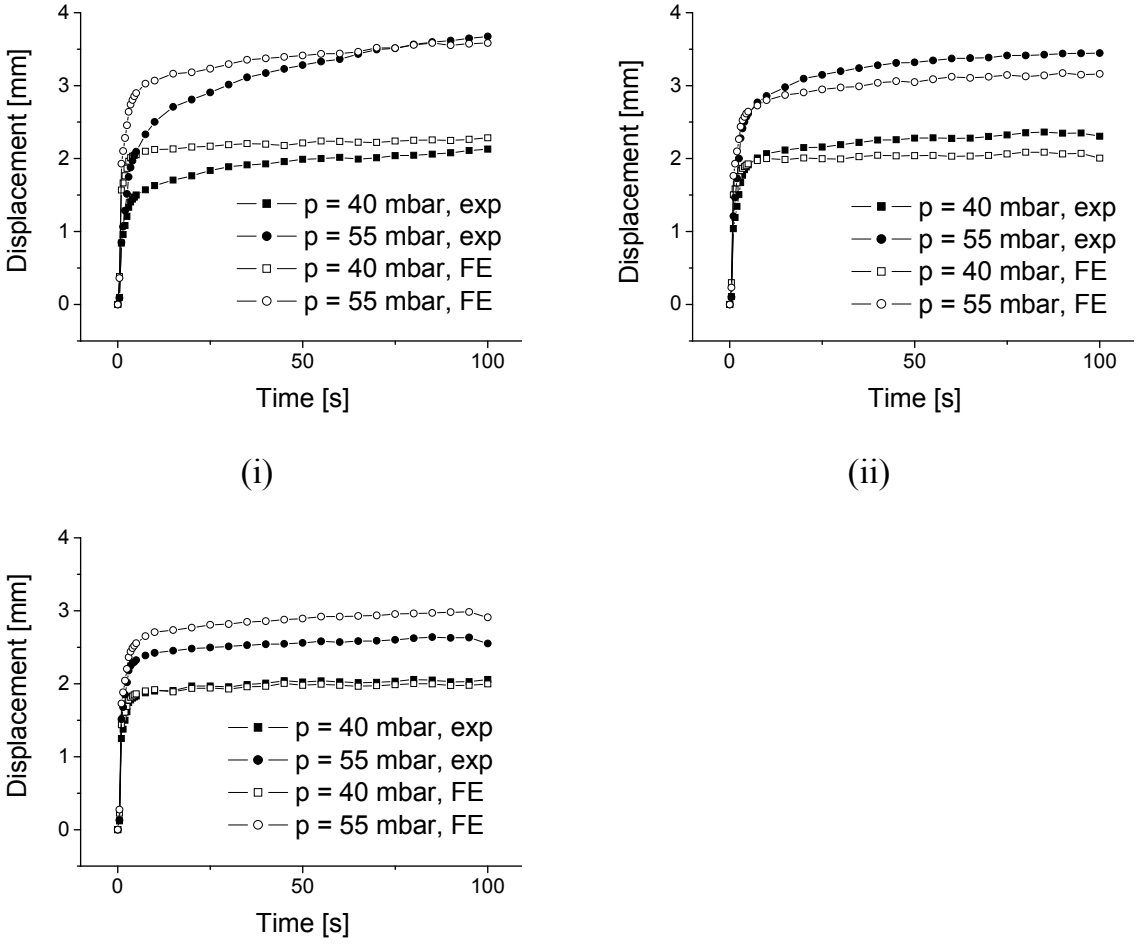

Figure 4.9. Comparison between experimental data and simulation for the Arruda-Boyce model for pre-strain $\lambda_p = 3$ (i), $\lambda_p = 4$ (ii) and $\lambda_p = 5$ (iii). The abbreviation 'exp' is used for experimental data and 'FE' is used for finite element simulation.

Experiments and simulations agree to a great extent, especially for the Yeoh strain energy form. The aspiration tests characterize the biaxial behavior of the elastomer whereas the circular strain tests also include the influence of the electromechanical coupling.

4.4 Compression tests

4.4.1 Introduction

A compression test device is used for further characterization of the elastomer behavior. A sample with thickness z is squeezed by two circular plungers with radius r.

The compression test also exerts a pressure on the elastomer as does the circular strain test. In contrast to the circular strain test where no information about forces is available, the average pressure is measured in the compression test.

These tests have various boundary conditions. The circular strain test corresponds to a mainly biaxial deformation state. In the compression test, the VHB 4910 film adheres to the plunger's surface since the film is very sticky. This effect and the fact that the film is nearly incompressible results in a 'mixed mode' deformation state (see section 4.5). The characterization of the compression behavior provides further verification of the constitutive model.

4.4.2 Experimental details

Compression tests were performed with a Zwick (Z010) machine under displacement control conditions at room temperature (23 °C), Figure 4.10. The radius, r, of the plungers was 1.78 cm. In order to obtain a sample thickness which is of the same magnitude as the radius r, five layers of un-stretched VHB 4910 were glued one on top the other. The sample with an initial thickness of z_0=5 mm was then fixed to a circular frame with an inner radius of R = 75 mm.

Figure 4.10. Sketch of the two plungers of the compression test

The two concentric plungers with the radius r = 1.78 cm of the test device compressed the sample in the middle of the circular frame. The distance z between the plungers was provided by the Zwick (Z010) machine. The control profile of the displacement $d=z_0-z$ is illustrated in Figure 4.11. Two identical samples were tested under identical conditions. The force histories of both experiments are close, see Figure 4.12.

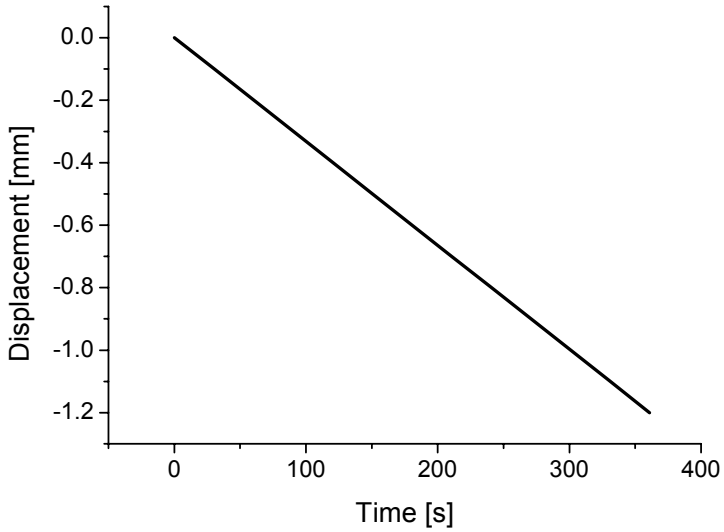

Figure 4.11. Control profile for the compression tests. The displacement is plotted against time

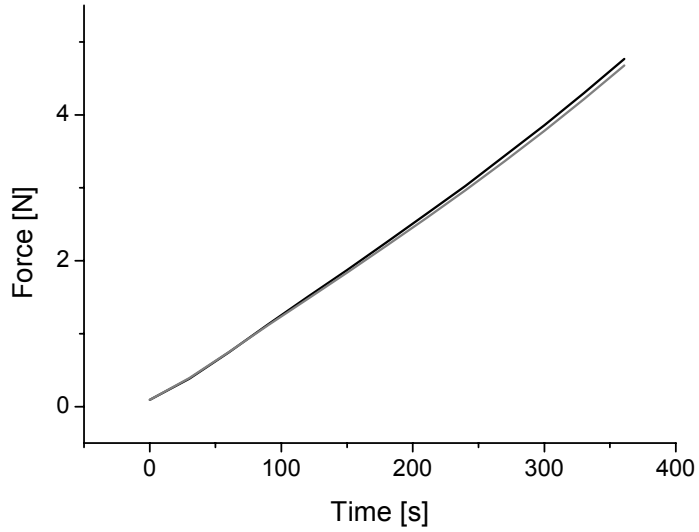

Figure 4.12. Force vs. time for the two compression tests

4.4.3 Finite element simulations

The compression test simulations were performed with ABAQUS 6.5.1 [ABAQUS 2004]. The axially symmetrical model consists of 4-node elements (CAX4H: 4-node bilinear axisymmetric quadrilateral, hybrid, constant pressure), Figure 4.13. Due to the good adherence of the material

(i) the five layers were considered to be one layer with a thickness of z = 5 mm and

(ii) the two plungers were not directly included in the model. Instead, the nodes of Border a and b are fixed in radial direction (Figure 4.13).

As further boundary condition the nodes of Border b were fixed in the vertical direction and the vertical displacement, u_2, of the nodes of Border a corresponds to the displacement history in Figure 4.11.

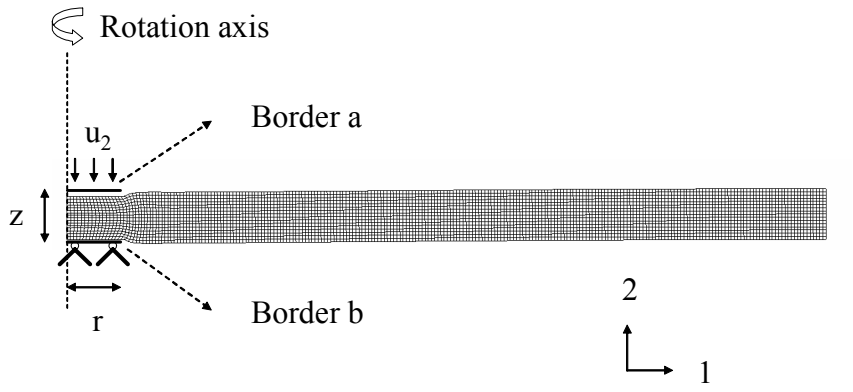

Figure 4.13. Finite element model of a circular dielectric elastomer actuator

The quasilinear visco-hyperelastic model with the parameters of Table 4.1 and Table 2 in article 3 were used. The output of the simulation was the distribution of Cauchy-stresses s_{22} in the vertical direction at Border a as a function of the radius, r. In order to obtain the total force in the vertical direction, the Cauchy stresses s_{22} along Border a were multiplied by the corresponding area and summed up.

4.4.4 Results

Figure 4.14 shows the finite element model of the compression test and Figure 4.15 illustrates the comparison of the force history from experiment and simulation.

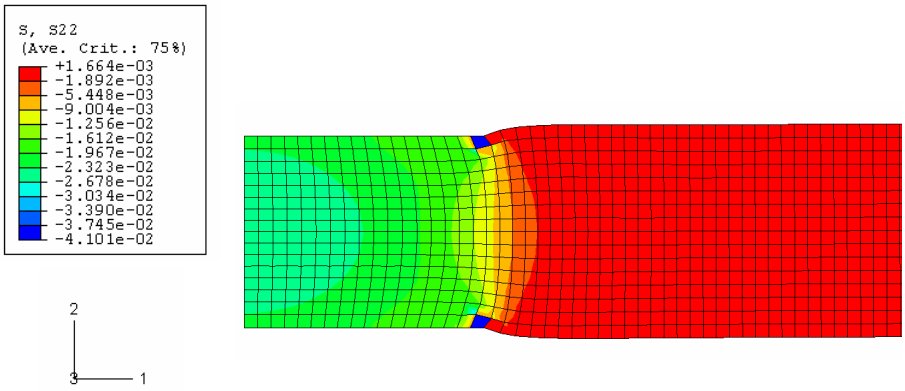

Figure 4.14. Finite element model of the compression test. The stress component s22 is given in MPa.

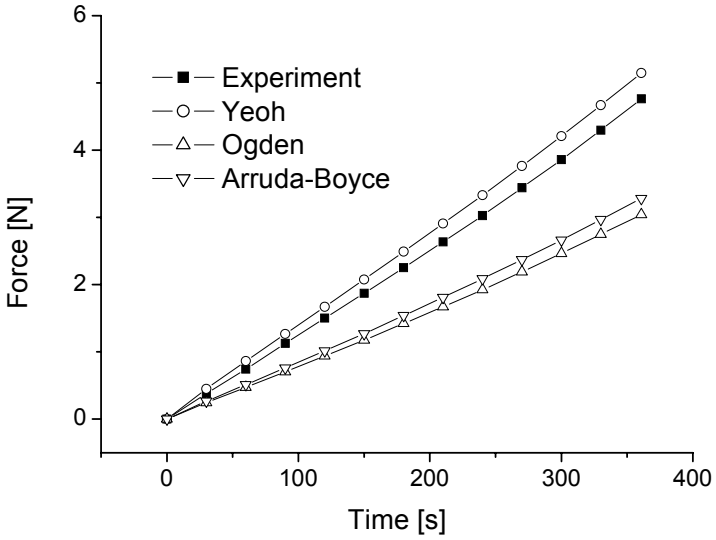

Figure 4.15. Comparison between the experimental and numerical force history

The Yeoh strain energy form yields good agreement between simulation and experiments. By contrast, the force values of the Ogden- and the Arruda-Boyce-strain energy forms are about 40% too small. This finding corresponds with the results shown in Figure 4.1: for small strains (up to 20%) the uniaxial behavior is predicted well with the Yeoh model (Figure 4.1 (i)) whereas the Ogden and the Arruda-Boyce strain energy forms (Figure 4.1 (ii) and (iii)) underpredict the force values.

4.5 Deformation state in the experiments

4.5.1 Introduction

The circular actuators made of VHB 4910 have a large deformation range. The deformation corresponds to a biaxial deformation state with stretch ratios (including the prestrain) of up to 6. In the uniaxial tensile tests, the stretch ratios are also as large as 6. One possibility of analyzing the corresponding deformation states and ranges [Bird 1977 and Treloar 1975] is to plot the first Invariant I_1 as a function of the second invariant I_2 of the left Cauchy-Green deformation tensor. For an incompressible material, the first and the second invariants are

$$I_1 = \lambda_1^{\,2} + \lambda_2^{\,2} + \lambda_3^{\,2} \tag{4.1}$$

$$I_2 = \lambda_1^{\,-2} + \lambda_2^{\,-2} + \lambda_3^{\,-2} \tag{4.2}$$

where the stretch ratios λ_1, λ_2 and λ_3 are the principal values of the deformation gradient and incompressibility yields $\lambda_1\lambda_2\lambda_3=1$. Three important deformation states are uniaxial extension, equi-biaxial stretching and shear [Treloar 1975]. Uniaxial extension is described by the stretch ratios as

$$\lambda_2 = \lambda_3 = \frac{1}{\sqrt{\lambda_1}} \tag{4.3}$$

where $\lambda_1>1$. The equi-biaxial behavior is given by

$$\lambda_3 = \frac{1}{\lambda_1^2} = \frac{1}{\lambda_2^2} \tag{4.4}$$

where λ_1 and λ_2 represent the in-plane stretch ratios and λ_3 the out-of-plane stretch ratio, $\lambda_1 \geq 1$. The shear behavior [Treloar 1975] is given by

$$\lambda_3 = 1/\lambda_1, \ \lambda_2 = 1 \tag{4.5}$$

where $\lambda_1 \geq 1$. A map of deformations is generated by plotting I_1 vs. I_2 for all three deformation states [Bird 1977], Figure 4.16. All combinations of I_1 and I_2 within the shaded zone are accessible [Bird 1977]. Each experiment represents a curve in this plot. The uniaxial and the equi-biaxial behavior stand for the boundaries of the allowable deformation range [Bird 1977].

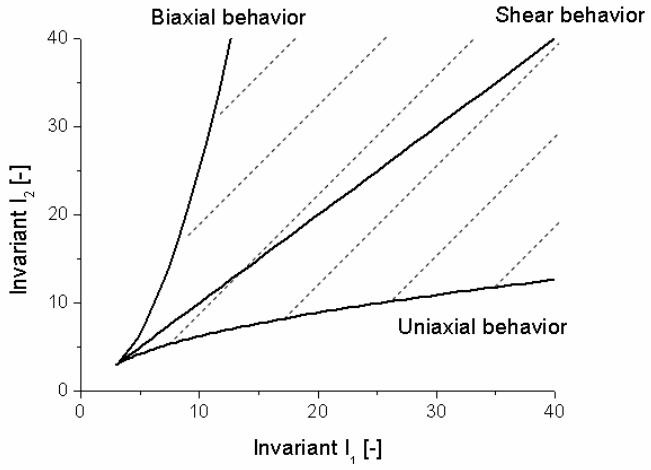

Figure 4.16. Map of deformation range for the classical tests for hyperelastic materials: uniaxial, equi-biaxial and shear behavior

The quality of a three-dimensional model can be evaluated based on its ability to predict the mechanical response for different deformation states. To this end,

experimental data from different test configurations are necessary. In the following sections, the deformation states for the experimental procedures applied in the present work are discussed.

4.5.2 Uniaxial tensile tests

The stretch ratio ranges from 1 to 6 for the uniaxial tensile and relaxation tests. The first invariant I_1 vs. the second invariant I_2 for the uniaxial behavior (λ_1 = 1 to 6) is illustrated in Figure 4.17.

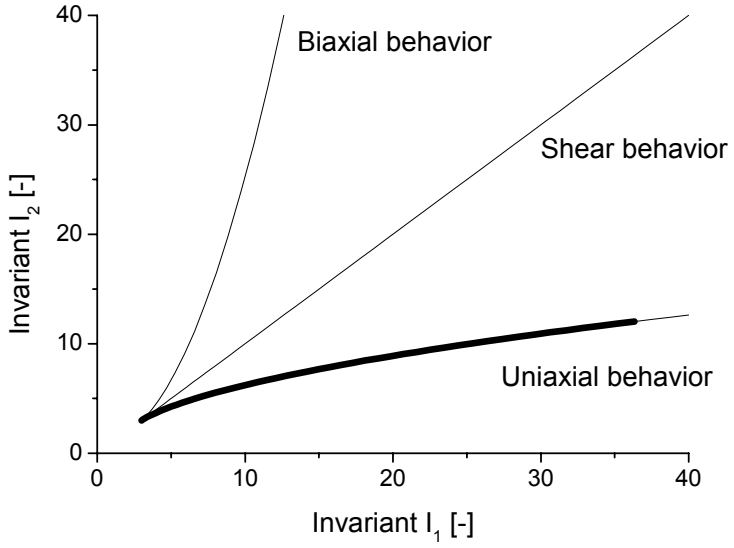

Figure 4.17. Map of deformation range. The curve for the tensile test is indicated in bold.

4.5.3 Circular strain test

The deformation of the active part of the circular actuators is mainly biaxial. The validity of the mechanical model is estimated from Figure 12 in article 3 for the Yeoh strain energy form. The smallest deformation is λ_1= 3 corresponding to a pre-stretch ratio λ_p=3 without activation. The largest stretch ratio where the model still provides reasonable predictions is λ_1= 5.75. This corresponds to 15% nominal strain for the pre-stretch ratio 5. In Figure 4.18, I_1 is plotted logarithmically vs. I_2 for a biaxial behavior from λ_1= 3 to 5.75.

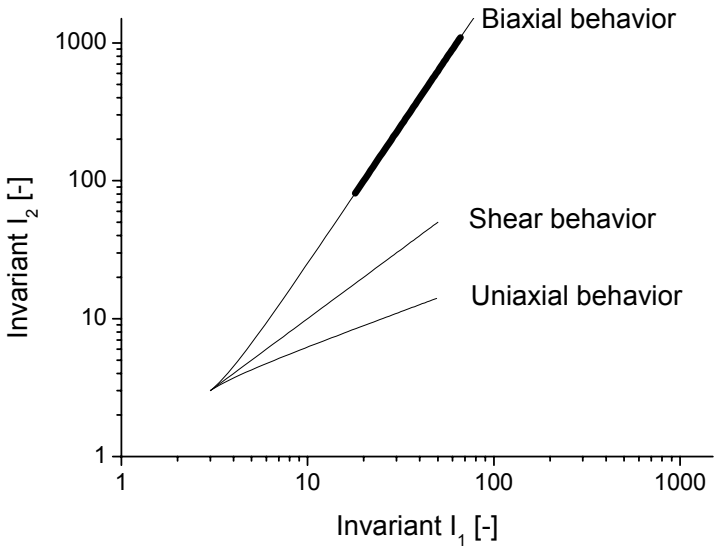

Figure 4.18. Map of deformation range (logarithmic scale). The curve for the circular strain test is indicated in bold.

4.5.4 Aspiration test

The aspiration test corresponds to a great extent to a biaxial configuration. The upper boundary for the stretch ratio λ_1 was taken from the ABQAUS output file at point P (Figure 4.2) for the Yeoh strain energy form. The largest value of λ_1 is 6.09, achieved at prestrain 5. The lowest value is λ_1= 3 corresponding to a pre-stretch ratio λ_p=3, identical to the circular strain test. The deformation range of the aspiration test lies between λ_1= 3 to 6.09, see Figure 4.19.

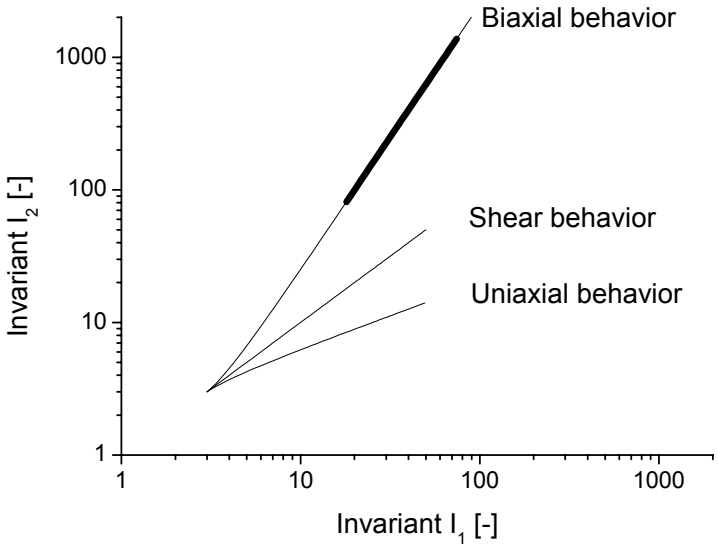

Figure 4.19. Map of deformation range (logarithmic scale). The curve for the aspiration test is indicated in bold.

4.5.5 Compression test

For the compression test, the deformation behavior is strongly dependent on the location of the material points. Therefore, four material points (volume elements with the numbers 1690, 1699, 3601 and 3618) are considered in order to analyze the deformation behavior, see Figure 4.20. In Figure 4.21 I_1 is plotted against I_2 for the four elements. The dependencies between the invariants I_1 and I_2 were taken from the output of the ABAQUS simulation.

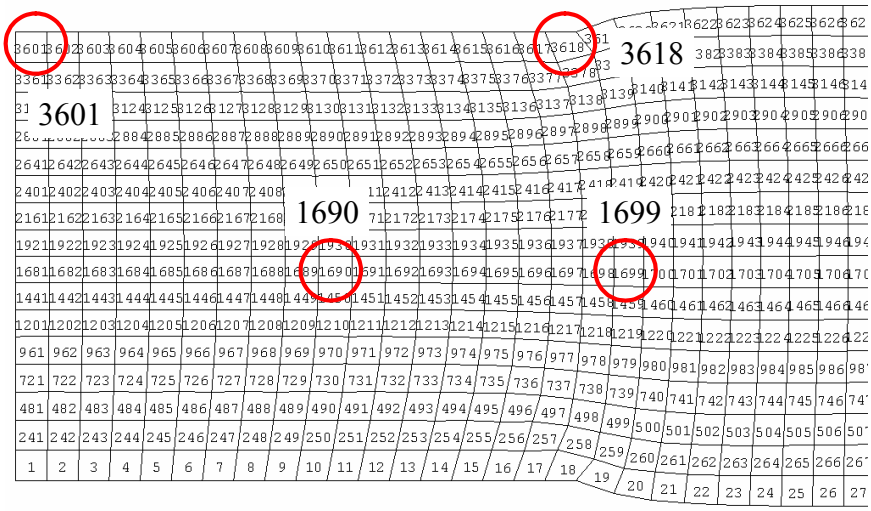

Figure 4.20. Finite element model of the compression test. The elements with the numbers 1690, 1699, 3601 and 3618 were used for the analysis of the deformation behavior.

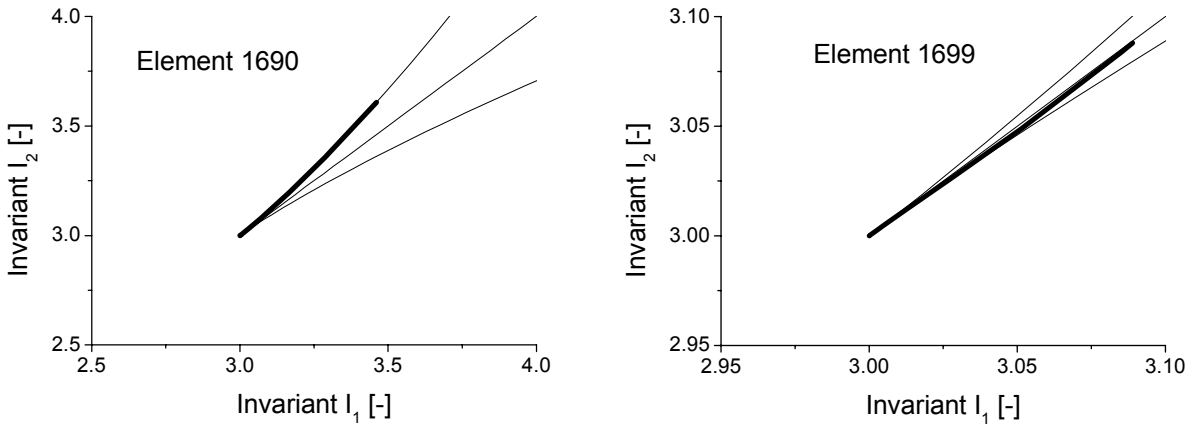

(a) (b)

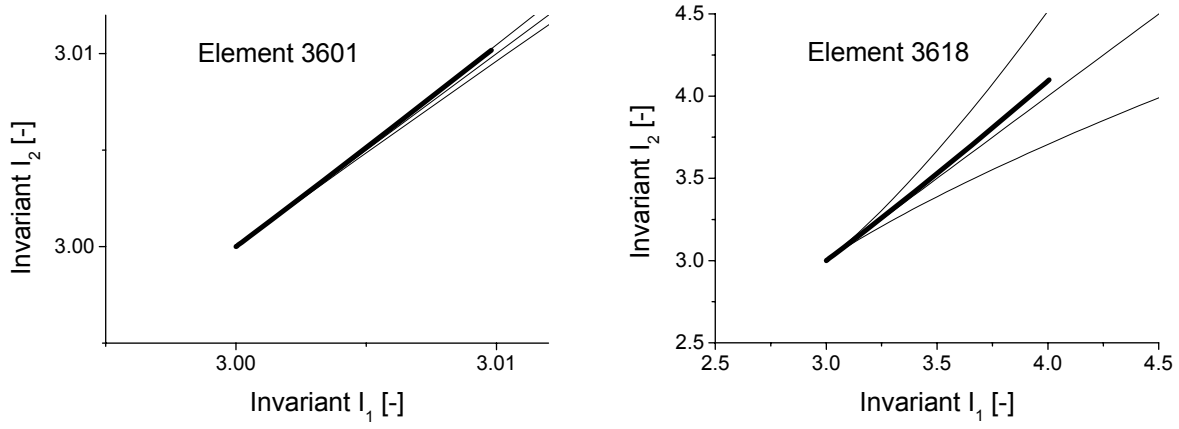

(c) (d)

Figure 4.21. Map of deformation range. The curves for the compression test are indicated in bold for (a) element 1690, (b) element 1699, (c) element 3601 and (d) element 3618.

Elements 1690 and 3601 exhibit a pure equi-biaxial deformation. The deformation of element 3601 is very small compared to element 1690. Element 3618 undergoes a deformation which is similar to the simple shear test. An interesting deformation behavior is shown by element 1699. At small strains the deformation is similar to the uniaxial tensile test and at higher strains the deformation corresponds rather to simple shear.

4.5.6 Discussion

All the findings of section 4.5.2 to 4.5.5 for the uniaxial tests, the circular strain tests, the aspiration tests and the compression tests are presented in one map, Figure 4.22. The deformation range for which the simulations are in agreement with the experiments is wide. From this point of view, the mechanical model (in particular the Yeoh strain energy form) has excellent predictive capabilities. It is clear from the corresponding curves that the circular strain and the aspiration test exhibit a similar deformation behavior. A comparison between the circular strain and aspiration tests therefore provides information about the validity of the model for electromechanical coupling. The deformation range with reliable predictions is larger for the aspiration test than for the circular strain test.

The deformation of the circular strain test and the aspiration experiment are mainly equi-biaxial and thus comparable. However, simulation results are in better agreement with experimental data for the aspiration test than for the circular strain test. The agreement between experimental data and simulation is good for the circular strain test up to 20-25% nominal strain and for the aspiration test up to 55% at λ_p=3, 40% at λ_p=4

and 22% at λ_p=5. This might lead to the conclusion that the disagreement between simulation and experimental data in the circular strain test is due to Pelrine's equation failing to describe the electromechanical coupling at voltages which cause strains greater than 20-25%. The electromechanical coupling at high voltages should be further investigated in more detail.

The compression test covers a much smaller deformation range compared to the other experiments but it has the advantage that different deformation states occur in one single test.

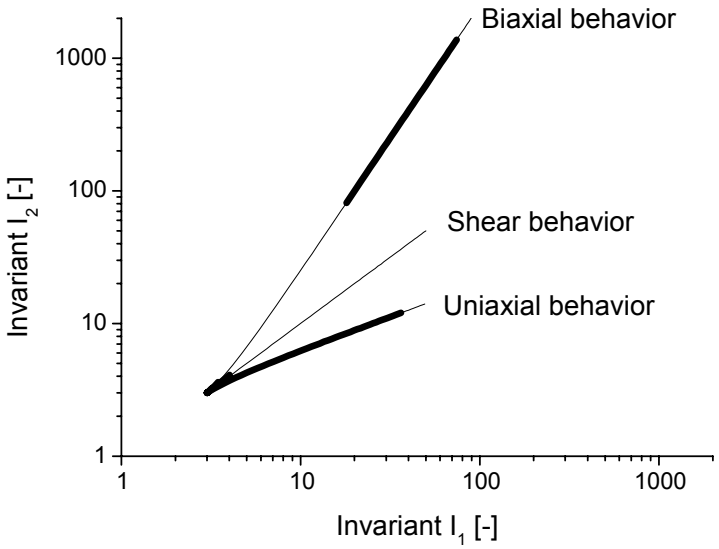

Figure 4.22. Map of deformation range with all tests (bold lines): uniaxial tensile tests, circular strain tests, aspiration tests and compression test.

4.6 Influence of the passive part of a spring roll activation

4.6.1 Introduction

In article 4 the value of the dielectric constant at a prestrain of 4 was determined as 3.2 by spring roll experiments and confirmed by LCR-measurements. As explained in the article, the spring rolls had an active and a passive part.

By the evaluation of the dielectric constant with the spring rolls, it is assumed that the geometrical ratio, r, corresponds to the ratio of force reduction, k. The ratio r is the coated area divided by the whole area of the spring roll ($r=x_a/x_1$, Figure 11, article 4); k is the axial force of a spring roll with ratio r divided by the axial force of a

geometrical identical spring roll without a passive part (r=1). As explained in the article, r=k is an approximation.

In this section, the relationship between r and k is investigated. The results provide a verification of the dielectric constant determination by spring roll experiments. Furthermore, the relationship between r and k is important for the design of spring rolls which are used as artificial muscles [Kovacs 2006] and for walking robots [Pei 2003]. Analytical and numerical calculations are performed for the evaluation of the relationship between r and k. Viscoelastic effects are neglected. The analytical model is more useful than the numerical one because it also contains the electromechanical coupling. But with the analytical model it is not possible to consider the influence of the intersection between the active and passive zones. Therefore the numerical model serves as a verification of the analytical model.

4.6.2 Analytical model

Three planar configurations are considered for the analytical model, Figure 4.23. The notation is slightly different from that in article 4. The configurations are:

(i) the undeformed configuration with the dimensions X, X_a, X_b, Y and Z,

(ii) the prestrained configuration (denoted with the index 'I') with the dimensions x_a^I, x_b^I, x^I, y^I and z^I and

(iii) the activated configuration (denoted with the index 'II') with the dimensions x_a^{II}, x_b^{II}, x^{II}, y^{II} and z^{II}.

The index 'a' refers to the active part and the index 'b' to the passive part.

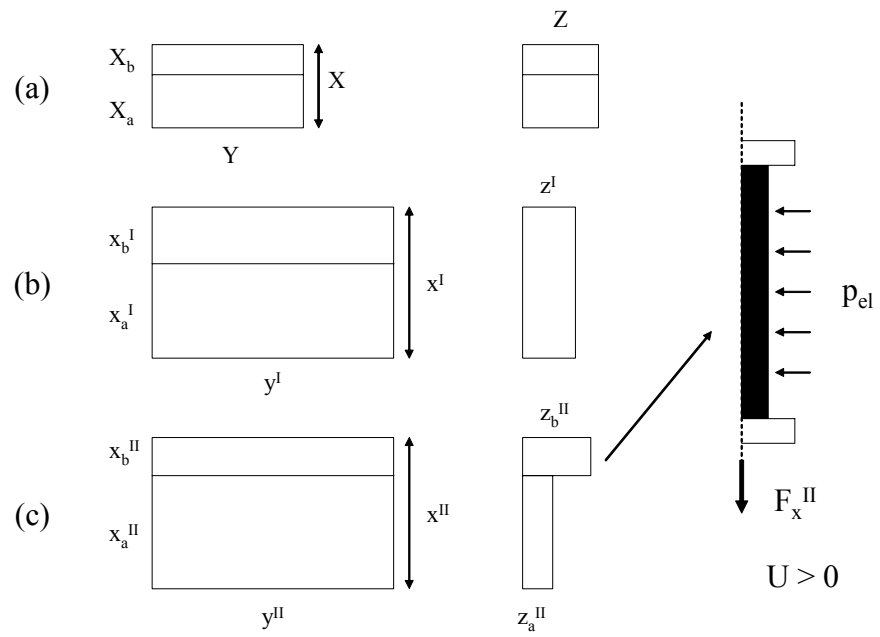

Figure 4.23. Three configurations of deformation for the spring roll: (a) undeformed, (b) prestrained and (c) activated configuration

A Cartesian and not a polar coordinate system is introduced for simplicity. For the calculation results it is assumed that this approach is valid as long as the thickness of one layer is much smaller than the radius of the spring roll.

The original thickness of the film, Z, is assumed to be 1 mm (this corresponds to the film thickness of VHB 4910). The geometrical ratio r is

$$r = \frac{X_a}{X} = \frac{x_a^I}{x^I} \tag{4.6}$$

The nominal actuation strain, s_z, for the deformation of the actuator is introduced for later reference

$$s_z = \frac{z_a^{II}}{z^I} - 1 \tag{4.7}$$

4.6.2.1 Kinematics

For the pre-strained configuration the stretch ratios are

$$\lambda_x^I = \frac{x^I}{X} = \lambda_x \tag{4.8}$$

$$\lambda_y^I = \frac{y^I}{Y} = \lambda_y \tag{4.9}$$

$$\lambda_z^I = \frac{z^I}{Z} = \frac{1}{\lambda_x \cdot \lambda_y} \tag{4.10}$$

where λ_x and λ_y correspond to the pre-stretch ratios of the spring roll. z^I is given by

$$z^I = \frac{Z}{\lambda_x \cdot \lambda_y} \tag{4.11}$$

The stretch-ratios in the y-direction in the active part λ_{ya}^{II} and the passive part λ_{yb}^{II} do not change during activation.

$$\lambda_{ya}^{II} = \lambda_{yb}^{II} = \lambda_y \tag{4.12}$$

By transforming eq. (4.7), z_a^{II} becomes

$$z_a^{II} = (s_z + 1) \cdot z^I \tag{4.13}$$

and thus the stretch ratio of the active area in the z-direction is

$$\lambda_{za}^{II} = \frac{z_a^{II}}{Z} = \frac{s_z + 1}{\lambda_x \cdot \lambda_y} \tag{4.14}$$

Due to incompressibility ($\lambda_{xa}^{II}\ \lambda_{ya}^{II}\ \lambda_{za}^{II}$)=1, the stretch-ratio in the x-direction of the active part is

$$\lambda_{xa}^{II} = \frac{x_a^{II}}{X_a} = \frac{\lambda_x}{s_z + 1} \tag{4.15}$$

With eq. (4.15) the x-coordinate of the active part x_a^{II} is

$$x_a^{II} = \frac{\lambda_x}{s_z + 1} \cdot X_a \tag{4.16}$$

and x_b^{II} is the difference between x^I (eq. (4.8)) and x_a^{II} (eq. (4.16))

$$x_b^{II} = x^I - x_a^{II} \tag{4.17}$$

A combination of eqs. (4.6), (4.16) and (4.17) yields the following expression for the stretch ratio λ_{xb}^{II}

$$\lambda_{xb}^{II} = \frac{x_b^{II}}{X_b} = \lambda_x \cdot \frac{s_z + 1 - r}{(1 - r) \cdot (s_z + 1)} \tag{4.18}$$

where the relationship X_b=X-X_a has been used. Incompressibility yields for the stretch ratio λ_{zb}^{II} in the z-direction

$$\lambda_{zb}^{II} = \frac{1}{\lambda_{xb}^{II} \cdot \lambda_{yb}^{II}} = \frac{1}{\lambda_x \cdot \lambda_y} \cdot \frac{(s_z + 1) \cdot (1 - r)}{s_z + 1 - r} \tag{4.19}$$

4.6.2.2 Kinetics

For an incompressible material, the principal Cauchy stresses, t_i, are determined by the derivative of the strain energy potential, W, with respect to the stretch ratio, λ_i, see article 1.

$$t_i = \lambda_i \cdot \frac{\partial W}{\partial \lambda_i} - p = G(\lambda_i) - p \tag{4.20}$$

where i refers to a principal direction (x, y or z), p is the hydrostatic pressure and G is defined here as:

$$G(\lambda_i) = \lambda_i \cdot \frac{\partial W}{\partial \lambda_i} \tag{4.21}$$

For the pre-strained configuration the stress in the z-direction has to be zero

$$t_z^I = G(\lambda_z^I) - p^I = 0 \tag{4.22}$$

The stress in the x-direction for the prestrained configuration is obtained by using eqs. (4.20) and (4.22).

$$t_x^I = G(\lambda_x^I) - G(\lambda_z^I) \tag{4.23}$$

The axial force F_x^I in the x-direction for the prestrained configuration is

$$F_x^I = t_x^I \cdot y^I \cdot z^I \tag{4.24}$$

In the activated configuration, the stress t_{za}^{II} in the z-direction for part a is

$$t_{za}^{II} = G(\lambda_{za}^{II}) - p_a^{II} = -p_{el} \tag{4.25}$$

where p_{el} is the electrostatic pressure. Solving for p_a^{II} and using eq. (4.20) for the x-direction leads to

$$t_{xa}^{II} = G(\lambda_{xa}^{II}) - G(\lambda_{za}^{II}) - p_{el} \tag{4.26}$$

The axial force of the active and the passive part have to be equal.

$$F_x^{II} = t_{xa}^{II} \cdot y^{II} \cdot z_a^{II} = t_{xb}^{II} \cdot y^{II} \cdot z_b^{II} \tag{4.27}$$

By evaluating the stress t_{xb}^{II} in the y-direction for the passive part and using eqs. (4.26) and (4.27), t_{xb}^{II} is

$$t_{xb}^{II} = \frac{s_z + 1 - r}{1 - r} \cdot [G(\lambda_{xa}^{II}) - G(\lambda_{za}^{II}) - p_{el}] \tag{4.28}$$

Using eq. (4.20), t_{xb}^{II} can also be expressed as

$$t_{xb}^{II} = G(\lambda_{xb}^{II}) - p_b^{II} \tag{4.29}$$

The stress t_{zb}^{II} of the passive part in the z-direction is zero

$$t_{zb}^{II} = G(\lambda_{zb}^{II}) - p_b^{II} = 0 \tag{4.30}$$

Combining eqs. (4.29) and (4.30) gives for t_{xb}^{II}

$$t_{xb}^{II} = G(\lambda_{xb}^{II}) - G(\lambda_{zb}^{II}) \tag{4.31}$$

4.6.2.3 Electromechanical coupling

By equating eqs. (4.28) and (4.31), the following relationship is obtained

$$t_{xb}^{II} = \frac{s_z + 1 - r}{1 - r} \cdot [G(\lambda_{xa}^{II}) - G(\lambda_{za}^{II}) - p_{el}] = G(\lambda_{xb}^{II}) - G(\lambda_{zb}^{II}) \tag{4.32}$$

The electromechanical pressure, p_{el}, is given by Pelrine's equation [Pelrine 1998]

$$p_{el} = \varepsilon_r \cdot \varepsilon_0 \cdot \left(\frac{U}{z_a^{II}} \right)^2 \tag{4.33}$$

Solving for U and using eqs. (4.11), (4.13), (4.32) and (4.33) gives

$$U = \frac{Z \cdot (s_z + 1)}{\lambda_x \cdot \lambda_y \cdot \sqrt{\varepsilon_r \cdot \varepsilon_0}} \cdot \left(G(\lambda_{xa}^{II}) - G(\lambda_{za}^{II}) - \frac{1 - r}{s_z + 1 - r} \cdot (G(\lambda_{xb}^{II}) - G(\lambda_{zb}^{II})) \right)^{1/2} \tag{4.34}$$

This relationship represents a connection between the voltage, the geometrical dimensions, the prestrain of the spring roll, the strain s_z, the hyperelastic material parameters and the dielectric constant.

The parameter k is determined by evaluating the force differences ΔF and ΔF_{eff}. The force difference, ΔF_{eff}, corresponds to the difference of eqs. (4.24) and (4.27)

$$\Delta F_{eff} = F_x^{II} - F_x^{I} \tag{4.35}$$

The force difference ΔF of a spring roll without a passive part is

$$\Delta F = p_{el} \cdot y^I \cdot z^I = \varepsilon_r \cdot \varepsilon_0 \cdot \left(\frac{U}{z^I}\right)^2 \cdot y^I \cdot z^I \tag{4.36}$$

and with eq. (4.11) yields:

$$\Delta F = \varepsilon_r \cdot \varepsilon_0 \cdot U^2 \cdot \frac{Y}{Z} \cdot \lambda_x \cdot \lambda_y{}^2 \tag{4.37}$$

The ratio k is given by $k=\Delta F_{eff}/\Delta F$. The whole system is described by the derived equations. The equations are implemented into Matlab [Matlab 2004]. For the comparison between analytical and numerical calculations, two different prestrain levels, 1x1 ($\lambda_x=\lambda_y=1$, no prestrain) and 4x4 ($\lambda_x=\lambda_y=4$), are considered. The selected parameters for the analytical model are listed in Table 4.2. The initial thickness at prestrain 4x4 is the value of undeformed VHB 4910, 1mm. For prestrain 1x1 a value of 50µm was chosen in order to ensure that the thickness is much smaller than the radius of the elastic core of the spring roll which is an assumption of the analytical model. The dielectric constant, ε_r, was 3.2 for both prestrains and the ratio r was 0.77. The Yeoh strain energy form was used for W with the material parameters listed in Table 4.1.

Table 4.2. Parameters for the analytical model

	Prestrain 1x1	Prestrain 4x4
Dielectric constant ε_r [-]	3.2	3.2
Ratio r [-]	0.77	0.77
Initial thickness Z [mm]	0.05	1
C_{10} [MPa]	0.0537433	0.0537433
C_{20} [MPa]	-4.857E-04	-4.857E-04
C_{30} [MPa]	3.809E-06	3.809E-06

4.6.3 Numerical considerations

Two axially symmetrical finite element models with hyperelastic material behavior (the viscoelastic part was neglected) were created in ABAQUS in order to verify the analytical calculations.

The first model was a spring roll with a prestrain 1x1 ($\lambda_x=\lambda_y=1$, no prestrain) and the second model had a prestrain of 4x4 ($\lambda_x=\lambda_y=4$). For both models, the geometrical ratio, r, was chosen as r=77%. The element type (4-node bilinear axially symmetrical quadrilateral, reduced integration) was applied and the Yeoh model was used for the material model with the parameters in Table 4.1.

A single layer was considered for both spring rolls in the finite element model (Figure 4.24). The spring roll with prestrain 4x4 was simulated in three steps, Figure 4.24:

(i) prestraining with a factor of 4 in the x-direction, the edge DC was displaced vertically and the edge AB was fixed in the x-direction

(ii) prestraining in the z-direction (the edge AD was displaced) in such a way that the stretch ratio in the z-direction and the r-direction was 4 after step (ii). The geometrical parameters after step (ii) corresponded to the actual geometry of the spring rolls in article 4, Figure 11: x_1 = 143 mm, x_a = 110 mm and z_1 = 62.5 µm. The radius of the spring roll, r_0, was 3.5 mm

(iii) applying a displacement, u_r, in the (negative) r-direction, see Figure 4.24

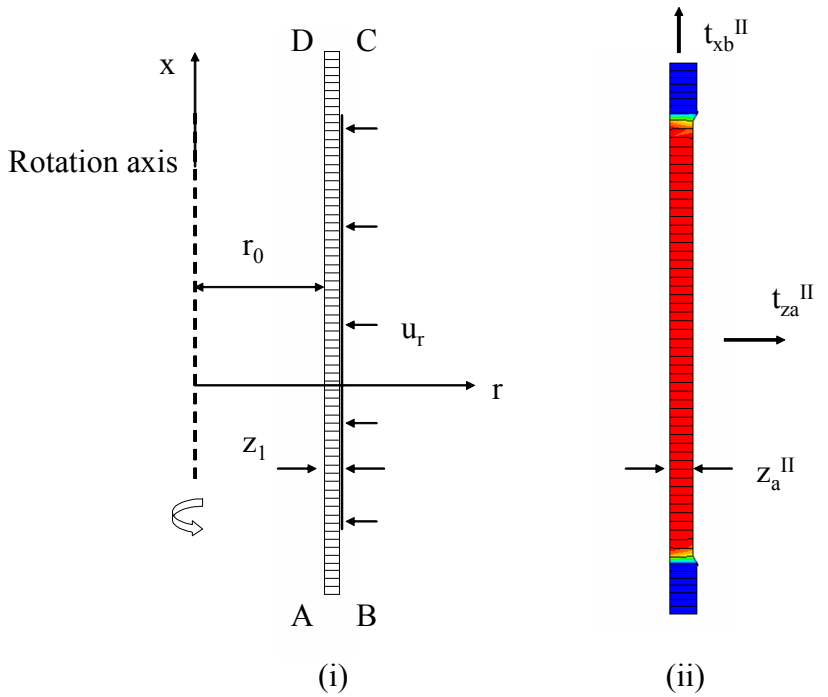

Figure 4.24. Finite element model of the spring roll (prestrain 4x4), (a) sketch and (b) finite element model, the scale factor in the radial direction is 100.

Only step (iii) was performed for the spring roll with prestrain 1x1. The thickness z_1 was chosen as 50 µm and the radius r_0 as 5 mm. The same material parameters as for the analytical model were applied for both simulations. The thickness, the prestrain (in the radial and axial directions) and the ratio r were identical for the analytical and the numerical models for each single prestrain, 1x1 and 4x4.

4.6.4 Results

A comparison between analytical and numerical calculations is shown in Figure 4.25. The stresses t_{za}^{II} of the active part and t_{xb}^{II} of the passive part are plotted against the thickness z_a^{II}.

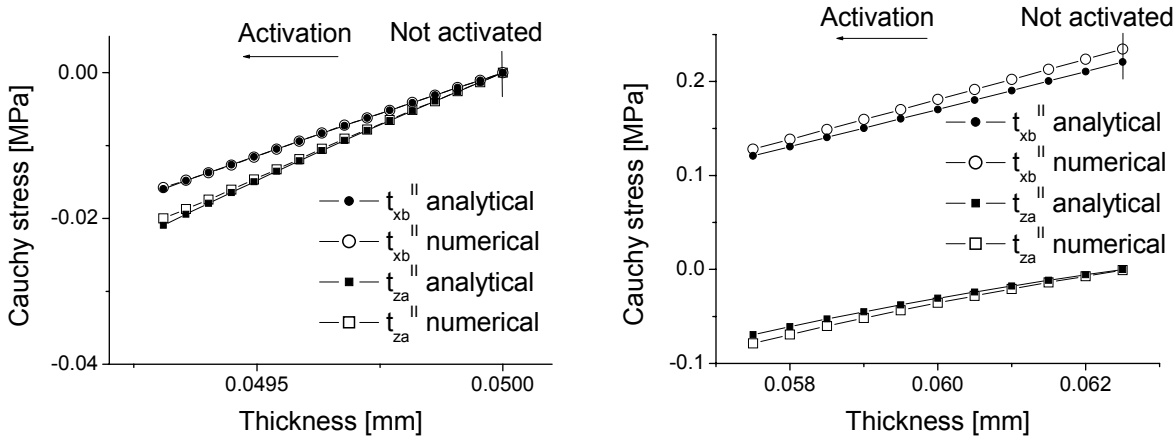

(a) (b)

Figure 4.25. Analytical vs. numerical calculations for (a) a spring roll with prestrain 1x1 and (b) a spring roll with prestrain 4x4. The stresses are plotted against the thickness.

The finite element and analytical results agree to a great extent and this provides a verification of both the analytical and the numerical model. The distinctions between analytical and numerical model are larger for prestrain 4x4 than 1x1. The discrepancies between the analytical and numerical models might come from the transition between the active and the passive part. The analytical model allows the voltage, U, to be plotted against k for different ratios r. For prestrain 4x4, the voltage U is calculated as function of k for the geometrical ratios r = 0.7, 0.8 and 0.9, Figure 4.26.

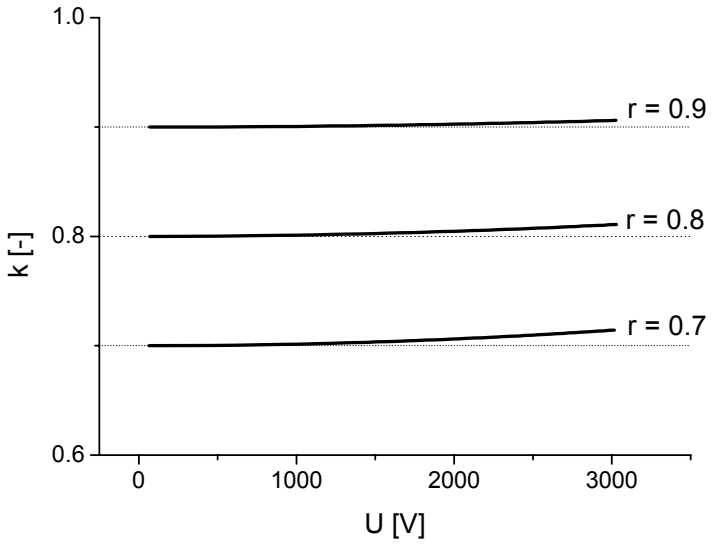

Figure 4.26. Voltage U vs. ratio k for different geometrical ratios r = 0.7, 0.8 and 0.9.

The analytical and numerical models are in agreement for spring rolls with prestrain 1x1 and prestrain 4x4. The ratio k depends on the following parameters: the geometrical ratio, r, the voltage, U, the dielectric constant, ε_r, the pre-stretch ratios, λ_x and λ_y, the initial thickness, Z, and the material parameters, C_{10}, C_{20} and C_{30}. When the voltage is zero, the ratio k corresponds to the ratio r. By increasing the voltage, k increases only slightly.

From an experimental point of view, the ratio k should be considered as constant, as confirmed by the fact that fitting the experimental electromechanical pressure with Pelrine's equation gives an excellent result. In this sense, the slight dependence of k on the voltage is in agreement with the experiments.

The analytical model does not consider the electrodes. The electrode seems not to have a strong influence. By assuming k=r, force measurements of spring rolls provide a value for the dielectric constant of 3.24. This is in agreement with dielectric constant measurements (article 4).

Future work should consider the influence of the electrodes by a spring roll activation which can deform in the axial direction (no fixation).

5 Conclusions and Outlook

5.1 Main contributions of the present work

An important contribution of this thesis is represented by the mechanical model (including the corresponding material parameters) valid over a wide deformation range for dielectric elastomer actuators made of VHB 4910. A large number of experiments including circular strain tests, uniaxial tests, aspiration tests and compression tests were performed and the test data were shared with the scientific community for model verification purposes. A finite element model was created and simulations were performed for each test. Comparisons between experiments and simulations showed that the constitutive model (in particular with the Yeoh strain energy form) is able to describe the material behavior for several deformation and activation configurations.

Electromechanical coupling has been investigated and a new physical interpretation of Pelrine's equation was found. The dielectric constant has been determined directly with a LCR-meter and with spring roll experiments. Specific conclusions were drawn based on the results presented in each article that constitute the main part of the present work.

Article 1 verifies the quasilinear visco-hyperelastic model, which includes large deformation and viscoelasticity. The condition of validity for quasilinear viscoelasticity (the stress relaxation function is independent of the magnitude of the deformation) is verified based on relaxation tests. The strain energy potential of Yeoh is used to describe large deformations. The material parameters were obtained by fitting experimental data using an optimization algorithm. An inverse finite element technique is introduced for the calculation of the circular actuator. Simulation results have shown a good agreement between experiments and simulations for the circular strain test.

Article 2 presents an analytical model for circular actuators. An equation that links the voltage, the prestrain and the active strain was derived. The analytical model was verified numerically. The analytical model is valid for hyperelastic materials (time-dependent effects are neglected) and might be useful for the design of silicone actuators with less pronounced viscoelastic behavior. The analytical model allows the investigation of electromechanical instabilities which might lead to failure of the actuators.

Article 2 demonstrates that the fitting of uniaxial data for the strain energy forms of Yeoh, Ogden and Mooney-Rivlin leads to different simulation results in the (multiaxial) VHB 4910 actuator behavior. This shows the importance of characterizing the biaxial response of the elastomer. This step was omitted in most previous work (see section 1.4) on dielectric elastomers, where material models are proposed based on uniaxial test data only.

In article 3 an extensive experimental study on circular actuators is presented. A novel finite element technique was used which allows direct simulation of actuator activation by the applied voltage. Three different constitutive model formulations were evaluated, viz. the strain energy forms of Yeoh, Ogden (six parameters instead of only two as in article 2) and Arruda-Boyce. The corresponding material parameters were determined with an enhanced optimization procedure.

The behavior of three actuators at prestrain 3, 4 and 5 was included in the optimization procedure. With the optimized material parameters, the actuator behavior was reasonably described by the model over a large strain range. By contrast, the uniaxial tensile test simulation did not fit the experimental data. This discrepancy has been further analyzed in article 4. Furthermore, limitations of the proposed quasilinear visco-hyperelastic model were demonstrated when applied to the prediction of the actuator behavior for a large number of activation cycles.

In article 4 the electromechanical coupling was investigated. Pelrine's equation was verified by an analytical approach. A numerical investigation provides the charge, electric field and electrostatic force distribution for a circular actuator. It is found that the electromechanical pressure acts in the thickness direction and with the same magnitude in the lateral direction. By considering a superimposed hydrostatic stress state the resulting out-of-plane pressure corresponds to the result obtained by Pelrine.

Measurements of the dielectric constant demonstrated that its value decreases with increasing prestrain. The dielectric constant of VHB 4910 is about 3.2 and not 4.7 (as proposed by Kofod and used by many researchers) in the relevant prestrain range. This was also verified with the spring roll experiments.

With the findings of this paper the material parameters of the constitutive model were adapted. A comparison between simulations (demonstrated with the Arruda-Boyce strain energy form) and experiments showed a significant improvement for the uniaxial behavior.

In section 5 the constitutive model parameters for the Yeoh and the Ogden strain energy form were adjusted based on a new value of the dielectric constant. Results

have shown, that for all three strain energy formulations the uniaxial behavior is well described.

Aspiration and compression tests are presented for the verification of the multiaxial response predicted using the constitutive model. The results showed that the Yeoh formulation yields excellent agreement between experiments and simulations. This is not only a confirmation of the validity of the constitutive model but also, indirectly, of the electromechanical coupling.

The deformation range of all performed experiments was studied by plotting the first invariant vs. the second invariant of the left Cauchy Green deformation tensor. This showed that the constitutive model is valid over a large deformation range.

The influence of the geometrical ratio between the active and passive parts of spring rolls was investigated. This is important for (i) the design of spring rolls and (ii) the interpretation of the measurements of the dielectric constant. Results showed that the geometrical ratio, r, corresponds in a good approximation to the so-called force ratio, k, introduced in article 4.

5.2 General design considerations and suggestions for future work

The performance of dielectric elastomer actuators depends on the material properties of the elastomer and their geometrical characteristics. Here, some considerations are proposed on the material behavior and the geometrical design of the actuator with respect to the findings of the present work.

5.2.1 Material behavior of the elastomer

The constitutive model presented in this work is valid for VHB 4910. For a different material, but which is also incompressible and quasilinearly viscoelastic, the same constitutive model formulation can be applied, provided the respective material parameters are determined, e.g. with the procedures described in the present work. For rubber-like materials (e.g. silicones) without a dissipative behavior, time dependence does not have to be considered. Thus, the analytical model as proposed in article 2 might be used for the optimization of the actuators.

Models with internal state variables (e.g. [Rubin 2002]) that can be interpreted as describing changes in the material microstructure, can be applied for elastomers with a significant dissipative and history-dependent response.

For the characterization and modeling of a new DE material one of two cases may occur:

(i) the material is given and an adequate constitutive model has to be determined and

(ii) the desired constitutive model is given (due to the required actuator performance) and an adequate material has to be found or synthesized.

The formulation and the determination of the mechanical material parameters and the dielectric constant are necessary to define a constitutive model for a given material. As shown in the present work, the multiaxial material behavior has to be considered in the fitting process of the material parameters.

The second case occurs when input voltages and the mechanical output (stresses/strains) of the actuator are prescribed. A suitable elastomer is required which can be, for example synthesized. For this purpose, it is useful to evaluate the link between the microstructure of the elastomer and the constitutive model. For example, the Arruda-Boyce strain energy form [Arruda 1993] is based on statistical mechanics and the parameters are physically linked to the chain lengths and orientations involved in the deformation of the three-dimensional network structure of the rubber [Holzapfel 2000]. By fitting the constitutive model parameters in such a way that the required actuator output is achieved in the simulations, the material parameters (e.g. shear modulus and number of chain segments) can be used as a basis for the synthesis of the elastomer.

5.2.2 Geometrical design of the actuator

The results of the present work make fundamental contributions to the modeling of dielectric actuators (not only their material). In particular, circular actuators have been simulated. Suitable numerical models have to be developed for the design of actuators for general applications. The design of the actuator can be optimized based on the model presented here. One relevant design parameter in particular is the level of prestretch (in each planar direction) to be applied. For spring rolls used as artificial muscles [Kovacs 2006] or walking robots, axially symmetrical finite element models can be created with axially symmetrical elements similar to the procedure described for circular actuators. For applications with complex geometries such as shell-like structures [Lochmatter 2006b] or blimps [Michel 2006], three-dimensional finite element models with thin shell elements are required. Standard shell elements are not able to transfer the electromechanical pressure in the lateral direction for hyperelastic materials. New program codes have to be developed for the design of such structures.

The results of article 4 offer novel design possibilities for actuators. The finding that high lateral forces arise at the lateral surface area might be useful for enhancing the efficiency of the electromechanical coupling. The absorption of a larger charge density would increase the electrostatic forces. This could be achieved by a smart design of the electrodes: By applying a material with a high dielectric constant (e.g. ceramics) at the lateral boundaries, the electrode could absorb a greater charge due to the high polarization of the material with high dielectric constant.

In general, further investigation of the electrodes and the electromechanical coupling are required to improve the predictive capabilities of the models, in particular for high activation voltages. The physical mechanism of electrostatic force transmission from the electrodes to the elastomer in the out-of-plane and in-plane directions has to be understood in order to optimize the selection of electrode material.

5.2.3 Reliability

A further challenge is to describe the failure mechanisms by experiments and simulations. In [Plante 2006a and Plante 2006b] three failure mechanisms are described, viz. material strength failure, dielectric strength failure and pull-in instability failure. The material strength is purely a mechanical failure caused by stretching the elastomer over a certain limit. The dielectric strength is a purely electrical failure mechanism and occurs when the electrical field is higher than the electrical breakdown field. The pull-in instability occurs when the magnitude of the electromechanical pressure increases at a greater rate than the mechanical out-of-plane stress.

Plante performed experiments and calculations for circular actuators and for diamond actuators relating failure. Failure maps which compare the experimental and the calculated failure strain were created. For some cases, the experimental and the calculated values agreed, for other cases the analytical prediction was 57% over the experimental value. The failure models were only verified by a few pre-stretch ratios (e.g. for the diamond actuator only one pre-stretch ratio was considered).

In general, reliability should be investigated more in detail. It is a relevant aspect for dielectric elastomer technology, especially for the development of commercial applications. For future work, the following points should be considered:

(i) The quantitative connection between failure mechanism of circular actuators and ‘real applications’ needs to be understood. The circular actuator is a good model system as shown in the present work.

(ii) The influence of the electrode should be evaluated. The electrode composition and shape might influence the failure behavior of the actuators.

(iii) The fatigue behavior of actuators should be investigated more in detail. Both cyclic mechanical and actuator tests are required.

(iv) The influence of pre-stretching the elastomer with respect to failure behavior needs to be understood. In general, time-dependent failure mechanisms have to be identified.

(v) Different elastomers should be investigated, in order to evaluate their differences and commonalities in failure mechanisms.

Bibliography

ABAQUS/Standard Manual, 2004. Version 6.5.1, Hibbitt, Karlsson & Sorensen, Inc.

Aoki T., T. Ohashi, et al., (1997). The pipette aspiration applied to the local stiffness measurement of soft tissues, *Ann. Biomed. Eng.*, vol. 25, pp. 581 - 587

Arruda E.M., M.C. Boyce (1993). A three-dimensional constitutive model for the large stretch behavior of rubber elastic materials, *J. Mech. Phys. Solids*, vol. 41, No.2, pp. 389 - 412

Aschwanden M., A. Stemmer (2006). Polymeric, electrically tunable diffraction grating based on artificial muscles, *Optical letters*, vol. 31, no. 17, pp. 2610-2612

Ashley S. (2003). Artificial muscles, *Scientific American*, vol. 289, no. 4, pp. 52-59

Bar-Cohen Y. (2001). Electroactive polymer (EAP) actuators as artificial muscles: Reality, potential and challenges, SPIE Press, Bellingham, Washington

Baughman R.H., C. Cui, et al. (1999). Carbon nanotune actuators, *Science*, vol. 284, pp. 1340-1344

Bergström J., M. Boyce (1998). Constitutive modeling of the large strain time-dependant behavior of elastomers, *Journal of Mechanics and Physics of Solids*, vol. 46, No. 5, pp. 931-954

Bird R.B., R.C. Armstrong, O. Hassager (1977). Dynamics of polymeric liquids – volume 1: Fluid mechanics, second edition, New York, Wiley

Boyce M.C., E.M. Arruda (2000). Constitutive models of rubber elasticity: A review, *Rubber Chemistry and Technology*, vol. 73, no. 3, pp. 504-523

Calvert P., J. O'Kelly, C. Souvignier (1998), Solid freeform fabrication of organic-inorganic hybrid materials, *Mat. Sci. Eng. C*, vol. 6, pp. 167-174

Carpi F., P. Chiarelli, et al. (2003). Electromechanical characterisation of dielectric elastomer planar actuators: comparative evaluation of different electrode materials and different counterloads, *Sens. Actuators A*, vol. 107, pp. 85-95

Carpi F., D. De Rossi (2004). Dielectric elastomer cylindrical actuators: electromechanical modeling and experimental evaluation, *Mat. Sci. Eng. C*, vol. 24, pp. 555-562

Christensen R.M. (1981). Theory of viscoelasticity: an introduction, Academic Press, New York

COMSOL Multiphysics, 2005, User's Guide, version 3.2, COMSOL, Inc.

Fung Y.C. (1993). Biomechanics. Mechanical properties of living tissues, 2nd edn., Springer-Verlag, New York, p. 277

Gandhi M.R., P. Murray, et al. (1995). Mechanisms of electromechanical actuation in polypyrrole, *Synthetic Metals*, vol. 75, pp. 247-256

Goulbourne N., M. Frecker, et al. (2003). Modeling of a dielectric elastomer diaphragm for a prosthetic blood pump, Proc. SPIE, vol. 5051, pp. 319-31

Goulbourne N., E. Mockensturm, M. Frecker (2005). A nonlinear model for dielectric elastomer membranes, *Journal of Applied Mechanics*, vol. 72, pp. 899 – 906

Heydt R., R. Kornbluh, et al. (1998). Design and performance of an electrostrictive-polymer-film acoustic actuator, *Journal of Sound and Vibration*, vol. 215, no. 2, pp. 297-311

Holzapfel A. (2000). Nonlinear solid mechanics – a continuum approach for engineering, John Wiley & Sons, Chichester, UK

Kim J., J.Y. Kim, S.J. Choe (2000). Electro-active papers: its possibility as actuators, Proc. SPIE, vol. 3987, pp. 203-209

Kim H., S. Oh, et al. (2001). Actuator model of electrostrictive polymers (EPs) for microactuators, Proc. SPIE, vol. 4329, pp. 482-490

Kofod G. (2001a). Dielectric elastomer actuators, PhD. thesis, Riso-R-1286(EN)

Kofod G., R. Kornbluh, et al. (2001b). Actuation response of polyacrylate dielectric elastomers, Proc. SPIE, vol. 4329, pp. 141 – 147

Kofod G., P. Sommer-Larsen, et al. (2003). Actuation response of polyacrylate dielectric elastomers, *J. Intel. Mat. Syst. Str.*, vol. 14, pp. 787-793

Kofod G., P. Sommer-Larsen (2005). Silicone dielectric elastomer actuators: Finite-elasticity model of actuation, *Sens. Actuators A*, vol. 122, pp. 273-283

Kornbluh R., R. Pelrine, et al. (1999). High-field electrostriction of elastomeric polymer dielectrics for actuation, Proc. SPIE, vol. 3669, pp. 149-161

Kornbluh R., R. Pelrine, et al. (2000). Ultrahigh strain response of field-actuated elastomeric polymers, Proc. SPIE, vol. 3987, pp. 51-64

Kovacs G., P. Lochmatter (2006). Arm wrestling robot driven by dielectric elastomer actuators, Proc. SPIE, vol. 6168, pp. 616807-1 - 616807-12

Lagarias J., J. Reeds, et al. (1998). Convergence properties of the Nelder-Mead simplex method in low dimensions, Siam. *J. Optim.*, vol. 9, no. 1, pp. 112-147

Lewis R., V. Torczon, M. Trosset (2000). Direct search methods: then and now, *Journal of Computational and Applied Mathematics*, vol. 124, pp. 191-207

Lochmatter P., S. Michel, G. Kovacs (2006a). Electromechanical model for static and dynamic activation of elementary dielectric elastomer actuators, Proc. SPIE, vol. 6168, pp. 61680F-1 - 61680F-13

Lochmatter P., G. Kovacs, P. Ermanni (2006b). Design and characterization of shell-like dielectric elastomer actuators, Proceedings of ICAST2006: 17th International Conference on Adaptive Structures and Technologies, Oct. 16-19, Taipei, Taiwan

Matlab 7.0, 2004, The MathWorks, Inc.

Maxwell J. C. (1954). A treatise on electricity and magnetism, Dover, Oxford

McMeeking R., C. Landis (2005). Electrostatic forces and stored energy for deformable dielectric materials, *Journal of Applied Mechanics*, vol. 72, pp. 581 – 590

Michel S., G. Kovacs, P. Lochmatter (2006). Propulsion unit for lighter-than-air aircraft, PCT-Patent, No. WO 2006/108311 A1

Mockensturm E., N. Goulbourne (2006). Dynamic response of dielectric elastomers, *International Journal of Non-Linear Mechanics*, vol. 41, pp. 388 – 395

Mooney M. (1940), A theory of large elastic deformation, *J. Appl. Phys.*, vol. 11, pp. 582-592

Nava A., E. Mazza, et al. (2004). Evaluation of the mechanical properties of human liver and kidney through aspiration experiments, *Health Care*, vol. 12, pp. 269 – 280

Nava A. (2007). In vivo characterization of the mechanical response of soft human tissues, Ph.D. thesis, Institute for Mechanical Systems, ETH Zurich, Switzerland

Nelder J., R. Mead (1965). A simplex method for function minimization, *Comput. J.*, vol. 7, pp. 308-313

Ogden R.W. (1972). Large deformation isotropic elasticity – on the correlation of theory and experiment for incompressible rubberlike solids, *Proc. R. Soc. Lond. A*, vol. 326, pp. 565-584

Pei Q., R. Pelrine, et al. (2003). Electroelastomer rolls and their application for biomimetic walking robots, *Synthetic Metals*, vol. 135- 136, pp. 129-131

Pelrine R., R. Kornbluh, J. Joseph (1998). Electrostriction of polymer dielectrics with compliant electrodes as a means of actuation, *Sens. Actuators A*, vol. A 64, pp. 77-85

Pelrine R., R. Kornbluh, et al. (2000a). High-speed electrically actuated elastomers with strain greater than 100%, *Science*, vol. 287, pp. 836-839

Pelrine R., R. Kornbluh, G. Kofod (2000b). High-strain actuator materials based on dielectric elastomers, *Adv. Mater.*, vol. 12, no. 16, pp. 1223-1225

Pelrine R., P. Sommer-Larsen, et al. (2001a). Applications of dielectric elastomer actuators, Proc. SPIE, vol. 4329, pp. 335-349

Pelrine R., R. Kornbluh, et al. (2001b). Dielectric elastomers: Generator mode fundamentals and applications", Proc. SPIE, vol. 4329, pp. 148-156

Pelrine R., R. Kornbluh, et al. (2002). Dielectric elastomer artificial muscle actuators: Toward biomimetic motion", Proc. SPIE, vol. 4695, pp. 126-137

Plante, J.S. (2006). Dielectric elastomer actuators for binary robotics and mechatronics, Ph.D. Thesis, Department of Mechanical Engineering, Massachusetts Institute of Technology, Cambridge, MA.

Plante J., S. Dubowsky (2006b). Large-scale failure modes of dielectric elastomer actuators, *International Journal of Solids and Structures*, vol. 43, pp. 7727–7751

Rivlin R.S., K.N. Sawyers (1971). Nonlinear continuum mechanics of viscoelastic fluids, *Ann. Rev. Fluid Mech.*, vol. 3, pp. 117-146

Rubin M.B., S.R. Bodner (2002). A three dimensional nonlinear model for dissipative response of soft tissue, *International Journal of Solids and Structures*, vol. 39, pp. 5081-5099

Shahinpoor M., Kim K.J. (2001). Ionic polymer-metal composites: I. Fundamentals, *Smart Mater. Struct.*, vol. 10, pp. 819-833

Sommer-Larsen P., G. Kofod, et al. (2002). Performance of dielectric elastomer actuators and materials, Proc. SPIE, vol. 4695, pp. 158-166

Su J., J.S. Harrison, et al. (1999). Electrostrictive graft elastomers and applications, MRS Symposium Proceedings, Warrendale, vol. 600, pp. 131-136

Sussman T., K.J. Bathe (1987). A finite element formulation for nonlinear incompressible elastic and inelastic analysis, *Journal Computers & Structures*, vol. 26, pp. 357-409

Treloar L. (1975). The physics of rubber elasticity, third edition, Oxford, Clarendon Press

Truesdell C., W. Noll (1992). The non-linear field theories of mechanics, 2nd edn., Springer-Verlag, Berlin

Vuskovic V. (2001). Device for in vivo measurement of mechanical properties of internal human soft tissues, Ph.D. thesis, No. 14222, ETH Zurich, Switzerland,

Wissler M., E. Mazza (2005). Modeling and simulation of dielectric elastomer actuators, *Smart Materials and Structures*, vol. 14, pp. 1396 - 1402

Wissler M., E. Mazza (2005). Modeling of a prestrained circular actuator made of dielectric elastomers, *Sens. Actuators A*, vol. 120, pp. 184-192

Wyrsch J. (2006). Untersuchung des elektromechanischen Verhaltens von Aktoren aus dielektrischen Elastomeren, Bachelerarbeit at Empa Dübendorf, Laboratory for Materials and Engineering, Dubendorf, Switzerland

Yang E., M. Frecker, E. Mockensturm (2005). Viscoelastic model of dielectric elastomer membranes, Proc. SPIE, vol. 5759, pp. 82 – 92

Yeoh O.H. (1990). Characterization of elastic properties of carbon-black-filled rubber vulcanizates, *Rubber Chem. Technol.*, vol. 63, pp. 792-805

Yeoh O.H. (1993). Some forms of the strain energy function for rubber, *Rubber Chem. Technol.*, vol. 66, pp. 754-771

Zhang Q.M., V. Bharti, X. Zhao (1998). Giant electrostriction and relaxor ferroelectric behavior in electron-irradiated poly(vinylidene-fluoride-trifluorethylene) copolymer, *Science*, vol. 280, pp. 2101-2104

Zhang Q. M., H. Li, et al. (2002). An all-organic composite actuator material with a high dielectric constant, *Nature*, vol. 419, pp. 284-287

Zhang R., A. Kunz, et al. (2004). Dielectric elastomer actuators for a portable force feedback device, The 4th European Conference on EuroHaptics 2004, Munich Germany, June 2004, pp. 300-307

Zhang X., C. Löwe, et al. (2005). Dielectric elastomers in actuator technologies, *Advanced Materials Engineering*, vol. 7, no. 5, pp. 361-367

Curriculum Vitae

Name:	Michael Wissler
Date of birth:	25th October 1976
Citizen of:	Sumiswald (BE), Switzerland

Education

1983 - 1985	Primary school, Oberrieden, Switzerland
1985 - 1991	Secondary school, Oberrieden, Switzerland
1991 - 1996	High School, MNG Rämibühl (Typus C), Zurich, Switzerland
1996 - 2002	Tertiary education at the ETH Zurich, Department of Materials. Graduation as Dipl. Werkstoff.-Ing. ETH (Degree in Materials Engineering)
2003 - 2007	Doctoral student at the Laboratory for Materials and Engineering, Empa, Dübendorf, Switzerland and the Institute of Mechanical Systems, ETH Zurich, Zurich, Switzerland

Professional experience

1996	Practical training for six weeks at Landis und Stäfa, Zug, Switzerland
1998	Practical training for three month at Copenhagen Pectin SA, Lille Skensved, Denmark
2003 - 2007	Research assistant at the Laboratory for Materials and Engineering, Empa, Dübendorf, Switzerland and the Institute of Mechanical Systems, ETH Zurich, Zurich, Switzerland